White Rose Research Online

eprints@whiterose.ac.uk
https://eprints.whiterose.ac.uk
Universities of Leeds, Sheffield and York

Deposited via The University of Leeds.

White Rose Research Online URL for this paper:
https://eprints.whiterose.ac.uk/id/eprint/102470/

Version: Accepted Version

Article:
Gannoun, A, Burton, KW, Day, JMD et al. (2016) Highly Siderophile Element and Os Isotope Systematics of Volcanic Rocks at Divergent and Convergent Plate Boundaries and in Intraplate Settings. Reviews in Mineralogy and Geochemistry, 81 (1). pp. 651-724. ISSN: 1529-6466

https://doi.org/10.2138/rmg.2016.81.11

© 2016, Mineralogical Society of America. This is an author produced version of a paper published in Reviews in Mineralogy and Geochemistry. Uploaded in accordance with the publisher's self-archiving policy.

Reuse
Items deposited in White Rose Research Online are protected by copyright, with all rights reserved unless indicated otherwise. They may be downloaded and/or printed for private study, or other acts as permitted by national copyright laws. The publisher or other rights holders may allow further reproduction and re-use of the full text version. This is indicated by the licence information on the White Rose Research Online record for the item.

Takedown
If you consider content in White Rose Research Online to be in breach of UK law, please notify us by emailing eprints@whiterose.ac.uk including the URL of the record and the reason for the withdrawal request.

UNIVERSITY OF LEEDS
University of Sheffield
UNIVERSITY of York

Highly siderophile element and Os isotope systematics of volcanic rocks at divergent and convergent plate boundaries and in intraplate settings

Abdelmouhcine Gannoun[1], Kevin W. Burton[2], James M.D. Day[3], Jason Harvey[4], Pierre Schiano[1], Ian Parkinson[5]

[1]Laboratoire Magmas et Volcans,
Université Blaise Pascal, CNRS-IRD, BP 10448,
63000 Clermont Ferrand, France
M.Gannoun@opgc.univ-bpclermont.fr

[2]Department of Earth Sciences,
Durham University, Science Labs,
Durham DH1 3LE, United Kingdom
kevin.burton@durham.ac.uk

[3]Geosciences Research Division,
Scripps Institution of Oceanography,
La Jolla, CA 92093-0244, USA
jmdday@ucsd.edu

[4]Institute of Geophysics and Tectonics,
School of Earth and Environment,
University of Leeds
Leeds, LS2 9JT, United Kingdom
feejh@leeds.ac.uk

[5]School of Earth Sciences
University of Bristol
Bristol BS8 1RJ, United Kingdom
Ian.Parkinson@bristol.ac.uk

INTRODUCTION

Terrestrial magmatism is dominated by basaltic compositions. This definition encompasses mid-ocean ridge basalts (MORB), which account for more than eighty percent of Earth's volcanic products and which are formed at divergent oceanic plate margins; intraplate volcanic rocks such as ocean island basalts (OIB), continental flood basalts (CFB) and continental rift-related basalts, and highly magnesian ultramafic volcanic rocks that dominantly occur in Archean terranes, termed komatiites. All of these broadly basaltic rocks are considered to form by partial melting of the upper mantle, followed by extraction from their source regions and emplacement at the Earth's surface. For these reasons, basalts can be used to examine the nature and extent of partial melting in the mantle, the compositions of mantle sources, and the interactions between Earth's crust and mantle. Because much of Earth's mantle is inaccessible, basalts offer some of the best 'proxies' for examining mantle composition, mantle convection and crust-mantle interactions. By contrast, at arcs, volcanism is dominated by andesitic rock compositions. While some arcs do have basaltic and picritic magmatism, these magma types are rare in convergent plate margin settings and reflect the complex fractional crystallization and often associated concomitant assimilation processes occurring in arc settings. Despite the limited occurrence of high MgO magmas in arc volcanics, magmas from this tectonic setting are also important for elucidating the behavior of the HSE from creation of basaltic compositions at mid-ocean ridges to the subduction of this crust beneath arcs at convergent plate margins.

The highly siderophile elements (HSE; comprising Re and Au, along with the six platinum-group elements [PGE] Os, Ir, Ru, Rh, Pt and Pd) combined with the ^{187}Re-^{188}Os and ^{190}Pt-^{186}Os systems that are embedded within these elements, have found significant utility in the study of basaltic rocks (e.g., Shirey & Walker, 1998; Carlson, 2005; Day, 2013). The greatest strengths of the HSE lie in the fact that they strongly partition into metal or sulfide phases, and so record evidence for processes that are not revealed from other isotope systems commonly used in high-temperature geochemical studies (e.g., He-O-Sr-Nd-Hf-Pb). Partial melting over much of Earth's geological history has resulted in significant fractionation of the HSE between the mantle and the crust (oceanic and continental). The HSE show contrasting behavior during melting, with the platinum-PGE (PPGE; Pt, Pd), Re and Au usually behaving as moderately compatible to moderately incompatible elements during melting and crystallisation, and the iridium-PGE (IPGE; Os, Ir and Ru) acting as highly compatible elements (Barnes et al., 1985). The differential response of the HSE to partial melting is demonstrated by differences in both the absolute and relative abundances of the HSE in mantle-

derived melts and in residual mantle rocks themselves. High degree melts, such as komatiites (e.g. Puchtel et al., 2009) show a smaller enrichment of PPGE over IPGE than relatively lower degree melts, such as MORB (e.g. Rehkämper et al., 1999; Bezos et al., 2005) (**Figure 1a**). Mantle peridotites often show a complementary depletion of PPGE relative to the IPGE that reflects the degree of melt depletion (**Figure 1b**), consistent with preferential removal of Re > Au > Pd > Pt > Rh > Ir ≥ Ru ≥ Os (Pearson et al., 2004; Becker et al., 2006; Fischer-Gödde et al., 2011). In the broadest sense, these observations suggest that the HSE in mantle and mantle-derived melts are controlled by both: (i) the degree of melting and; (ii) the mineralogy of mantle rocks. The IPGE are preferentially retained in mantle rocks at low-degrees of melting, consequently, moderate- to low-degree melts such as MORB have relatively low IPGE abundances.

Furthermore, because Pt is moderately compatible, Re is moderately incompatible and Os is highly compatible during melt generation, the Re-Os and Pt-Os isotope systems differ significantly from other geologically useful long-lived radiometric systems (e.g., Rb-Sr, Sm-Nd, Lu-Hf, U-Th-Pb), where both the parent and the daughter elements are preferentially concentrated into the melt. In this chapter, we review the distribution of the HSE amongst mantle minerals and their behavior during melting, the HSE abundances and Os isotope compositions preserved at mid-oceanic ridge settings (divergent plate boundaries), intraplate settings and of magmas formed at arcs (convergent plate boundaries), to examine the behavior of these elements in a range of tectonic settings.

HIGHLY SIDEROPHILE ELEMENT DISTRIBUTION AND BEHAVIOR IN THE UPPER MANTLE

Core formation and the late accretion of impactor material.

The HSE have high affinity for both Fe-metal and sulfide over coexisting silicate minerals or silicate melt. Low-pressure metal-silicate partition coefficients determined experimentally are extremely high (between 10^4 and 10^{15}) (Kimura et al., 1974; Jones and Drake, 1986; Peach et al., 1990, 1994; Fleet et al., 1991, 1996; Borisov et al., 1994; O'Neill et al., 1995; Holzheid et al., 2000; Ertel et al., 2001; Fortenfant et al., 2003; Yokoyama et al., 2009; Mann et al., 2012; Brenan et al., 2015, this volume). Consequently, these elements should have been substantially partitioned into Earth's metallic core, leaving the silicate mantles effectively stripped of the HSE. Yet, HSE concentrations in Earth's upper mantle are much greater than predicted from low-pressure experimental data (see Day et al., 2015, this volume). Moreover, their relative abundances display a

broadly chondritic pattern, rather than reflecting differences in their respective metal-silicate partition coefficient (**Figure 2**). However, the siderophile behavior of some HSE may be greatly reduced at high pressure-temperature conditions, and on this basis it has been suggested that high-pressure equilibration at the base of a deep molten silicate layer or 'magma ocean' on the early Earth, may account for their abundances in the upper mantle (Murthy, 1991). High-pressure experiments that simulate the conditions of core formation do indeed indicate that the HSE are less siderophile under these conditions (e.g. Mann et al., 2012). However, the range of HSE partition coefficients, even at elevated P-T conditions, cannot account for either the absolute or relative abundances in the terrestrial mantle, suggesting that high-pressure equilibration was not the dominant process controlling their present distribution. Therefore, mantle HSE abundances have long been taken to suggest that between 0.5% and 0.8% by mass of 'late accreted' broadly-chondritic material was added to Earth after core formation was complete (e.g., Kimura et al., 1974; Chou, 1978). Differing absolute abundances, but similar chondrite-relative HSE abundances have also been inferred for the Moon, Mars and other meteorite parent-bodies (Day et al., 2007, 2010a, 2012, 2015 this volume; Day & Walker, 2015; Brandon et al., 2012; Dale et al., 2012a; Riches et al., 2012), suggesting that late accretion was a phenomenon common to all terrestrial planets, setting the HSE abundances in planetary mantles. In this way, core formation and late addition of meteorite material are thought to have established the HSE abundance in Earth's silicate mantle, providing a framework for understanding the long-term effects of mantle melting.

Highly siderophile elements in mantle minerals

The behavior of the HSE during partial melting of the mantle is controlled by their distribution amongst sulfides, platinum group minerals (PGM) and coexisting silicates and oxides in mantle rocks (see also Lorand and Luguet, 2015, this volume; O'Driscoll and González-Jiménez, 2015, this volume; Harvey et al., 2015, this volume; Becker and Dale, 2015, this volume).

Sulfide: In addition to their strongly siderophile behavior the HSEs are also known to be highly chacophile (sulfur-loving) hence it has long been known that sulfide in mantle rocks exerts a dominant control over the behavior of HSE (e.g. Mitchell and Keys, 1981) despite its extremely low abundance (the proportion of sulfide in mantle rocks is though to be in the range 0.0014 to 0.008%, Luguet et al., 2003). The exact magnitude of partitioning of the HSE between sulfide and silicate, however, remains poorly constrained with values ranging from 1000 to $>10^8$ (**Figure 3**) (Peach et al.,

1990; 1994; Fleet et al., 1996; Crocket et al., 1997; Andrews and Brenan, 2002a; Gannoun et al., 2004, 2007; Fonseca et al., 2009; Mungall and Brenan, 2014). At least some of this variation is likely to relate to compositional variations of sulfide and silicate, or the conditions under which equilibration occurred. Values at the low end of the range are usually found in natural occurrences of glass and sulfide (e.g. Gannoun et al., 2004, 2007), while the highest values are indirect estimates based on alloy-sulfide and alloy-silicate partitioning (e.g. Fonseca et al., 2009). A particular problem with the "indirect" estimates of alloy-silicate partitioning (Fonseca et al., 2009) is that they were determined for Fe and S-free compositions, precluding the possible formation metal-sulfide complexes (e.g. Gaetani and Grove, 1997). Moreover, the solubility of at least some HSE in silicate melts is enhanced in sulfur-bearing experiments, relative to sulfur-free (Laurenz et al., 2013) bringing partition coefficients into the range of other experimental estimates (Andrews and Brenan, 2002a; Mungall and Brenan, 2014). While the differences in partition coefficient that remain still span up to three orders of magnitude, estimates based on individual experiments or natural coexisting sulfide-silicate show significantly less variation. These data indicate that the PGE (Os, Ir, Ru, Pt and Pd) partition similarly into sulfide, with only Re showing a significant difference to the other HSE.

During mantle melting, sulfide will be removed in the silicate melt, as a function of temperature, pressure, oxygen fugacity and the iron content of the melt (Wallace and Carmichael, 1992; Mavrogenes and O'Neill, 1999; O'Neill and Mavrogenes, 2002). Given the estimated sulfur content of both the primitive mantle (~250±50 µg g^{-1} S; Lorand 1990; O'Neill 1991; Palme and O'Neill 2003) and the depleted mantle (~120-150 µg g^{-1} S; Salters and Stracke, 2004), and the relatively low degrees of partial melting required to produce most basalts, it is likely that they leave their source sulfide saturated (that is, sulfide remains as a stable mantle mineral). For example, the low HSE content of some low-degree alkali basalt partial melts can be explained by the presence of residual sulfide in the mantle source, while the high HSE content of high-degree mantle melts, such as komatiites, can be explained by exhaustion of sulfide in the source. However, sulfide behavior alone cannot account for the systematic depletion of HSE seen in mantle rocks, or the variable HSE content and very high Re abundances seen in MORB.

Silicate and oxides: Rhenium not only partitions into sulfide, but also into other mantle phases including clinopyroxene, orthopyroxene, garnet and spinel (Hart and Ravizza, 1996; Mallman and O'Neill, 2007; Righter and Hauri, 1998, Burton et al., 1999, 2000, 2002), particularly under reducing conditions (Mallman and O'Neill, 2007). The relatively low partition coefficients for Re between

175 silicate phases and melt, and the much lower coefficient for its partitioning between sulfide and
176 silicate melt compared to other HSE, makes this element moderately incompatible during partial
177 melting (Figure 3). The partitioning of Re into silicate then raises the question of to what degree the
178 HSE may also be incorporated into silicates or oxides in mantle rocks. Overall, natural and
179 experimental data suggest that silicate or oxide phases in the mantle do not exert a strong control on
180 the behavior of HSE during partial melting. Taking estimates of the proportion of silicate phases
181 present in the upper mantle (e.g. Workman and Hart, 2005), partial melting of a sulfide-free mantle
182 would yield melts that are slightly depleted in Os, Ir and Ru, relative to their source. Such a pattern is
183 consistent with that seen for high-degree melts, such as komatiites. Nevertheless, silicate and oxide
184 behavior cannot account for the fractionation of the HSE, and in particular the low Os, Ir and Ru
185 contents, seen in MORB basaltic rocks from all tectonic settings.
186
187 *Spinel:* Empirical estimates of partitioning derived from mineral separates suggest that Os, Ru and Ir
188 are highly compatible in Cr-bearing spinel with partition coefficients of up to 150, while Pt and Pd
189 are moderately compatible (Hart and Ravizza, 1996; Puchtel and Humayun, 2001). Experimental
190 work on spinel-silicate melt partitioning at moderate to high oxygen fugacity suggests that for Fe-
191 bearing spinels Ru, Rh and Ir are all highly compatible with partition coefficients of 20 to > 1000
192 (**Figure 4**), whereas Pd is barely compatible (Capobianco and Drake, 1990; Capobianco et al., 1994,
193 Righter et al., 2004). More recently it has been shown that the partition coefficients for Ir, Rh, and Ru
194 are strongly controlled by the ferric-iron content of the spinels. For Cr-bearing spinels, in which Fe^{3+}
195 is replaced by Cr^{3+}, partition coefficients for Ir and Rh are much lower than for Fe-rich compositions,
196 and Pt and Pd are highly incompatible (Brenan et al., 2012).
197
198 *Olivine:* Some of the first empirical data for olivine mineral separates were taken to indicate that Os
199 may be compatible in olivine with an inferred olivine-silicate partition coefficient of ~20 (**Figure 4**),
200 (Hart and Ravizza, 1996). However, other work on separated olivine suggested that Os is highly
201 incompatible (Walker et al., 1999; Burton et al., 1999, 2000, 2002). At this stage it is not clear
202 whether these variations reflect compositional differences between samples, or simply the presence
203 of micro-nuggets of sulfide or PGMs in the separated silicate phase. Experimental work, however,
204 suggests that many HSE are weakly compatible or only slightly incompatible in olivine, particularly
205 under reducing conditions (Brenan et al., 2003, 2005).
206
207 *Orthopyroxene and clinopyroxene:* Empirical constraints from Hart and Ravizza (1996) suggest that
208 Os may be compatible in orthopyroxene and clinopyroxene (**Figure 4**),, but other studies yield much

lower Os concentrations for these phases (relative to coexisting sulfide or olivine) (e.g. Burton et al., 1999, 2000). Experimental work indicates that Re may be mildly compatible in ortho- and clinopyroxene under reducing conditions (e.g. Mallman and O'Neill, 2007), but is incompatible under more oxidizing conditions (e.g. Watson et al., 1987; Righter and Hauri, 1998; Righter et al., 2004; Mallman and O'Neill, 2007). While Pt and Pd appear to be mildly compatible in clinopyroxene (Hill et al., 2000; Righter et al., 2004).

Overall, natural and experimental data suggest that silicate or oxide phases in the mantle do not exert a strong control on the behavior of HSEs during partial melting. Taking estimates of the proportion of silicate phases present in the upper mantle (e.g. Workman and Hart, 2005) partial melting of a sulfide-free mantle would yield melts that are slightly depleted in Os, Ir and Ru, relative to their source. Such a pattern is consistent with that seen for high-degree melts, such as komatiites (**Figure 1a**). Nevertheless, silicate and oxide behavior cannot account for the fractionation of HSEs, and in particular the low Os, Ir and Ru contents, seen in basaltic rocks from all tectonic settings (**Figure 1a**).

Refractory mantle sulfide: For natural magmatic and experimentally produced sulfide the data suggests that while the HSEs are strongly partitioned into this phase there is little fractionation between the elements (with the exception of Re). Mantle sulfides, however, dominantly comprise refractory monosulfide solid solution (MSS) and Cu-rich sulfides, which together control much of the HSE budget of the upper mantle (e.g. Alard et al., 2000). Petrographic observations suggest that MSS often occurs as inclusions trapped in silicate phases, and is characterized by high Os, Ir and Ru abundances, whereas the interstitial Cu-rich sulfides possess lower Os, Ir and Ru contents (**Figure 5**). The silicate hosted MSS sulfides were interpreted to be the refractory residues of partial melting, and the interstitial sulfides as having crystallised from a sulfide–bearing melt. On the basis of these observations it has been argued that the fractionation of HSE during mantle melting might be accomplished by partitioning between refractory "solid" MSS and liquid sulfide (Bockrath et al., 2004a). However, at mantle temperatures of 1300-1400°C and pressures of 5-16 kbar, that is, those appropriate for the generation of MORB (e.g. Klein and Langmuir, 1987) any refractory sulfide is likely to be completely molten well before the peridotitic silicate and oxide phases start to melt (Rhyzenko and Kennedy, 1973; Hart and Gaetani, 2006). Consequently, two phases of sulfide are unlikely to be stable during the melting that produces MORB, consistent with modeled depletion of mantle peridotites where MSS-sulfide melt partitioning cannot explain the observed variations in Pd, Pt and Au (Fisher-Godde et al., 2011). However, under conditions of melting at lower temperatures, for example, due to the presence of volatiles such as H_2O and at fO_2 lower than that at which sulfide

is oxidized to sulfate, MSS fractionation may play a role in generating melts with low Os, Ir and Ru contents (Mungall, 2002, Mungall et al., 2006; Dale et al. 2012b; Botcharnikov et al., 2013)

Os-Ir-Ru metallic alloys: Osmium, Ir and Ru (the IPGE) are not only strongly concentrated in refractory monosulfide solid solution, but also in platinum-group minerals (PGM), which encompass alloys and sulfides where Ru, Os and/or Ir are the major metallic elements. It is clear from the distribution and absolute concentrations of IPGE in PGM (**Figure 6**) that precipitation and accumulation of such phases should have a profound effect on IPGE/PPGE fractionation (Brenan and Andrews, 2001). In addition, Pt-rich PGM, such as Pt-Ir alloys, have also been found in upper mantle lithologies (Luguet et al., 2007; Lorand et al., 2010). Palladium-rich PGM also exist, which also may contain Pt, but typically Pd combines with bismuth and/or tellurium to form bismuthotellurides which are thought to be indicators of refertilisation rather than residual to melting (e.g. Lorand et al., 2010). Thus, Os-Ir-Ru and, to a lesser extent, Pt can all be retained by PGM during melting, while Pd is not.

Some have argued that PGE-alloys may represent material that was once part of the core, either as a result of incomplete segregation of metal to the core, or due to the entrainment of outer core material into the mantle at the core-mantle boundary (Bird and Weathers, 1975; Bird and Bassett, 1980; Bird et al., 1999). However, recent experimental data suggests that metal originating in the outer core would possess similar concentrations of Os, Pt and Re, rather than show an enrichment in Ru-Os and Ir (van Orman et al., 2008; Hayashi et al., 2009) likewise any metal trapped in the mantle during core formation (e.g. Mann et al., 2012). The solubility of Os, Ir and Ru is extremely low in silicate melts (e.g. Borisov and Palme, 2000; Brenan et al., 2005). Therefore, it has been argued that Os-Ir-Ru-rich PGM may precipitate directly from a silicate melt, through nucleation on nanoclusters of HSE molecules (Tredoux et al., 1995). Furthermore, on the basis of the high solubility of Ir and Ru in sulfide melts it has been proposed that crystallisation of Ru-Ir-Os alloys in the presence of a sulfide liquid is unlikely (Brenan and Andrews, 2001). Rather it has been argued that such alloys can only precipitate from a melt that is sulfide-undersaturated (Brenan and Andrews, 2001; Andrews and Brenan 20002b; Bockrath et al., 2004b; Barnes and Fiorentini, 2008).

Together, these observations have been taken to suggest that the relationship between Os-Ir-Ru alloys and refractory sulfides in the mantle is key to understanding the behavior of the HSE during higher degrees of partial melting (e.g. Fonseca et al., 2012), where the removal of sulfur in silicate melts leads to a decrease in the proportion of sulfide in the source. All the while that sulfide remains present the HSE are quantitatively retained, and can reach wt. % levels in sulfide. However, as soon

as sulfide has been completely dissolved, Os-Ir-Ru-Pt alloys form in response to lowering of fS_2 and diminished metal-sulfide complexation in the silicate melt (Fonseca et al., 2012). Effectively, much of the HSE budget of the mantle, with the exception of Re, remains in the mantle until sulfide has been completely removed, after which time Os-Ir-Ru and Pt are hosted by PGM phases rather than being liberated in a silicate melt. This model is consistent with an increasing number of petrographic observations indicating the presence of PGM phases in melt-depleted mantle peridotite (Luguet et al., 2003, 2007; Pearson et al., 2004; Brandon et al., 2006; Kogiso et al., 2008, Lorand et al., 2010, 2013; Fisher-Gödde et al., 2012).

The degree of partial melting needed to trigger PGM formation will depend on how much sulfur there is in the mantle source at the onset of melting, and is also a result of the solubility of S being inversely proportional to pressure (Mavrogenes and O'Neill, 1999). The mantle that melts to produce MORB is already significantly depleted (e.g. Hofmann, 1997), and the melting occurs at relatively shallow levels (e.g. Klein and Langmuir, 1987). However, there is considerable uncertainty as to the amount of sulfur in the depleted mantle, with estimates ranging down to ~120 µg g^{-1} (Salters and Stracke, 2004) compared to the concentration in primitive "fertile" (unmelted) mantle at 250 µg g^{-1} (Lorand, 1990; O'Neill, 1991; Palme and O'Neill, 2003). Taking the S content of the MORB source mantle to be 120 µg g^{-1}, then 15% melt extraction is needed to exhaust sulfide from the source, and thereby allow the generation of PGM in the mantle residue (Fonseca et al., 2011, 2012; Mungall and Brenan, 2014). While these calculations indicate that even the depleted mantle requires significant degrees of melting to remove sulfide, such melt proportions are well within the range of estimates for the generation of MORB (e.g. Klein and Langmuir, 1987). In this case PGM formation in the upper mantle may be a potential cause for the characteristic depletion of Os, Ir Ru and Rh, relative to Pt and Pd observed in MORB (**Figure 7**). The absence of significant fractionation of the HSE in komatiites, considered to represent higher-degrees of melting than MORB, suggests that alloys are not stable at the higher pressures and temperatures conditions required for the generation of such melts (cf. Mungall and Brenan, 2014).

Overall, the natural and experimental data for mantle minerals indicates that whenever sulfide is present in the mantle, the HSE are largely retained during partial melting, the exception being Re that is not as strongly incorporated into sulfide, and is relatively soluble in silicate melts. However, if base metal sulfide is removed from the system during high degrees of melting, at the pressure temperature conditions appropriate for MORB melting, then this will result in the formation of Os-Ir-Ru alloys and/or sulfides.

311 **Highly siderophile element behavior accompanying fractional crystallisation**
312
313 The major and trace element variations preserved in mid-ocean ridge basalts indicates that their
314 composition has been extensively modified by fractional crystallisation, prior to eruption on the
315 ocean floor (e.g. Klein and Langmuir, 1987). The principal silicate phases involved in the fractional
316 crystallisation that generates MORB are olivine, plagioclase and clinopyroxene (e.g. Klein and
317 Langmuir, 1987; Grove et al., 1993). In general, the more evolved MORB (that is, those with lower
318 MgO and Ni contents, due to the crystallisation and removal of olivine) possess lower HSE contents
319 (**Figure 7**). On the basis of early empirical estimates for the partitioning of Os into olivine, this
320 relationship has led some to suggest that the HSE are compatible in this phase and removed from the
321 silicate melt. However, as discussed previously, with the exception of Re, there is little evidence to
322 suggest that the HSE are strongly partitioned into olivine, plagioclase or clinopyroxene (**Figure 4**).
323
324 Most MORB are thought to be sulfur saturated (Wallace and Carmichael, 1992) and sulfide is a
325 ubiquitous phase. Nevertheless, even if MORB melts are sulfur saturated at their source, they are
326 likely to arrive at the surface undersaturated, because the sulfur content at sulfide saturation increases
327 dramatically at lower pressures (e.g. Mavrogenes and O'Neill, 1999). In this case the only viable
328 mechanism by which MORB melts can become sulfur saturated is through extensive fractional
329 crystallisation, driving the residual melt to higher S contents. Therefore, it seems most likely that it is
330 the fractional crystallisation of olivine, plagioclase and clinopyroxene that drives the melt to sulfur
331 saturation, resulting in the precipitation of sulfide. Hence, the relationship between Ni (concentrated
332 in olivine) and HSE (concentrated in sulfide) can be attributed to the coupled crystallisation of
333 silicates and sulfide.
334
335 Sulfide may be present at relatively high proportions in MORB (up to ~0.23% by mode, Kiseeva and
336 Wood, 2015), and it strongly incorporates most HSE (section 2.3, **Figure 3**) with partition
337 coefficients between 10^4-10^6. In contrast, Re, while still being compatible compatible in sulfide, has a
338 sulfide-silicate melt partition coefficient, at least, two orders of magnitude lower than that of the
339 other HSE (D_{Re}~10-10^3). Consequently, MORB sulfides have high Os (and other HSE) contents, and
340 low Re/Os relative to their parental melt, and the effect of sulfur saturation and sulfide crystallisation
341 will be to decrease absolute HSE abundances, and to raise the Re/Os ratio in the residual melt.
342
343

THE ^{187}Re-^{187}Os ISOTOPE SYSTEM AND THE FORMATION OF MID-OCEAN RIDGE BASALTS

Introduction

Mid-ocean ridge basalts form by partial melting of the Earth's upper mantle, and variations in their radiogenic isotope compositions or concentration ratios of incompatible elements are considered to reflect compositional heterogeneity in the mantle source (Tatsumoto, 1966; O'Nions et al., 1977; Kay, 1985; Hofmann, 1997). These compositional variations occur on a variety of scales and tectonic settings, ranging from the global-scale of the so-called DUPAL anomaly (centred on the Indian ocean) (Dupré & Allègre, 1983; Hart, 1984; Hamelin & Allègre, 1985; Hamelin et al., 1986; Michard et al., 1986; Price et al., 1986; Dosso et al., 1988; Mahoney et al., 1989, 1992; Rehkamper & Hofmann, 1997; Escrig et al., 2004); to those associated with ocean-island volcanics or near-ridge seamounts (White & Schilling 1978; Zindler et al., 1984; Brandl et al., 2012); to minor pervasive variations within ridge segments of normal MORB (e.g. Hofmann, 1997; Agranier et al., 2005). A number of processes have been put forward to account for these compositional variations including variable degrees of mantle depletion by prior partial melting (e.g. DePaolo & Wasserburg, 1976; Zindler et al., 1984), the infiltration of silicate melts or fluids (e.g. Green, 1971), or recycling of lithospheric material into the mantle (e.g. Hofmann, 1997).

The ^{187}Re-^{187}Os isotope system, based on the long-lived β decay of ^{187}Re to ^{187}Os, potentially provides an exceptional tracer of recycled lithosphere in Earth's mantle. This is because both oceanic and continental crust possess exceptionally high Re/Os (parent/daughter ratios), and develop radiogenic Os isotope compositions over time (e.g. Pegram & Allègre, 1992; Shirey & Walker, 1998; Hauri, 2002). In contrast, portions of the lithosphere have low Re/Os, and evolve to unradiogenic Os isotope compositions relative to that of the primitive upper mantle (PUM) (Walker et al., 1989; Pearson et al., 1995). These distinctive isotope signatures can be readily traced as recycled material if mixed back into the convective mantle. For example, the ^{187}Os/^{188}Os variations seen in HIMU (= high μ = elevated ^{238}U/^{206}Pb) ocean island basalts indicate the presence of material that has evolved over a long-time period with high Re/Os, consistent with models indicating recycled oceanic lithosphere in the source of these volcanic rocks (Zindler and Hart, 1986; Day et al., 2010b; Day, 2013).

Some of the earliest measurements of ^{187}Os/^{188}Os in MORB also yielded isotope compositions more radiogenic than estimates for the primitive upper mantle (e.g. Martin, 1991; Roy-Barman and

Allègre, 1994) and these were attributed either to contamination by seawater derived Os or melting of a heterogeneous mantle (e.g. Martin, 1991; Roy-Barman and Allègre, 1994). The work of Schiano et al (1997) on normal MORB, however, not only indicated relatively radiogenic Os isotope compositions but also that these compositions appeared to covary with the Sr-Nd and Pb isotopes of the same samples. For the DUPAL anomaly, radiogenic Os isotope compositions were taken to indicate the presence of mafic continental crust in the mantle source (Escrig et al., 2004). While radiogenic $^{187}Os/^{188}Os$ isotope compositions for MORB from the south Atlantic were attributed to metasomatism of the asthenospheric mantle, and local effects from plume-ridge interaction (Escrig et al., 2005). At first sight the data from these studies might be taken to suggest that the Os isotope variations reflect those of the MORB mantle source, rather than a secondary process, and that Os isotopes do indeed act as a sensitive tracer of different recycled or enriched material in the mantle.

However, these data also indicate a covariation between the Os isotope composition and the Os elemental abundance in these samples (Schiano et al., 1997; Escrig et al., 2005). Covariations between Os, Ni and Mg contents in MORB are most readily explained by fractional crystallisation (e.g. Burton et al., 2002) but in this case it is then difficult to attribute the Os isotope variations to a mantle source, leading some to propose that the radiogenic Os isotope ratios reported by these studies must result from seawater derived contamination (e.g. Shirey and Walker, 1998; Hart et al., 1999; Standish et al., 2002; Peucker-Ehrenbrink et al., 2003). Subsequent work demonstrated that many of the MORB previously analysed (Schiano et al., 1997; Escrig et al., 2004, 2005) had been affected by an analytical artefact (Gannoun et al., 2007), nevertheless a number of samples still possess relatively radiogenic isotope compositions (Gannoun et al., 2004, 2007; Yang et al., 2013, Burton et al., 2015).

Despite the potential utility of this isotope system, in particular, for tracing the presence of recycled material in MORB, these studies highlight the particular difficulties of both the measurement and the interpretation of ^{187}Re-^{187}Os isotope data in MORB. Mid-ocean ridge basalts possess extremely low Os concentrations, usually less than 10 parts per trillion (pg g^{-1}) which, not only makes their accurate measurement exceptionally challenging, but also renders MORB highly susceptible to effects that are rarely seen in lithophile elements isotope systems (such as Rb-Sr or Sm-Nd). Such effects include; (i) Radiogenic ingrowth of ^{187}Os, produced from the decay of ^{187}Re over very short periods of time, (ii) seawater contamination, both direct on the sea floor or indirect in the magmatic plumbing system, and (iii) sample heterogeneity, due to variable contamination in glass or amongst coexisting magmatic phases or through sulfide nugget effects.

Analytical techniques.

Osmium has seven naturally occurring isotopes, two of which ^{187}Os and ^{186}Os are the decay products of long lived radioactive isotopes, ^{187}Re and ^{190}Pt. Of these two decay systems, the Re-Os method has been used as a dating tool and geochemical tracer for over four decades (Shirey and Walker, 1998). Despite its great potential as a geochemical tool, analytical difficulties initially limited the application of the osmium isotope method, mainly because of the high ionization potential of Os (ca. 9eV). The discovery that a solid Os sample could yield negative molecular ions by conventional thermal ionisation (Creaser et al., 1991; Volkening et al., 1991) rendered largely obsolete all the excitation methods for atomic osmium used before (Hirt et al., 1963; Luck and Allègre, 1982; Walker and Fasset, 1986). In the N-TIMS method Os is measured as osmium trioxide (OsO^{3-}) via heating on platinum filaments with an electron donor. A Ba–Na emitter solution is employed to lower the work function of the filament, which enhances the emission of negative ions. The formation of the Os oxide species is also advantaged by bleeding oxygen into the source (Walczyk et al., 1991). The ionisation efficiency increases significantly with decreasing Os loads and can reach above 30% at the pg Os level (Birck, 2001; Gannoun and Burton, 2014).

Another major problem with Re-Os isotopic analysis has been the chemical behavior of Os in solution because of the numerous oxidation states including the volatile tetraoxide species (OsO_4). At present, no single technique is equally applicable to all matrices particularly when organic matter and/or refractory mineral phases are present because the variable oxidation states may inhibit the complete homogenisation of Os between sample and spike.

High temperature (~ 250°C) oxidising digestions using either Carius tubes (Shirey and Walker, 1995) or high-pressure asher (HPA) digestion vessels (Meisel et al., 2003) have the merit of dissolving acid-resistant phases such as chromite and HSE alloys. These methods have been supplemented by employing HF digestion after Carius tube/HPA digestion (e.g., Ishikawa et al., 2014), but with mixed results (Day et al., 2015). However, such techniques can potentially yield high Os blanks (> 1pg) that can contaminate low Os (±PGE and Re) abundance samples, such as MORB. Mid-ocean ridge basalt glass possesses low Os abundances, with some samples in the range of 0.2 and 3 pg g^{-1}, in which refractory minerals are usually absent. For these reasons low-temperature digestion techniques have been used in preference to other approaches when analysing Os in MORB. These use HF and HBr in sealed Teflon vessels at temperature of ≤ 140 °C, followed by extraction of Os in liquid bromine (Birck et al., 1997). Extremely low blanks of <50 fg of Os have been achieved with this method (Gannoun et al., 2004; 2007). Furthermore, MORB glasses are likely to be completely dissolved in HF-HBr acids mixtures even at room temperature.

Mid-ocean ridge basalt sulfide grains can be extracted directly using a magnet and handpicked under a binocular microscope (Gannoun et al., 2004; 2007; Harvey et al., 2006) or removed from hand-polished slabs using a diamond scribe to etch around and under the grains (Warren and Shirey, 2012). The grains are weighed, spiked with ^{185}Re-^{190}Os and dissolved with high purity HBr. The Os fraction is then purified using microdistillation (Birck et al., 1997; Gannoun et al., 2007, Harvey et al., 2006). It is also possible to undertake dissolution simultaneously with microdistillation (Pearson et al;, 1998). The purified Re and Os are analysed by NTIMS following the method described by Pearson et al. (1998). Osmium analysis in sulfides can also be achieved using in situ laser ablation techniques. The strength of this technique lies in the ability to relate Os isotope information from individual sulfide to their precise spatial and textural setting in the rock (Pearson et al., 2002). However single sulfide Os data analysed by the N-TIMS technique are typically of a much higher precision than in situ analysis (cf. Gannoun et al., 2007; Harvey et al., 2006; Pearson et al., 1998) even for sulfide with low Os contents (i.e. less than 10 µg g^{-1}). Moreover, for in situ analysis, because of the isobaric interference of ^{187}Re on ^{187}Os accurate measurement of ^{187}Os/^{188}Os is only possible for sulfides with low ^{187}Re/^{188}Os (Pearson et al., 2002). Such conditions are only met in the case of mantle sulfides.

Rhenium-Osmium elemental variations in MORB glass.

The fractionation of Re and Os accompanying the generation of MORB is one of the key processes controlling the distribution of these elements between Earth's mantle and crust. Osmium behaves as a highly compatible element during partial melting, and is preferentially retained in the residual mantle. Consequently, MORB have much lower concentrations, ranging from 0.18 to 170 pg g^{-1} (with a mean of 10 pg g^{-1}) than mantle peridotite, ranging from 800 to 13000 pg g^{-1} (with a mean of 3900 ng g^{-1}). In contrast, Re is moderately incompatible during partial melting and preferentially enters the melt. Accordingly, MORB have high Re concentrations, ranging from 480 to 3000 pg g^{-1} (with a mean of 1023 pg g^{-1}) compared to 10 to 450 pg g^{-1} in mantle peridotite (with a mean of 200 pg g^{-1}) (**Figure 8**).

By comparison, komatiiites have generally much higher Os concentrations, up to 10,000 pg g^{-1}, with a similar range of Re concentrations as MORB. These high Re and Os concentrations are generally attributed to higher degrees of melting. Ocean island basalts (OIB) have Os concentrations that range from 1 to 500 pg g^{-1}, and arc lavas from 0.1 to >10 pg g^{-1}. The low Os concentration of many arc lavas is likely due to extensive removal during fractional crystallization and indeed in cases where basaltic compositions have been sampled Os concentrations can be greater than 50 pg g^{-1} (Dale

et al., 2012b). The relatively low Re concentration of many arc lavas and OIB was originally thought to reflect differences in the mineralogy of the mantle source or the extent of melting, but it is likely that for many of these samples the low Re concentrations result from volatile behaviour during sub-aerial eruption (e.g. Lassiter, 2003; Day et al., 2010b; Gannoun et al., 2015b). As outlined previously, the low Os concentration of MORB is likely to result, in part, from preferential partitioning into residual mantle sulfide and/or PGM phases and, in part, to the low solubility of Os in silicate melts. In addition, the Os composition of primitive MORB melts will be further reduced by sulfide segregation during fractional crystallisation. In contrast, the relatively high Re concentrations result, in part from Re being much less strongly incorporated in mantle sulfide and PGM phases and, in part, from much of the Re budget being controlled by silicate phases, and having a much higher solubility in silicate melts. Rhenium, is removed into both silicates and sulfide during fractional crystallisation.

A remarkable feature of MORB, and indeed all other terrestrial basalts, is the relatively constantly increasing fractionation of Re/Os with decreasing Os content. The values range from mantle Re/Os values of around 0.01 for Os concentrations of 2-7 ng g^{-1}, to Re/Os values of ~1000 for lavas with concentrations of 0.1 pg g^{-1} (**Figure 9**). The systematic nature of this fractionation, suggests either that it is dominantly controlled by a single process, such as mantle melting or fractional crystallisation, or else that several process act to have the same effect, for example, fractionation by refractory mantle sulfide and also by sulfide segregation during fractional crystallisation.

Rhenium shows a broad positive covariation with Al_2O_3 and sulfur consistent with the incompatibility of all these elements during mantle melting (**Figure 10**). The positive Re–S covariation might be explained by the fact that both elements will be removed into sulfide during fractional crystallization, resulting in a decreasing S and MgO content during the differentiation of S-saturated MORB (Mathez, 1976; Bezos et al., 2005; Ballhaus et al., 2006). Despite significant scatter, Os broadly covaries with Ni in MORB (**Figure 11**), consistent with a role for olivine crystallisation in Os partitioning. Although previous studies have attributed the Os–Ni covariation directly to the compatibility of Os in olivine (Brügmann et al., 1987; Hart and Ravizza, 1995), natural samples and experiments indicate that Os is much less compatible. Burton et al., (2002) have shown that Os is in fact extremely incompatible in olivine. Rather it is the crystallisation of olivine that drives the melt to sulfur saturation, which in turn results in sulfide precipitation (in which Os is highly compatible) that is trapped within the olivine as 'melt inclusions' (Walker et al., 1999; Burton et al., 2002, Brenan et al., 2003, 2005). In summary, Re and Os display similar overall behaviour in MORB from the three major ocean basins. Osmium is highly compatible during melting and fractional crystallisation, whereas Re is moderately incompatible.

The $^{187}Os/^{188}Os$ isotope variations in MORB glass.

The $^{187}Os/^{188}Os$ isotope compositions for MORB from the Pacific, Atlantic and Indian Oceans are shown against the reciprocal of the concentration in **Figure 12**. Mid-ocean ridge basalts from the three major oceans show a similar range of $^{187}Os/^{188}Os$ isotope compositions, ranging from 0.126 to 0.148 with a mean value of 0.133 ±0.009 (2σ st. dev.) (Gannoun et al., 2004, 2007; Yang et al., 2013; K W Burton, unpublished data). There is no overall correlation with Os concentration (cf. Schiano et al., 1997; Escrig et al., 2004), however, in general MORB glasses have Os concentrations in the following order: Indian > Atlantic > Pacific, and those samples with a higher Os concentration have a tendency to possess more radiogenic $^{187}Os/^{188}Os$ compositions. Comparison of $^{187}Os/^{188}Os$ radiogenic ratios with the parent/daughter ratio, $^{187}Re/^{188}Os$, on a conventional isotope evolution diagram (**Figure 13**) indicates that there is no systematic covariation. The data do, nevertheless, indicate that MORB glasses with lower $^{187}Re/^{188}Os$ are generally found in the Indian > Atlantic > Pacific. In addition, those samples with the lowest $^{187}Re/^{188}Os$ tend to possess the most radiogenic isotope compositions.

With regard to the long-lived radiogenic isotopes of Sr, Nd and Pb, while the cross-linked data are limited, there are no systematic variations between $^{187}Os/^{188}Os$ and $^{87}Sr/^{86}Sr$, $^{143}Nd/^{144}Nd$, and $^{206}Pb/^{204}Pb$ (**Figure 14**). Similarly, there is no correlation between $^{187}Os/^{188}Os$ composition and ridge bathymetry or spreading rate (**Figure 15**) (using data compilation of DeMets et al., 2010 and Argus et al., 2011).

Analytical issues associated with MORB

Several studies have reported $^{187}Os/^{188}Os$ data for MORB glass (Schiano et al., 1997; Escrig et al., 2004) that could not be reproduced elsewhere, using lower blank techniques (Gannoun et al., 2007; K.W. Burton unpublished data). Comparison of these data shows that for many of the relatively unradiogenic samples there is reasonably good agreement between studies (**Figures 16 and 17**) but notably none of the very radiogenic values previously reported were reproduced for the same samples. Such a difference might be attributed either to the nature of the samples or the methods involved in their preparation for chemistry. The earlier studies used leaching techniques to remove any Fe-Mn oxyhydroxides that may have accumulated on the glass while on the sea floor. Iron-manganese precipitates, if present, are likely to possess a radiogenic Os isotope composition acquired from seawater ($^{187}Os/^{188}Os$ = ~1), therefore if present they might shift the measured $^{187}Os/^{188}Os$ to

more radiogenic values. However, experiments on some of the same glasses indicate that extensive leaching, with oxalic acid and HBr, yields indistinguishable results to those for the same glass samples simply rinsed in dilute HCl, ethanol and water. Another possibility is that because of the large sample sizes used in the earlier studies, between 1 and 5 g (Schiano et al., 1997; Escrig et al., 2004) compared to 300 to 500 mg (e.g. Gannoun et al., 2007), phenocrysts possessing radiogenic isotope compositions may have been inadvertently included in the material measured. Likewise, entrainment of included sulfides possessing very radiogenic compositions may have the same effect. If the radiogenic $^{187}Os/^{188}Os$ were due to the presence of entrained silicates or sulfides, then some variation in the parent/daughter ratio might be expected (cf. Figure 9 of Day 2013). Such heterogeneity is spectacularly displayed in two samples from the same locality in the Indian Ocean, where significant variations in the isotope and elemental composition of MORB glass can be attributed to the variable presence of sulfide inclusions. However, duplicate and triplicate measurement of eleven of the samples showed no resolvable variation, and there is no evidence for isotope and elemental heterogeneity in any of these glass samples. Therefore, it seems more likely that the difference in measured $^{187}Os/^{188}Os$ composition is an analytical artefact. One possibility is that this is due to interference from $^{187}ReO_3^-$ on the measured $^{187}OsO_3^-$, although this can be carefully monitored during N-TIMS analysis through the direct measurement of $^{185}ReO_3^-$. More likely is that the earlier data were under-corrected for the total procedural blank during chemical purification. The blanks of the original studies possessed a radiogenic $^{187}Os/^{188}Os$ composition, and the difference between the earlier data (Schiano et al., 1997; Escrig et al., 2004) and those samples that were re-analysed increases with decreasing Os concentration in the sample, consistent with increasing contribution from the blank (**Figure 17**). Overall, these studies highlight the analytical difficulties of obtaining accurate $^{187}Os/^{188}Os$ data for MORB glass many of which possess low Os concentrations (i.e. between 0.2 and 5 pg g^{-1}).

The origin of the Os isotope variations in MORB glass

Notwithstanding any shifts that arise from analytical problems, the data obtained thus far, for all the major oceans, indicates a resolvable variation in the $^{187}Os/^{188}Os$ isotope composition of MORB, ranging from values similar to those expected for the primitive upper mantle (e.g. Meisel et al., 1996) to radiogenic compositions akin to those found in ocean island basalts (e.g. Day, 2013). It is unlikely that these data have also been compromised by analytical problems; first, because there is no covariation between the corrected $^{187}Os/^{188}Os$ and the Os concentration, as might be expected if

582 the blank concentration was not correctly determined. Second, replicates with differing sample
583 weights and subject to different dissolution technique yield indistinguishable $^{187}Os/^{188}Os$ values
584 (Gannoun et al., 2007; Yang et al., 2013, Burton et al., 2015). Moreover, those samples with
585 radiogenic $^{187}Os/^{188}Os$ compositions are actually those with the highest Os concentrations, and
586 therefore would be less susceptible to any blank effect. Finally there is no significant covariation
587 between Os and Sr, Nd or Pb isotopes, as might be expected if the variations were due to
588 compositional heterogeneity in the mantle source.
589
590 ***Radiogenic growth of ^{187}Os since MORB eruption.*** For lithophile elements, such as Sr or Nd,
591 parent/daughter ratios in MORB glass and coexisting silicates are relatively low, consequently shifts
592 in their radiogenic isotope composition are unlikely to have a measurable effect for timescales less
593 than 10^3 million years (e.g. Hofmann, 1997). Therefore variations in Sr or Nd isotope composition
594 preserved in MORB can be attributed to compositional heterogeneity in the upper mantle source (e.g.
595 Hofmann, 1997). For the ^{187}Re-^{187}Os system however, silicate phases and glass possess exceptionally
596 high $^{187}Re/^{188}Os$ (parent/daughter). This then raises the possibility that radiogenic ^{187}Os could be
597 produced in situ from the decay of ^{187}Re over relatively short periods of time (that is a few hundred
598 thousand years or less; e.g. Hauri et al., 2002, Gannoun et al., 2004, 2007). For example, MORB
599 glass possesses $^{187}Re/^{188}Os$ with values ranging from 30 to 8000 (Gannoun et al., 2007; Yang et al.,
600 2013), and a glass with $^{187}Re/^{188}Os = 4000$ would produce a shift in $^{187}Os/^{188}Os$ from mantle values
601 of 0.1296 to a value of 0.14 in less than 250 thousand years (Gannoun et al., 2007). This effect is
602 illustrated in **Figure 13**, where timescales of between 50 ka and > 1 Ma could produce the range of
603 $^{187}Os/^{188}Os$ preserved in the MORB glasses if they were simply due to the decay of Re.
604 One approach to determining the age of crystallisation of the MORB glasses is the
605 measurement of short-lived isotopes of Th-U and Ra in the same samples. Such Th-U-Ra data were
606 obtained for a few MORB glasses spanning much of the observed range of $^{187}Os/^{188}Os$ compositions
607 for the datasets in Gannoun et al. (2004, 2007). Of those samples measured, if it is assumed that they
608 initially possessed a PUM-like composition at the time of crystallization, then between 700 kyr and
609 1.25 Myr would be required to generate their given $^{187}Os/^{188}Os$ isotope compositions. However, the
610 same samples possess $^{230}Th/^{232}Th$ activity ratios greater than 1, suggesting that they must be $\leq$ 350
611 kyr old (that is, the maximum time available before all ^{230}Th has decayed). Moreover, all but one
612 sample has a $^{226}Ra/^{230}Th$ activity ratio that is also greater than 1, suggesting those samples must be $\leq$
613 8 kyr old. Therefore, for these samples, at least, the radiogenic $^{187}Os/^{188}Os$ compositions cannot be
614 explained solely as a result of in situ decay of ^{187}Re subsequent to igneous crystallisation (Gannoun
615 et al., 2004, 2007).

An alternative approach that can be used with phenocryst-bearing MORB samples is to obtain Re-Os isotope data for the constituent phases in MORB, including sulfide, glass, spinel, olivine, clinopyroxene and spinel (Gannoun et al., 2004). If these coexisting phases are in Os isotope equilibrium, then they may yield an isochron that will give the age of crystallisation, and the initial Os isotope composition defined by the best-fit line will correspond to that of the mantle source. However, if some of the phases were assimilated from previously crystallised basalts, gabbro (from deeper in the oceanic crust), or contaminated by seawater, then they may possess different isotope information to that of the host glass or other minerals (Gannoun et al., 2004). ^{187}Re-^{187}Os data were obtained for coexisting phases from two MORB samples from the FAMOUS region on the mid-Atlantic ridge (**Figures 18** and **19**). These results illustrate the age information that can be obtained from MORB glass and coexisting phases, some of the processes involved in MORB genesis, and the ^{187}Os/^{188}Os composition of the MORB source. Sample ARP1974-011-018 (36.85°N; 33.25°W) is an olivine basalt containing olivine (Fo_{90}–Fo_{80}), plagioclase (An_{91}–An_{95}), and clinopyroxene ($Wo_{44}En_{15}Fs_5$–$Wo_{40}En_{15}Fs_9$) phenocrysts (up to 1 to 2 mm in diameter) and microphenocrysts in a hyalocrystalline matrix, and, in places, a glassy pillow rim (e.g. Le Roex et al., 1981*)*. The ^{187}Re-^{187}Os isotope data for matrix, glass, plagioclase, and olivine yield a best-fit line corresponding to an age of 565 ±336 ky and an initial ^{187}Os/^{188}Os ratio of 0.1265 ±0.0046 (**Figure 18**). The data for clinopyroxene are distinct from this best-fit line, suggesting either an older age or a different and more radiogenic source for this phase. Sample ARP1973-010-003 (36.8372°N; 33.2482°W; 2760-m water depth) is a porphyritic, picritic basalt with abundant olivine phenocrysts (Fo_{91}–Fo_{89}; up to 5 mm in diameter) set in a glassy to hyalocrystalline matrix. Cr-spinel [Cr/(Cr + Al) = 48.01] phenocrysts and sulfide [~14 weight percent (wt %) Ni] blebs (up to 1 mm in diameter) occur as inclusions in olivine or discrete crystals in the groundmass. Plagioclase (An_{80}) microlites are also common (Le Roex et al., 1981, Su and Langmuir, 2003). The ^{187}Re-^{187}Os data for olivine, plagioclase, glass, and sulfide yield a best-fit line corresponding to an age of 2.53 ±0.15 My and an initial ^{187}Os/^{188}Os ratio of 0.129 ±0.002 (**Figure 19**). Spinel, which is relatively Os-rich (Table 1 of Gannoun et al., 2004), possesses a distinct isotope composition from this best-fit line and is probably the phase responsible for the displacement of the matrix from the same line.

The simplest interpretation of these data is that the ages represent the time of igneous crystallization and the initial Os isotope composition represents that of the mantle source. The crystallization ages are, however, much older than might be expected from age-distance relations with the ridge axis that suggest ages of 5 to 10 kyr (Selo and Storzer, 1979). They are also different to the ages inferred from the Th-U-Ra isotope composition of the glass. Glass from sample

ARP1974-011-018 gives a $^{226}Ra/^{230}Th$ activity ratio close to 1, suggesting that the sample is ≤ 8 ky old, whereas the $^{230}Th/^{232}Th$ activity ratio is 1.273, suggesting that the sample is ≤ 350 ky old, consistent with previous ^{230}Th data for the same sample (Condomines et al., 1981). Arguably the ^{187}Re-^{187}Os age of 565±336 kyr is indistinguishable from the ^{230}Th age constraints. Glass from sample ARP1973-010-003 gives $^{226}Ra/^{230}Th$ ratio of 1.3, which might at first be taken to indicate that the sample is less than 8 ky old. However, the same sample has a $^{234}U/^{238}U$ ratio of 1.043, and such elevated values are often taken to indicate seawater contamination, consistent with previously published data for this sample (Condomines et al., 1981), which raises the possibility that Ra has also been affected by the same seawater contamination. It might be argued that the best-fit lines are due to contamination by radiogenic Os from seawater, rather than having some age significance. This would require that the contamination occurred during mineral crystallization and has affected phases such as olivine and plagioclase in a systematic manner; otherwise, it is difficult to imagine how different phases would align to yield the correlations observed.

Alternatively, the data may indicate that few if any of the constituent phases crystallized in their present basalt host (i.e., they are xenocrysts not phenocrysts). There is evidence for assimilation of xenocrystic phases in samples from the FAMOUS region (e.g. Clocchiati, 1977; le Roex et al., 1981; Shimizu, 1998). For example, in this sample high-Al spinel is considered to be a relict from high-pressure crystallization (Sigurdsson and Schilling, 1976), which suggests that spinel is not in Os isotopic equilibrium with the other phases. However, if most of the phases lie on the same best-fit line, then this interpretation demands that all such minerals are xenocrysts. For the picritic basalt, if eruption occurred about 5 to 10 kyr ago, then the Re–Os isotopic data indicate that original crystallization of the minerals occurred about 2.5 Myr prior to this event. In this case, the xenocrysts were assimilated from previously solidified "olivine–plagioclase" basalts, or cumulates through which the present host basalts have ascended.

Taken together, these results demonstrate that the radiogenic $^{187}Os/^{188}Os$ composition of MORB glass can be readily generated from the decay of ^{187}Re over very short timescales (that is, a few hundred thousand years or less). Nevertheless, the ages obtained for the samples from the FAMOUS region on the mid-Atlantic ridge are much older than might be expected on the basis of their distance from the ridge axis, and this can only be explained either by seawater contamination (that occurred during the crystallisation of magmatic minerals) or by the entrainment of crystals (i.e. xenocrysts) from older oceanic crust.

683 ***Extreme $^{187}Os/^{188}Os$ heterogeneity in MORB glass.*** Occasionally MORB itself shows
684 significant Os isotope and elemental heterogeneity. For example, replicate measurements of the
685 MORB sample EN026 10D-3 show significant heterogeneity, with $^{187}Os/^{188}Os$ isotope compositions
686 that range from 0.128 to > 0.15 (Day et al., 2010b). For MORB glass this is exemplified by two
687 samples from the same locality on the central Indian ridge, MD57 D9-1 and D9-6 (8.01°S; 68.07°E)
688 which show $^{187}Os/^{188}Os$ compositions ranging from 0.126 to 0.254, with covariations in Os
689 concentration (**Figure 20**). Those samples with the least radiogenic $^{187}Os/^{188}Os$ composition possess
690 unusually high Os concentrations (up to 220 pg g^{-1}). Sulfides from the same samples possess
691 $^{187}Os/^{188}Os$ between 0.126 to 0.132, and concentrations between 136 and 246 ng g^{-1}. Given the
692 presence of Os-rich sulfides in these samples, it seems most likely that this heterogeneity is due to the
693 entrainment of this phase. If the radiogenic $^{187}Os/^{188}Os$ isotope composition of the glass is simply due
694 to the radiogenic growth of ^{187}Os from the decay of ^{187}Re, since the time of igneous crystallization,
695 then the initial ratio determined from elemental or parent/daughter ratios may reflect the composition
696 of the source (cf. Day, 2013). Alternatively, if the radiogenic composition of the glass is due to
697 seawater contamination or altered oceanic crust then the initial $^{187}Os/^{188}Os$ isotope composition
698 determined from such covariations may have little relationship with that of the mantle source.
699
700 ***Seawater contamination or assimilation of altered oceanic crust.*** The age constraints from
701 spreading rates, Th-U-Ra disequilibria and ^{187}Re-^{187}Os isotope data for MORB glass and coexisting
702 minerals suggest that the radiogenic $^{187}Os/^{188}Os$ isotope compositions of MORB glass cannot be
703 solely explained by an age effect following igneous crystallisation. An alternative possibility is that
704 these radiogenic compositions could be due to seawater contamination, either occurring directly
705 during quenching of the glass on the ocean floor or through the assimilation of hydrothermally
706 altered oceanic crust in the magmatic plumbing system. Seawater possesses a very radiogenic
707 $^{187}Os/^{188}Os$ composition (~1.026-1.046) (e.g. Sharma et al., 2012, Gannoun and Burton, 2014) and a
708 $^{187}Re/^{188}Os$ ratio of ~3400, (calculated using the Os concentrations from Sharma et al., 2012,
709 Gannoun and Burton, 2014 and Re from Anbar et al., 1992, Colodner et al., 1993). In this case,
710 seawater contamination could account for both the radiogenic Os isotope composition and the
711 tendency of such samples to possess relatively low $^{187}Re/^{188}Os$.
712 Trace elements that are enriched in seawater, such as Cl or B could potentially be used as
713 indicators of seawater contamination. At first sight, however, there is no apparent covariation of
714 either B or Cl with $^{187}Os/^{188}Os$ in the MORB glasses. Rather the variations that do exist indicate that
715 many of the samples with radiogenic Os compositions possess low Cl and B concentrations,
716 inconsistent with seawater contamination (**Figure 21**). The difficulty in interpreting Cl and B is that

both are highly incompatible elements, and therefore they are strongly affected by partial melting and fractional crystallisation (Michael and Schilling, 1989; Chaussidon and Jambon, 1994; Jambon et al., 1995; Michael and Cornell, 1998). Indeed, Cl and B for the same MORB glasses show a negative covariation with MgO suggesting that fractional crystallisation has strongly influenced their abundances, thereby masking any subtle effects from seawater contamination. Like Cl and B, K also behaves as a highly incompatible element during melting and crystallisation, in this case an alternative approach is to use incompatible element ratios such as B/K or Cl/K that are not significantly fractionated during crystallisation to place some constraints on potential contamination by seawater. For example, mantle Cl/K ratios are lower than 0.08, whereas altered oceanic crust has a Cl/K ratio ~0.1, and seawater ~50 (Michael and Schilling, 1989; Jambon et al., 1995; Michael and Cornell, 1998). However, again there is no clear co-variation of Cl/K with $^{187}Os/^{188}Os$, rather the radiogenic Os values appear to possess low Cl/K (Gannoun et al., 2007).

A more robust tracer of seawater interaction is provided by $^{11}B/^{10}B$ of the MORB glasses. The upper mantle is thought to possess a $\delta^{11}B$ value (Chaussidon and Marty, 1995) of −10‰, (where $\delta^{11}B = 1000 \times[(^{11}B/^{10}B_{sample} / ^{11}B/^{10}B_{standard}) - 1]$ relative to the borate standard NBS 951 with an $^{11}B/^{10}B$ ratio of 4.04558). In contrast, for altered oceanic crust $\delta^{11}B$ ranges from +2 to +9‰, seawater has a $\delta^{11}B$ = +39.5‰ (e.g., Spivak and Edmond, 1987; Smith et al., 1995) and serpentinized oceanic mantle samples can range from +9‰ to +39‰ (Boschi et al., 2008; Vils et al., 2009; Harvey et al., 2014a). While melting and crystallisation processes are unable to significantly fractionate boron isotopes, mixing with altered oceanic crust and mantle can account for the $\delta^{11}B$ range of −7 to −1‰ observed in MORB (Chaussidon and Jambon, 1994).

The $\delta^{11}B$ values of MORB glasses for which $^{187}Os/^{188}Os$ data are available range from −9 to +2‰, and those samples with high $\delta^{11}B$ values also possess radiogenic $^{187}Os/^{188}Os$ compositions (**Figure 22**). The B concentration of seawater is ~4.6 μg g^{-1} which is some 5–10 times higher than that of unaltered MORB (<1 μg g^{-1}), whereas the Os concentration in seawater of 10^{-2} pg g^{-1} is some 3 orders of magnitude less than that of average MORB. Direct mixing of seawater would be dominated by B at the low mixing proportions suggested in **Figure 22** (that is, a horizontal vector in Os versus $\delta^{11}B$) indicating that the radiogenic $^{187}Os/^{188}Os$ and high $\delta^{11}B$ values cannot be easily explained by direct contamination from seawater. Conversely, contamination from Fe-Mn crust with a seawater Os isotope composition would produce far greater shifts in $^{187}Os/^{188}Os$ than B. Rather, the co-variations are entirely consistent with the assimilation of between 5-10% of altered oceanic crust with a variable $^{187}Os/^{188}Os$ composition.

It might be argued that the relatively heavy $\delta^{11}B$ values (> −5‰), and the radiogenic $^{187}Os/^{188}Os$ could be due to the presence of recycled oceanic crust (present as pyroxenite) in the

MORB mantle source. Recycled oceanic crust can lose substantial amounts of Re during subduction (~50% or more, Becker, 2000; Dale et al., 2007) but Re/Os ratios are still sufficiently elevated to produce radiogenic $^{187}Os/^{188}Os$ values with time. However, recent studies suggest that during dehydration of the subducting slab, B is preferentially partitioned into the released fluids, leaving a depleted residue (Moran et al., 1992; Bebout et al., 1993; Peacock and Hervig, 1999; Nakano and Nakamura, 2001; Harvey et al., 2014b). Furthermore, boron isotope fractionation occurs during such dehydration and the residue becomes increasingly enriched in the light B isotope (^{10}B) generating light $\delta^{11}B$ values (You et al., 1996; Ishikawa et al., 2001; Leeman et al., 2004), rather than the heavy values required to generate the ranges observed in MORB.

Notwithstanding analytical difficulties, the Os isotope and elemental variations in MORB glass, the mismatch in age constraints and measured $^{187}Os/^{188}Os$ compositions, and the covariations with B isotopes suggest that assimilation of seawater-altered oceanic crust is likely to be the dominant process responsible for the radiogenic Os isotope signal seen in many of the MORB glasses studied thus far.

SULFIDES IN MID-OCEAN RIDGE BASALTS

Petrology and chemistry

Sulfide is a ubiquitous phase in MORB glass, indicating that these melts were sulfur saturated (Wallace and Carmichael, 1992). Because decompression will drive the melt away from sulfide saturation (e.g. Mavrogenes and O'Neill, 1999) it might be expected that most MORB would be undersaturated when transported to lower pressures during eruption. The presence of sulfide globules in early crystallising phases, however, clearly indicates that MORB are sulfur saturated during the initial stages of magmatic evolution (Mathez and Yeats, 1976; Patten et al., 2012; Yang et al., 2014) and, as previously suggested for MORB, this sulfur saturation is most likely to result from fractional crystallisation itself. In addition, MORB contain more sulfur than subaerially erupted basalt, because degassing is impaired by the overlying pressure of seawater.

Sulfides occur as spherules embedded in the walls of large vesicules (Moore and Calk, 1971; Moore and Schilling, 1973), as small irregular grains in microcrystalline aggregates of plagioclase and olivine (Mathez and Yeats, 1976) and as well-developed spherical globules, in glass or in phenocrysts (Mathez and Yeats, 1976; Czamanske and Moore, 1977; Patten et al., 2012; Roy-Barman et al., 1998) (**Figures 23a and 23b**). The globules, which range from 5 to 600 μm in diameter, have

784 different textures that can be divided into three groups (Moore and Calk, 1971; Mathez, 1976;
785 Mathez and Yeats, 1976; Czamanske and Moore, 1977; Peach et al., 1990; Roy-Barman et al., 1998;
786 Patten et al., 2012; 2013). The first, comprise a fine grained micrometric intergrowth of Fe-Ni-rich
787 and Cu-Fe-rich sulfide phases that represent quenched monosulfide solid solution (MSS) and
788 intermediate solid solution (ISS). The second, comprise globules of coarser grained intergrowth of
789 MSS and ISS with pentlandite and oxide (Mathez, 1976; Czamanske and Moore, 1977; Patten et al.,
790 2012) and the third group comprise zoned globules that consist of two massive and distinct grains of
791 MSS and ISS, first identified recently by Patten et al. (2012).
792 Pentlandite and oxide occur to a lesser extent in all types of textures. Sulfide droplets with
793 different sizes and textures may coexist in the same MORB sample. Patten et al. (2012) have shown
794 that sulfide droplets exhibiting all three textures may be present in the same sample separated by only
795 few millimetres, (cf. Czamanske and Moore, 1977). Patten et al. (2012) also observed a relationship
796 between the size of the droplets and their textures. Below 30 μm, over 90% of the droplets have a
797 fine grained texture and between 30 and 50 μm, 60% of the sulfide droplets are coarse-grained. In
798 contrast, above 50 μm all the droplets are zoned.
799 Sulfide globules usually comprise fine-grained exsolution of Fe-Ni and Cu-rich sulfide
800 phases. When the bulk compositions of sulfide are calculated to 100%, in order to estimate liquidus
801 temperature of the MSS using the Ebel and Naldrett (1997) approach for O-free systems, they
802 showed low variability in S content, moderate variability in Fe contents and high variability in Cu
803 and Ni contents (Patten et al., 2012). **Figure 24** shows the bulk composition of sulfide globules in the
804 Fe-Ni-Cu system. The limited field of such bulk compositions confirms the agreement between
805 different studies (Czamanske and Moore, 1977; Roy-Barman et al., 1998; Patten et al., 2012). The
806 dashed lines in **Figure 24** indicate the sulfide liquid at crystallisation temperatures of the MSS at
807 1100, 1050 and 1000°C from Ebel and Naldrett (1997). The liquidus temperature of the sulfide
808 globules from MORB determined in this way, range from slightly above 1100°C to 1030°C where
809 globules are randomly distributed over this temperature interval irrespective of their size or textures
810 (cf. Patten et al., 2012).
811 Pentlandite occurs to a lesser extent than MSS and ISS in all textures of sulfides. Oxide also
812 occurs either inside MSS, inside ISS or at their interface, comprising up to 7% of some sulfide
813 globules. Oxides are best developed in zoned droplets and electron probe analyses reveal that they
814 are Ti-free magnetite (Patten et al., 2012) in agreement with Czamanske and Moore (1977), who
815 suggested that a few percent of magnetite is common in sulfide globules in MORB.
816
817

^{187}Re-^{187}Os behaviour in MORB sulfide

If present, sulfide dominates the Os budget in MORB, where sulfide-silicate partition coefficients for Os in basaltic system are in the range ~10^4–10^6 (Roy-Barman et al., 1998; Gannoun et al., 2004, 2007). In contrast, Re while still being highly compatible in sulfide, has a partition coefficient at least two orders of magnitude lower than that of Os (~10^1-10^3; Roy-Barman et al., 1998; Gannoun et al., 2004, 2007) similar to that of Cu (Peach et al., 1990; Gaetani and Grove, 1997). As a result of the difference in partitioning of Re and Os, MORB sulfides have high Os concentrations (tens to a few hundreds of ng g^{-1}) and a low Re/Os relative to their coexisting glass (some 3 orders of magnitude lower). Consequently, sulfide is much less susceptible to the effects of seawater assimilation, or radiogenic in-growth, than coexisting silicate minerals or glass (Roy-Barman et al., 1998; Gannoun et al., 2004, 2007).

For those sulfides for which Os isotope and elemental abundances have been measured thus far, there is a clear covariation between ^{187}Os/^{188}Os and the Os concentration (**Figure 25**). Where those sulfides with low Os concentrations (i.e ≤ 10 ng g^{-1}) possess ^{187}Os/^{188}Os compositions > 0.15, and those with high Os concentrations (i.e. ≥ 100 ng g^{-1}) possess ^{187}Os/^{188}Os compositions around ~0.13 or less. At first sight, this relationship might be taken to indicate that the sulfide globules, like their host glass have been systematically affected by contamination with material derived from altered oceanic crust. There is no clear relationship between the Os concentration of the sulfide and that of the host glass. However, with one exception, sulfides possess ^{187}Os/^{188}Os values that are less radiogenic than their glass host, where in general, the more radiogenic the host glass the greater the difference in ^{187}Os/^{188}Os with coexisting sulfide (**Figure 26**). It is difficult to explain such a difference between sulfide and glass simply by radiogenic decay of ^{187}Re, rather it suggests that the ^{187}Os/^{188}Os composition of the glass has been more significantly affected by the assimilation of older oceanic crustal material than the coexisting sulfide.

If MORB sulfides preserve ^{187}Os/^{188}Os compositions that are systematically less radiogenic than their host silicate glass then this has some important implications for the timing of contamination relative to crystallisation. If contamination of the silicate melt occurred before sulfide precipitation then the sulfide should possess an Os isotope composition that is indistinguishable from that of the melt. Therefore, the contrasting Os isotope composition of the glass and sulfide suggests that the silicate melt experienced contamination after the segregation of sulfide in the melt.

At the high temperatures of MORB eruption (~1200°C) most sulfides will be present as liquid globules rather than as a solid phase, and diffusional equilibration between silicate and sulfide liquids is likely to be rapid. The time in which a sulfide globule will equilibrate its Os isotope composition

852 with a melt can be assessed using simple diffusion calculations. Using an implicit finite difference
853 model (Crank, 1975) and assuming a sulfide globule radius of 250 μm and a silicate-sulfide melt
854 diffusion coefficient of 10^{-8} cm^2 s^{-1} the sulfide will equilibrate with the melt in ~12 h (Gannoun et
855 al., 2007). This is a relatively conservative estimate because cation diffusion in most basaltic melts is
856 10^{-5} to 10^{-6} cm^2 s^{-1} (Watson and Baker, 1975), whereas diffusion rates in pyrrhotite are likely to be
857 faster than 10^{-9} cm^2 s^{-1} at magmatic temperatures (Brenan et al., 2000). Therefore, under normal
858 circumstances, complete equilibration between sulfide and glass would be expected, with both
859 possessing an indistinguishable $^{187}Os/^{188}Os$ composition. However, because of the large
860 concentration difference between the sulfide and the silicate liquid, a large amount of melt has to
861 exchange with a small sulfide bleb before the sulfide reaches Os isotope equilibrium with the glass. It
862 is possible to calculate the volume (and mass) of melt that is needed to equilibrate the sulfide using
863 simple mass balance equations and the concentration and isotopic data for the glass and sulfides
864 obtained here. Assuming initial $^{187}Os/^{188}Os$ for the sulfides of 0.125 and a sulfide globule radius of
865 250 μm, then sulfides will have only equilibrated with <0.5 cm^3 of melt (or less if the sulfide blebs
866 were smaller). This suggests that the sulfides have only exchanged with the immediate melt
867 surrounding the sulfide. Furthermore, a sulfide that contains >200 ng g^{-1} Os would have to exchange
868 with <50 cm^3 of melt in order to completely equilibrate with that melt. Thus, the absence of any Os
869 isotope or elemental covariation between the sulfides and their host glass suggests that Os isotope
870 exchange is likely to have been limited. These observations are consistent with Pd elemental data for
871 MORB from the SouthWest Indian Ridge taken to suggest that segregated sulfides were poorly
872 equilibrated with their host silicate magmas (Yang et al., 2013).
873 Nevertheless, many, if not all of the sulfides analysed thus far are likely to have been
874 modified by contamination, depending on their Os concentration. The sulfides with $^{187}Os/^{188}Os$
875 compositions > 0.13 have most likely been significantly modified through partial exchange with the
876 contaminated silicate melt. Although those sulfides with a high Os concentration (>20 ng g^{-1}) may
877 have also been affected by such exchange they do, however, yield the least radiogenic compositions
878 yet observed in normal MORB samples.
879
880 **The $^{187}Os/^{188}Os$ isotope composition of the MORB mantle source**
881
882 The MORB glass measured thus far preserves variations in $^{187}Os/^{188}Os$ extending from
883 unradiogenic values as low as 0.125, comparable to estimates for the primitive upper mantle, to
884 radiogenic values up to 0.25. There are no clear covariations with lithophile element isotopes, such as
885 Sr or Nd, as might be expected from Os isotopic heterogeneity inherited for a mantle source. Rather,

886 the radiogenic Os isotope compositions show a relationship with B isotopes that is most simply
887 attributed to seawater-derived contamination that occurs during magma ascent. In this case, to a
888 greater or lesser extent all MORB glass has been affected by seawater contamination. Individual
889 sulfide grains appear to provide a much more robust record of the primary Os isotope signature (Roy-
890 Barman et al., 1998; Gannoun et al., 2004; 2007, Burton et al., 2015) although even this phase
891 appears to be susceptible to seawater-derived contamination. In this case it is difficult to assess the
892 extent to which any radiogenic signal, preserved in either glass or sulfide, is due to an age effect
893 caused by ^{187}Re decay following igneous crystallisation, or the presence of Re-enriched material,
894 such as recycled oceanic crust in the MORB source.
895 Assuming that the Os isotope information preserved by high-Os sulfide grains has been
896 minimally affected by seawater contamination then they potentially provide some unique constraints
897 on the nature of the MORB source. A fundamental assumption underlying the use of radiogenic
898 isotopes, such as Sr, Nd and Os, in mantle derived basalts is that they are in equilibrium with their
899 mantle source (e.g., Hofmann and Hart, 1978). Abyssal peridotites are ultramafic rocks thought to
900 represent the residue of the melting responsible for generating MORB (Dick et al., 1984; Johnson and
901 Dick, 1992; Brenan et al., 2000). Consequently during melting and basalt genesis the composition of
902 long-lived isotopes of heavy elements in both MORB and residual abyssal peridotites should be the
903 same. The average ^{187}Os/^{188}Os composition of abyssal peridotites is 0.127 ±0.015 (n = 129) (**Figure**
904 **27**), however, like MORB, abyssal peridotites are also susceptible to seawater alteration during their
905 exhumation on the sea floor, which may shift the composition towards radiogenic values. In this case
906 individual abyssal peridotite sulfides are likely to yield a more reliable indication of their primary Os
907 isotope composition, and these yield an average ^{187}Os/^{188}Os composition of 0.125±0.021 (n = 63).
908 The best estimate for the ^{187}Os/^{188}Os composition of the primitive upper mantle, that is a theoretical
909 mantle composition with high Al_2O_3 that is considered to have experienced no depletion through
910 melting, is 0.1296±0.009 (2σ; n = 117) (Meisel et al., 2001). By comparison, the high-Os (>20 ng g^{-1})
911 sulfides from MORB yield an average composition of 0.129±0.005 (n = 31) with values as low as
912 0.1236 (**Figure 27**). Therefore, these high-Os sulfides show no evidence for significant Re
913 enrichment in the MORB source that might accompany the presence of recycled oceanic crust.
914 Rather they indicate that the upper mantle source of these samples has experienced a long-term
915 depletion of Re, similar to that observed in abyssal peridotites, and consistent with the incompatible
916 nature of this element during mantle melting.
917
918
919

LOWER OCEANIC CRUST

The oceanic crust comprises some 1-1.5 km of basalt and dolerite that is underlain by 4-5 km of gabbro. Therefore, mid-ocean ridge basalts are thought to be evolved lavas formed by fractional crystallisation in the lower oceanic crust, that itself comprises plutonic rocks and cumulates, from primitive magmas. Given that Re is moderately incompatible while Os is compatible during mantle melting, one might expect that gabbros in the lower crust would have higher Os and lower Re concentration and accordingly low Re/Os ratios than evolved MORB assuming that the phases that control solid/liquid partitioning of Re and Os during crystallization are similar to those involved during partial melting. Gabbroic lower oceanic crust should therefore dominate the PGE budget of the oceanic crust as whole.

However, the first reported siderophile element data for gabbros from Ocean Drilling Program (ODP) Site 735 (Blusztajn et al., 2000) yielded rather low PGE concentrations (**Figure 28**), even lower than average MORB (Bezos et al., 2005; Gannoun et al., 2007) pointing to their evolved compositions. Indeed, Dick et al. (2000) and Hart et al. (1999) noted that the average composition of gabbro from ODP Site 735B is closer to that of average MORB (on the basis of major and trace element systematics). Consequently, the gabbro recovered at this site cannot be considered as the primitive complement to typical evolved MORB. More recently, Peucker-Ehrenbrink et al. (2012) have argued that all prior geochemical work on in situ upper oceanic crust such as DSDP-ODP sites 417, 418 and 504 (Bach et al., 2003; Peucker-Ehrenbrink et al., 2003), and 801 (Reisberg et al., 2008), and evolved gabbros at ODP 735 (Hart et al., 1999; Blusztajn et al., 2000), and site 894 (Lecuyer and Reynard, 1996) failed to reproduce the true average for the complementary crustal reservoir to MORB lavas and therefore needs to be complemented with more detailed geochemical and petrologic studies of primitive gabbroic material from the lower crust.

In order to more accurately assess the global HSE chemistry of the whole oceanic crust Peucker-Ehrenbrink et al. (2012) obtained data for an oceanic crust section from the Oman ophiolite that includes the crust-mantle transition. The mean weighted composition of the 4680 m Oman section yielded Re 427 pg/g, Os 55pg/g, Ir 182 pg/g, Pd 2846 pg/g, Pt 4151 pg/g and initial $^{187}Os/^{188}Os$ of 0.142, indicating higher PGE concentration and lower Re concentration than all data previously reported on partial sections of ocean crust that lack cumulate lower crust. Assuming that these data are truly representative of the lower oceanic crust then they suggest that these rocks are the main

PGE reservoir in the oceanic crust as a whole and that the average Re in these gabbros is much lower than in MORB lavas (Re ~1070 pg/g; Hauri and Hart, 1997; Gannoun et al., 2007; This chapter). The Oman gabbros are characterised by a distinct subchondritic average Os/Ir ratio of ~ 0.3 which is significantly different from the chondritic ratio or the primitive upper mantle value of ~ 1.1 (Becker et al., 2006; Lodders et al., 2009). This difference is surprising because Ir is generally viewed as a geochemical analogue of Os during magmatic processes (Becker et al., 2006; Puchtel and Humayun, 2000). The Os/Ir fractionation observed in the Oman gabbros, while within the range observed in MORB (0.2-1.4 average 0.6), is the opposite of that observed in the upper crustal part from DSDP 504B (average Os/Ir of ~2.4; Peucker-Ehrenbrink et al., 2003). However the Os/Ir of abyssal peridotites in general and in the harzburgitic mantle section of Oman in particular, remains chondritic (Hanghoj et al., 2010). If such harzburgites are representative of the mantle source then the subchondritic Os/Ir ratio in Oman gabbros cannot reflect a source signature. Hanghoj et al. (2010) report both superchondritic and subchondritic Os/Ir ratios in Oman dunites (0.5 - 8.3). As Os and Ir alloys included in chromites have been observed in Oman dunites (Ahmed and Arai, 2002; Ahmed et al., 2006), Peucker-Ehrenbrink et al. (2012) suggested that such a phase may be responsible for the fractionation of Os from Ir during melting, melt extraction or crystal fractionation.

Estimating the HSE inventory of the whole ocean crust remains challenging because of the discontinuous nature of the field sampling and the question of how representative are the samples that have been analysed thus far. Peucker-Ehrenbrink et al. (2012) used data from Site 504B for the upper oceanic crust (Peucker-Ehrenbrink et al., 2003) combined that for the Oman ophiolite for the lower oceanic crust (Peucker-Ehrenbrink et al., 2012). The weighted chemical and isotope characteristics of this "composite" oceanic crust (**Figure 28**), corrected for Re decay since emplacement, are 736 pg/g Re, 45 pg/g Os, 133 pg/g Ir, 2122 pg/g Pd, 2072 pg/g Pt, $^{187}Re/^{188}Os$: 80 and $^{187}Os/^{188}Os$: 0.144. Such crust is more enriched in Re and less depleted in PGE than observed in average gabbros from ODP Hole 735D. Therefore, unless fundamentally altered during subduction, subducted oceanic crust will evolve to form a PGE-depleted, Re-rich mantle component that over time will evolve to radiogenic $^{187}Os/^{188}Os$ isotope compositions. However, the projected ingrowth of radiogenic $^{187}Os/^{188}Os$ may be inhibited by the loss of Re from the basaltic upper part of the crust during eclogite-facies metamorphism (Becker et al., 2000; Dale et al., 2007) but not the gabbroic lower part of the crust (Dale et al., 2007).

Assimilation of gabbroic lower crust

Recent work has shown that the crystallization of gabbros, troctolites and other plutonic rocks of the lower oceanic crust may be protracted, and that these rocks sometimes possess ages that are several million years older than predicted from the magnetic ages of the overlying basaltic crust (e.g. Schwartz et al., 2005; Grimes et al., 2008). This extended timescale for the growth of the lower oceanic crust has been attributed to the crystallisation of gabbros in the mantle followed by uplift to lower crustal depths (Schwartz et al., 2005; Grimes et al., 2008). Such uplift may relate to unroofing by low-angle detachment faults, typical of asymmetrical spreading ridge segments (e.g. Lissenburg et al., 2009).

Over a timescale of several million years gabbros and troctolites, and their constituent phases, in the lower oceanic crust will rapidly evolve to radiogenic Os isotope compositions. This raises the possibility that younger melts passing through older lower crust may acquire a radiogenic Os isotope composition, either by remelting and assimilation of older material or through the physical entrainment of older crystals. Primitive xenocrysts are commonly found in MORB (e.g. Dungan and Rhodes, 1978; Coogan, 2014) with evidence for mixing shortly before eruption (e.g. Moore et al., 2014). Indeed, as discussed previously, the old ages of phenocryst phases in basalts that are thought to have been erupted just 5 to 10 ka (**Figures 18 and 19**), may indicate that these are rather xenocrysts physically entrained from previously solidified "olivine–plagioclase" bearing plutonic rocks through which the present host basalts have ascended. In this case, it is possible that some MORB glass may acquire a radiogenic Os isotope composition without interaction with seawater altered oceanic crust, or the presence of a radiogenic mantle source. For MORB glass such a signature might be distinguished by the absence of any covariation with Cl abundance or B isotopes.

HSE ABUNDANCES AND RE-OS ISOTOPE SYSTEMATICS OF INTRAPLATE VOLCANISM

The HSE and Re-Os systematics of intraplate volcanism were reviewed recently by Day (2013). The purpose of this section is to briefly summarize the likely origins of intraplate volcanism, based specifically upon HSE abundance and Re-Os isotope constraints, and to provide a brief update of developments in the field since 2013. In particular, and mostly as a function of the difficulties associated with producing precise $^{186}Os/^{188}Os$ data (e.g., Chatterjee and Lassiter, 2015), there has been no significant advances in the application of the Pt-Os isotope system to intraplate volcanism since Day (2013); the interested reader is referred to this earlier review article for an up to date appraisal of Pt-Os systematics.

The origin of intraplate volcanism has been variously attributed to (i) mantle plumes (Wilson, 1963; Morgan, 1971), (ii) plumes which are not particularly "hot" (e.g., Falloon et al., 2007; Putirka et al., 2007), (iii) stress-driven processes (Anguita and Hernan, 1975) or (iv) chemical heterogeneities preserved in the upper mantle (e.g., Courtillot et al., 2003; Arndt, 2012). The occurrence of intraplate volcanism does not appear to be related to proximity to plate boundaries (cf. Hawaii; Wilson, 1963 versus the Canary Islands; Morgan, 1971) and does not occur systematically on either the continents or within oceanic basins, even spanning continental–oceanic margins (i.e., the Cameroon Line; Rehkämper et al., 1997; Gannoun et al., 2015a). Intraplate volcanism can be associated with convergent (e.g. Samoa; Wright and White, 1987) and divergent (e.g. Iceland; Morgan, 1971) tectonic settings.

In general, intraplate volcanism is controlled by anomalous thermo-chemical and/or tectonic conditions capable of producing large volumes of extrusive products. Many investigations into the HSE of intraplate volcanic rocks have predominantly featured primitive, high-MgO rocks, e.g., komatiites and picrites (e.g. Connolly et al., 2011; Ireland et al., 2009, respectively), because of the compatibility of the HSE during fractional crystallisation, and the sensitivity of $^{187}Os/^{188}Os$ to crustal assimilation processes in more evolved magmas (e.g., Chu et al., 2013). However, evolved potassic and sodic mafic-alkaline volcanic rocks and phonolites, trachytes and rhyolites, which may have experienced extensive fractional crystallisation, are also observed and have recently been investigated for their HSE abundance and Re-Os isotope systematics (e.g., Chu et al., 2013; Li et al., 2014; Wang et al., 2014). For this reason, we adopt the same definition used by Day (2013) for intraplate 'hotspot' volcanism, i.e., *"Volcanic rocks that are unassociated with conventional plate tectonic boundary magmatic processes and that may require anomalous thermo-chemical and/or tectonic conditions to induce small- to large-scale melting"*.

Mantle melting processes

The composition of the mantle source may be expressed by a variety of end-member compositions based upon its history of prior melt depletion i.e., depleted versus fertile peridotite (e.g., Niu, 2004; Godard et al., 2008) and overall lithology, i.e., peridotite versus pyroxenite (Hirschmann and Stolper 1996; Yaxley, 2000; Kogiso et al., 2004; Lambart et al., 2012, 2013). In addition, fertile heterogeneities in the mantle nucleate magmatic channels that focus melts up to the surface and hinder their re-equilibration with ambient peridotite (Katz and Weatherley, 2012). Therefore, the chemical signature of hybrid melts of peridotite and pyroxenite can be retained in the composition of mantle-derived basalts. Day (2013) discussed the significance of the 'shape' that a melting regime can have, discussing two end-member geometries; (i) batch melting of a columnar (cylindrical) region (e.g., Rehkämper et al., 1999), and (ii) regions of adiabatic melting in triangular or corner-flow melting regime (e.g., Plank and Langmuir, 1992). Each of these melting regimes aggregate melt pooled from over the melting volume, accounting for the overall composition of the magma generated.

Briefly, model (i) is most consistent with an upwelling 'mantle plume-like' melting regime. It assumes uniform melting throughout the source region and that HSE-rich sulfide is completely exhausted at 20–25% partial melting. This cylindrical melting model reproduces the HSE abundances of low-degree alkali basalts (e.g., Canary Island lavas; e.g., Day et al., 2009) and high-degree partial melts (e.g., komatiites; e.g., Rehkämper et al., 1999), but the HSE signature of some tholeiitic magmas generated by low degrees of partial melting are not predicted using this cylindrical melt volume (e.g., Momme et al., 2003, 2006). The triangular melting regime (model ii) assumes near-fractional melting in 1% increments with decreasing pressure, i.e., through adiabatic ascent (e.g. Rehkämper et al., 1999; Momme et al., 2003). In this melting regime, S-saturated low-degree partial melts with low HSE-concentrations mix with shallower, higher-degree (and potentially S-undersaturated) partial melt. Refinements to the two general classes of models described above have allowed distinct melt regimes in some continental flood basalt (CFB) provinces to be determined (Momme et al., 2006), whereas in the Icelandic rift zones depleted versus enriched mantle components have also been identified (Momme et al., 2003). Moreover, the use of these models has permitted the detection of a pyroxenitic component in primitive lavas from the Canary Islands (Day et al., 2009), and a similar component has been implicated in the generation of some Hawaiian lavas (Lassiter et al., 2000; Sobolev et al., 2007).

Source compositional estimates become increasingly complicated when the necessity arises to account for the contributions from mixtures of source lithologies (e.g., peridotite and recycled sediment or basalt) and the complex interplay of the HSE that each of these source reservoirs may contribute to a pooled melt (e.g., Hirschmann and Stolper, 1996).

Osmium isotopes as tracers of hotspot sources

Ocean island basalts. Many intraplate basalts retain HSE signatures of their mantle source region and osmium isotopes, when compared to lithophile element-based radiogenic isotopes, can offer a unique perspective on the petrogenesis of intraplate lavas. The large Re/Os fractionations generated during crust-mantle partitioning make it possible to model $^{187}Os/^{188}Os$ variations in OIB in the context of variably aged recycled crust and lithosphere (e.g., Hauri and Hart, 1993; Marcantonio et al., 1995; Widom et al., 1999; Day et al., 2009; Day, 2013). For example, ancient oceanic mantle lithosphere or SCLM has been implicated in the genesis of lavas from the Azores, Iceland and Jan Mayen (Skovgaard et al., 2001; Schaefer et al., 2002; Debaille et al., 2009), where measured unradiogenic $^{187}Os/^{188}Os$ values cannot be explained by melting exclusively of modern oceanic lithospheric material and thus require a mantle source or sources that have evolved in a low Re/Os environment (cf. unradiogenic abyssal peridotites reported by Snow and Reisberg, 1995; Alard et al., 2005; Harvey et al., 2006; Liu et al., 2008; Warren and Shirey, 2012; Lassiter et al., 2014). Intraplate basalts and specifically ocean island basalts (OIB), are generated from mantle sources with distinct long-term time-integrated parent-daughter fractionations of Sr-Nd-Pb-Hf isotopes (e.g., Zindler and Hart, 1986; Hofmann, 2003; White, 2010), and also preserve a large range of $^{187}Os/^{188}Os$ compositions (e.g., Pegram and Allègre, 1992; Hauri and Hart, 1993; Reisberg et al., 1993; Marcantonio et al., 1995; Roy-Barman and Allègre, 1995; Widom and Shirey, 1996; Lassiter and Hauri, 1998; Brandon et al., 1999, 2007; Widom et al., 1999; Schiano et al., 2001; Eisele et al., 2002; Schaefer et al., 2002; Lassiter et al., 2003; Workman et al., 2004; Escrig et al., 2005b; Class et al., 2009; Day et al., 2009, 2010b; Debaille et al., 2009; Ireland et al., 2009; Jackson and Shirey, 2011). These signatures are only retained in instances where the melt produced at depth, albeit with ancient time-integrated compositions, and reflecting the recycling of material back into the convecting mantle (e.g., Zindler and Hart, 1986), are not significantly contaminated or overprinted though interaction with the lithosphere through which these basalts necessarily transit en route to the surface. For example, in a recent study of the Louisville Seamount Chain, Tejada et al. (2015) demonstrated that OIB erupted along this chain of oceanic volcanoes reach the surface with negligible chemical interaction with the lithospheric mantle that underlies the South Pacific. Moreover, unlike the

1119 Hawaiian-Emperor Seamount chain, whose compositions are readily explained by heterogeneous
1120 mantle sources (see following section), Os isotope signatures of these basalts have a very narrow
1121 range, consistent with their derivation from a primitive mantle source (cf. Meisel et al., 2001; Becker
1122 et al., 2006). Age corrected $^{187}Os/^{188}Os$ of the Louisville Seamount basalts range from 0.1245–
1123 0.1314, similar to other Pacific OIB, such as Rarotonga (0.125–0.129, Hauri and Hart (1993); 0.124–
1124 0.139, Hanyu et al. (2011) and some Samoan basalts (0.1230–0.1313, Hauri and Hart (1993);
1125 Jackson and Shirey (2011)). The age corrected $^{187}Os/^{188}Os$ for two aggregates of olivine phenocrysts
1126 separated from Louisville Seamount basalts (0.1272 and 0.1271–0.1275) agree with whole rocks
1127 from the same seamount (0.1253–0.1274; Tejada et al., 2015), supporting the hypothesis that early-
1128 crystallising olivine can preserve the pristine magmatic Os isotopic compositions of their source (cf.
1129 Jackson and Shirey, 2011; Hanyu et al., 2011) (**Figure 29**).
1130 Studies of HSE abundance complement and extend the knowledge of intraplate magma
1131 petrogenesis gleaned from Os isotope systematics. Only lavas with high-MgO contents and >0.05 ng
1132 g^{-1} Os should be considered as potentially being representative of the true HSE characteristics of
1133 intraplate magma and its mantle source. Such restrictions on the analysis of intraplate magmas mean
1134 that there is still a dearth of high quality HSE data on OIB. Much of what has been elucidated from
1135 HSE abundances in OIB comes from studies of Hawaiian lavas (Bennett et al., 2000; Crocket, 2002;
1136 Jamais et al., 2008; Ireland et al., 2009; Pitcher et al., 2009). These studies support the hypothesis
1137 that, in general, high-MgO lavas preserve early-formed Os-rich (+ HSE) phases that become
1138 incorporated in early forming phenocrysts such as olivine (e.g., Brandon et al., 1999; Ireland et al.,
1139 2009). Removing the effects of mineral fractionation on HSE abundances allowed Day (2013) to
1140 directly compare the absolute and relative HSE abundances and calculated Re/Os of parent melts in
1141 addition to $^{187}Os/^{188}Os$, of Hawaiian, Canary Island and Samoan lavas. Combined with the HIMU
1142 type $^{206}Pb/^{204}Pb$ compositions of Canary Island lavas, this led to the conclusion that, in contrast to
1143 Hawaiian and Samoan OIB, and komatiites, whose compositions suggest a relatively high proportion
1144 of peridotite in their parental melts, lavas from the Canary Islands, and specifically El Hierro and La
1145 Palma, contain recycled oceanic crust in their mantle source. Osmium isotope studies of HIMU-type
1146 OIB support and enhance Sr-Nd-Pb isotope and trace element arguments for a recycled oceanic
1147 lithosphere component in their mantle source (Hauri and Hart, 1993; Marcantonio et al., 1995;
1148 Widom et al., 1999; Eisele et al., 2002; Day et al., 2010b). The observed range of $^{187}Os/^{188}Os$ and
1149 $^{206}Pb/^{204}Pb$ of HIMU basalts (e.g., Becker et al., 2000; Dale et al., 2009a; van Acken et al., 2010)
1150 could be produced by direct melting (~50% to 90%) of recycled oceanic crust, but would result in
1151 melts that contain too much silica and too little magnesium (e.g., Yaxley and Green, 1998). Although
1152 field evidence suggests that pyroxenites account for ≤ 10% of mantle lithologies (e.g., Reisberg et al.,

1153 1991; Pearson et al., 1991), they melt disproportionately to peridotite under any P-T conditions (only
1154 1 to 2% pyroxenite may generate up to 50% of the melt at low degrees of partial melting), thus
1155 producing silica-undersaturated, iron-rich melts with high MgO (e.g., Hirschmann et al., 2003). This
1156 means that direct melting of recycled oceanic crust and lithosphere is not necessary to produce HIMU
1157 OIB.
1158 Spinel websterites have been suggested to be geochemically analogous to pyroxenites, at least
1159 in terms of their HSE systematics (Marchesi et al., 2014). The Re-Os fractionation generated as a
1160 result of peridotite versus pyroxenite (and/or spinel websterites) has been suggested as a likely
1161 contributor to the observed ^{186}Os-^{187}Os-rich compositions of some plume basalts (Luguet et al., 2008)
1162 previously attributed to interaction between the mantle and outer core (e.g., Brandon et al. 1998,
1163 2003; Puchtel et al., 2005; Walker et al., 1997). Subsequent studies (e.g., Baker and Jensen, 2004;
1164 Luguet et al., 2008; Scherstén et al., 2004) and, more recently, Marchesi et al. (2014) suggest that
1165 such enrichments could be attributed to processes requiring no input from the outer core. However,
1166 these models may require unreasonably high contributions from pyroxenitic / spinel websteritic
1167 lithologies in the mantle (as high as 90% in some cases, but potentially as low as 50%; van Acken et
1168 al., 2010; Marchesi et al., 2014), as a result of the comparatively low Os concentrations in pyroxene-
1169 rich lithologies.
1170 The enriched mantle (EM) signatures of other OIB have been attributed to the addition of
1171 subducted sediment or metasomatised lithosphere into their mantle sources (e.g., Workman et al.,
1172 2004). EM-type OIB span a range of compositions in Sr-Nd-Pb isotope space, varying from EMI
1173 (e.g., Pitcairn; Woodhead and McCulloch, 1998; and the Comores; Class et al., 2009), which exhibit
1174 a wide range of Os and Pb isotope compositions, but more restricted Sr isotope compositions, to
1175 EMII OIB (e.g., Samoa; Wright and White, 1987; Workman et al., 2004; Jackson and Shirey, 2011).
1176 These compositions are consistent with sediment, recycled oceanic crust and peridotite producing
1177 EMI-flavoured compositions with more radiogenic $^{187}Os/^{188}Os$ (Roy-Barman and Allègre, 1995;
1178 Class et al., 2009), while subducted sediment mixed with ambient peridotite produces enriched EMII
1179 compositions with lower $^{187}Os/^{188}Os$. Therefore, lithological variations in the mantle source play a
1180 key role in the composition of OIB, and HSE abundances combined with Re-Os systematics are
1181 critical in the identification of the various components mixed with variably depleted asthenospheric
1182 mantle.
1183
1184 ***Continental intraplate volcanism.*** The heterogeneous mantle sources described above are not
1185 restricted to OIB, or oceanic settings in general. These modifiers of magma composition also
1186 influence intraplate volcanism associated with continental regions. The main differences between

oceanic and continentally erupted intraplate magmas is the greater potential for the latter to be influenced by interaction with the thicker and older overlying sub-continental lithospheric mantle (SCLM) and continental crust, in addition to the potential compositional heterogeneities within the asthenospheric mantle. Recently, Sun et al. (2014) reported Re-Os systematics of ultrapotassic (>7 wt. % K_2O) basalts from the Xiaogulihe area of western Heilongjiang Province, NE China. The relatively unradiogenic Os isotope ratios ($^{187}Os/^{188}Os$ = 0.119 to 0.143) contrasted with the similarly potassic basalts from NE China reported by Chu et al. (2013) ($^{187}Os/^{188}Os$ = 0.13–0.17) and were attributed by Sun et al. (2014) to a dominantly peridotitic source, but one that required an unusually high K_2O content. In this particular setting, phlogopite-bearing garnet peridotite hosted within the lower part of the SCLM was implicated; its derivation being potassium-rich silicate melts produced by the subduction of ancient continent-derived sediments (>1.5 Ga). The observation that lherzolite xenoliths from Keluo and Wudalianchi contain phlogopite (Zhang et al., 2000, 2011) supports the hypothesis that SCLM, metasomatized by potassium-rich melts, is present beneath the WEK volcanic field and contributes to the basalts from Xiaogulihe.

Crustal and lithospheric mantle assimilation/contamination

Oceanic intraplate volcanism is often assumed to be immune to lithospheric contamination. Compared to continental intraplate eruptions, OIB do not interact with thermo-chemically complex SCLM. The low Os contents in OIB (typically <1 ng g^{-1}) makes the Re-Os isotope system a particularly sensitive indicator of lithospheric contamination, and the relatively unradiogenic $^{187}Os/^{188}Os$ compositions (<0.18) of OIB relative to local oceanic crustal reservoirs (typically $^{187}Os/^{188}Os$ >0.4; Reisberg et al., 1993; Marcantonio et al., 1995; Peucker-Ehrenbrink et al., 1995; Widom et al., 1999) make the tracing of assimilation of crustal or lithospheric mantle materials in OIB a straightforward process (e.g., Reisberg et al., 1993; Marcantonio et al., 1995; Lassiter and Hauri, 1998; Skovgaard et al., 2001; Gaffney et al., 2005). In particular, at the lowest levels of Os content, OIB are even more vulnerable to crustal contamination (Reisberg et al. 1993), while OIB with Os contents greater than 30 to 50 pg g^{-1} are typically assumed to be less susceptible to assimilation of lithospheric components (e.g., Reisberg et al., 1993; Eisele et al., 2002; Class et al., 2009). Crustal contamination thus rapidly drives Os isotope ratios to more radiogenic values resulting from the assimilation of oceanic crust with high Re/Os and $^{187}Os/^{188}Os$.

A consequence of the low HSE abundances of crustal material is that the addition of crust to a primitive melt should result in the dilution of HSE abundances in the resultant magma. Ireland et al. (2009) presented such a model, illustrating the effect of crustal contamination on Hawaiian picrites.

Briefly, three end-member scenarios are considered; (i) continental crust addition to komatiite; (ii) oceanic crust addition to tholeiite and, (iii) abyssal peridotite addition to alkali basalt. These models demonstrate that crustal contamination dilutes OIB HSE abundances at ≤20 % crustal or lithospheric assimilation. However, both $^{187}Os/^{188}Os$ and Re/Os can change dramatically in the evolving liquid, which has implications for the time integrated Os isotope ratio of such contaminated magmas and the effectiveness of using $^{187}Os/^{188}Os$ as a tracer for the mantle source of the magma. The effects of assimilation on HSE abundances (absolute or relative) in general, are less well-defined and where this issue has been addressed in the literature the consensus appears to be that fractional crystallisation exerts a stronger influence on HSE distributions than contamination factors (e.g., Chazey and Neal, 2005; Ireland et al., 2009). However, crustal contamination of continental flood basalts (CFB) can lead to a significant augmentation in the S content of a magma, sometimes resulting in S-saturation and significant HSE fractionation (e.g., Keays and Lightfoot, 2007; Lorand and Alard, 2010). This may also elevate concentrations of Re and the PPGE relative to Os, Ir and Ru. Assimilation of mantle lithosphere also has pronounced effects on Re/Os, but requires large additions to generate significant effects on magma HSE abundances. Conversely, Widom et al. (1999) demonstrated that unusually unradiogenic $^{187}Os/^{188}Os$ in some Canary Island lavas was most likely the result of the assimilation of peridotite xenoliths with sub-chondritic $^{187}Os/^{188}Os$ and >1 ng g^{-1} Os, prior to the eruption of the basalt at the surface. More recently, a similar process was described by Gannoun et al (2015a) to account for particularly unradiogenic Os concentrations in basalts from the Cameroon Line (**Figure 30**).

These simple crustal contamination models can be greatly complicated by the inclusion of fractional crystallisation processes, which are often intimately associated with crustal contamination. The combination of these processes will almost inevitably result in the generation of elevated Re, Pt and Pd abundances compared to Os, Ir and Ru in melts and crustal rocks, compared with their corresponding mantle residues. However, direct measurement of $^{187}Os/^{188}Os$ in early formed mineral phases handpicked from intraplate magmas, such as olivine (Debaille et al., 2009; Jackson and Shirey, 2011), generally yield more restricted ranges in $^{187}Os/^{188}Os$ than their associated whole-rocks, and may provide a means of seeing past bulk-rock contamination of OIB. As a result of these potential complications, a common sense approach, based upon a rigorous assessment of local potential contaminants and melt products was advocated by Day (2013) when applying thresholds for "contaminated" versus "uncontaminated" OIB. Both crustal and SCLM contamination of primitive melts have been reported in the literature (e.g., Ellam et al., 1992; Horan et al., 1995; Molzahn et al., 1996; Chesley and Ruiz, 1998; Keays and Lightfoot, 2007; Li et al., 2010; Chu et al., 2013). Successful modelling of SCLM or crustal assimilation is dependent upon the accurate determination

of likely end-member compositions, ranging from the parental primitive melt to its possible assimilants. Day (2013) successfully demonstrated the effect of contamination of primitive parent melts using North Atlantic Igneous Province (NAIP) picrites (Schaefer et al., 2000; Kent et al., 2004; Dale et al., 2009b) and intrusive rocks from the Rum Intrusion (O'Driscoll et al., 2009).

The origin of Continental Flood basalts (CFB) and Large Igneous Provinces (LIP)

Volcanic rocks from some CFB have been interpreted to have survived the transit from their asthenospheric source to eruption at the surface without any significant interaction with the SCLM or the crust (e.g., Schaefer et al., 2000; Zhang et al., 2008; Dale et al., 2009b; Rogers et al., 2010; Day et al., 2013). Many of these lavas are picritic in composition, have high-MgO (>13.5 wt. %), high Os concentrations, and $^{187}Os/^{188}Os$ ratios which are, in general, unradiogenic; consistent with their derivation from primitive mantle or a depleted mantle source (e.g., Schaefer et al., 2000; Dale et al., 2009b; Rogers et al., 2010). This chemical and isotopic signature has, in turn, been used to suggest that such CFB may be modern-day equivalents of uncontaminated Archaean komatiites, albeit from a cooler mantle, (cf., Brügmann et al., 1987; Wilson et al., 2003; Puchtel et al., 2009; Connolly et al., 2011).

In contrast, several studies have highlighted the importance of an interaction between asthenosphere-derived melts, SCLM and the crust to produce the observed spectrum of CFB compositions (e.g., Ellam et al., 1992; Horan et al., 1995; Molzahn et al., 1996; Chesley and Ruiz, 1998; Xu et al., 2007; Li et al., 2010; Heinonen et al., 2014) and the HSE fingerprint of some komatiites (Foster et al., 1996). Osmium isotope systematics, combined with other radiogenic isotope tracers in CFB demonstrate that the interplay between a primary magma and its potential lithospheric contaminants can be complex, as illustrated in a number of localities (e.g., Siberia - Horan et al., 1995; Ethiopia - Rogers et al., 2010; Emeishan, China, - Zhang et al., 2008). Correlations between $^{187}Os/^{188}Os$ and $^{87}Sr/^{86}Sr$ (Molzahn et al., 1996), $^{206}Pb/^{204}Pb$ (Xu et al., 2007), and possibly even $^{3}He/^{4}He$ (Dale et al., 2009b) illustrate the effects of lithospheric contamination on primary, asthenosphere-derived melts. However, observed variations in Os isotopes are not wholly consistent with SCLM or crustal contamination alone, suggesting that, like many OIB, some inherent heterogeneity within the asthenospheric source is present. For example, the 260 Ma Emeishan province (e.g., Li et al., 2010) requires a more depleted mantle source than 190 Ma Karoo CFB (Ellam et al., 1992). Some CFB provinces may therefore tap mantle sources that contain recycled material, similar to the source of some HIMU and EM flavoured OIB (e.g., Shirey, 1997; Dale et al., 2009b), while others are derived from an essentially primitive mantle (see review in Day, 2013).

Heterogeneity in the composition and distribution of sulfide types within a magma source region in the mantle (e.g., interstitial versus enclosed sulfides; Alard et al., 2002; see also Harvey et al., 2015, this volume) can have a profound influence on the composition of a basaltic melt (e.g. Harvey et al., 2010, 2011). The combination of source heterogeneity and degree of partial melting can therefore account for the observed differences in initial Os isotopic and HSE abundance variations in CFB provinces, that range from depleted DMM-like mantle compositions (e.g., Rogers et al., 2010) through undepleted basalts (e.g., Schaefer et al., 2000), to more radiogenic compositions, which provide strong evidence for recycled components in some CFB provinces (Shirey, 1997).

Coupled with the effects of adding subducted oceanic lithosphere back into the convecting mantle, i.e. the source of CFB and LIP, and the combinations of pelagic / terrigenous sediments, variably altered oceanic crust and serpentinized peridotite (Allègre and Turcotte, 1986), unravelling the sources of voluminous basaltic magmatism has sometimes been demonstrated to be problematic, often requiring both HSE and Re-Os isotope evidence used in concert with more traditional lithophile element-based isotope systems. For example, Heinonen et al. (2014) invoked a mixture of depleted Os-rich peridotite with ~10–30% of seawater-altered and subduction-modified MORB (with a recycling age of less than 1.0 Ga) as the likely source of the distinctive isotopic fingerprint found in CFB from the Antarctic Karoo province. A specific mixed peridotite-pyroxenite-like source was required to explain the unusual combination of elevated initial $^{87}Sr/^{86}Sr$ and Pb isotopic ratios, and low initial $^{187}Os/^{188}Os$ observed in the dykes sampled from around Ahlmannryggen, western Dronning Maud Land. In other words, simple, two-component mixing is often not consistent with the observed chemical and isotopic composition of CFB. In the example described by Heinonen et al. (2014), not only was a combination of mixed lithologies in the source, in addition to the inherent differences in their HSE and $^{187}Os/^{188}Os$ fingerprints required to account for the composition of the Ahlmannryggen dykes, but also a contribution from a seawater-altered subducted component was required.

A similar investigation into the nature of the Eastern North America (ENA) Central Atlantic Magmatic Province (CAMP) by Merle et al. (2014) also revealed the complex combination of chemical and isotopic fingerprints that can be preserved in large-volume basaltic eruptions. Although CAMP magmatism in general may have been produced as a result of either heat incubation under thick continental lithosphere (McHone, 2000; De Min et al., 2003; Puffer, 2003; McHone et al., 2005; Verati et al., 2005; Coltice et al., 2007), or by a plume head under the continental lithosphere (May, 1971; Morgan, 1983; White & McKenzie, 1989; Hill, 1991; Wilson, 1997; Courtillot et al., 1999; Ernst & Buchan, 2002; Cebria et al., 2003), Merle et al. (2014) proposed several increasingly complex scenarios to account for the chemical and isotopic signatures preserved in the ENA CAMP

basalts, including (i) direct derivation from a mantle plume (Wilson, 1997) or oceanic plateau basalt-type melts (e.g. Kerr & Mahoney, 2007); (ii) magmas derived from a mantle plume but contaminated by continental crust en route to the surface (Arndt et al., 1993); (iii) mixing between asthenospheric and ultra-alkaline mafic (lamproite, kimberlite, and kamfugite) melts (Arndt & Christensen, 1992; Gibson et al., 2006; Heinonen et al., 2010), possibly followed by crustal contamination; (iv) ternary mixing between OIB, MORB and SCLM-related melts, possibly followed by crustal contamination; (v) direct melting of a shallow source enriched in incompatible elements such as metasomatized SCLM or the mantle wedge above subduction zones (Puffer, 2001; De Min et al., 2003; Deckart et al. 2005; Dorais & Tubrett, 2008). Unfeasibly large degrees of crustal contamination would be required to produce the observed $^{143}Nd/^{144}Nd$, $^{206}Pb/^{204}Pb$ and $^{208}Pb/^{204}Pb$ isotopic compositions of the ENA CAMP basalts, and crustal contamination, assimilation (of continental crust) with fractional crystallization (DePaolo, 1981) and assimilation through turbulent ascent were discounted on the strength of the Re-Os and $^{187}Os/^{188}Os$ systematics i.e., initial $^{187}Os/^{188}Os$ ratios higher than 0.15 at Os concentrations lower than 50 ng g^{-1} (e.g., Widom, 1997).

Merle et al. (2014) determined that mixing involving either OIB or MORB-like parental melts, followed by crustal contamination, partially reproduces the compositions of the ENA CAMP basalts, but the trends observed in the Nd-Pb and Os-Nd isotopic diagrams require the addition of up to 35% continental crust, yet the assimilation of more than 20% of continental crust is thermodynamically unrealistic (Spera & Bohrson, 2001). Consequently, the hypothesis of a magma originating from mixing between OIB and SCLM-related melts and further contaminated by the continental crust was deemed unlikely. Therefore, the continental crust-like characteristics of the ENA CAMP were inferred to be present in the mantle source itself. Recent studies have suggested that such contrasting chemical characteristics may be derived from a metasomatized SCLM-type source (cf. Chu et al., 2013; Sun et al., 2014; Wang et al., 2014), where phlogopite in the SCLM was thought to be derived from the melting of subducted terrigenous sediments. To account for the measured Os isotope compositions of the ENA CAMP basalts, the Os isotopic composition of the source needed to be within the range of $^{187}Os/^{188}Os$ for off-cratonic SCLM (0·1180 to 0·1290; Carlson, 2005), therefore the model favored by Merle et al. (2014) to explain the multi-isotope system fingerprint of the EMA CAMP basalts required a reservoir that experienced progressive incorporation of subducted sediments derived from the local continental crust into a depleted sub-arc mantle wedge above a subduction zone.

Recent work has revealed that HSE abundances can be broadly modelled as a function of fractional crystallization in CFB. Day et al. (2013) studied the 1.27 Ga Coppermine CFB in northern Canada, which represents the extrusive manifestation of the Mackenzie large igneous province (LIP),

which includes the Mackenzie dyke swarm and the Muskox layered intrusion. These authors reported new HSE abundance and Re-Os isotope data for picrites and basalts from the CFB, as well as a highly unusual andesite glass flow. The glass contained high HSE contents (e.g., 3.8 ng g^{-1} Os) and mantle-like initial $^{187}Os/^{188}Os$ (γ_{1270Ma} Os = +2.2), but $\delta^{18}O$, εNd_i, and trace element abundances consistent with extensive crustal contamination, implicating a potential origin for sample CM19 as a magma mingling product formed within the Muskox Intrusion during chromitite genesis (cf. Day et al., 2008) and direct evidence for the processing of some CFB within upper-crustal magma chambers. These authors also modelled absolute and relative HSE abundances in CFB from the Coppermine, Parana and West Greenland, revealing that HSE concentrations decrease with increasing fractionation for melts with <8 ±1 wt.% MgO (**Figure 31**). The models reveal that significant inter-element fractionation between (Re+Pt+Pd)/(Os+Ir+Ru) are generated during magmatic differentiation in response to strongly contrasting partitioning of these two groups of elements into sulfides and/or HSE-rich alloys. Furthermore, fractional crystallization has a greater role on absolute and relative HSE abundances than crustal contamination under conditions of CFB petrogenesis due to the dilution effect of low total HSE continental crust. Day et al. (2013) found that picrites (>13.5wt.% MgO) from CFB (n = 98; 1.97 ±1.77 ng g^{-1}) having higher Os abundances than OIB picrites (n = 75; 0.95±0.86 ng g^{-1}) and interpreted these differences to reflect either higher degrees of partial melting to form CFB, or incorporation of trace sulfide in CFB picrites from magmas that reached S-saturation in shallow-level magma chambers.

Continental intraplate alkaline volcanism

Continental intraplate alkaline volcanic rocks (CIAV) comprise a wide spectrum of sodic and potassic compositions ranging from alkali basalts, picrites and basanites through to more evolved eruptive products that include nephelinites, carbonatites, melilitites, and kimberlites. The origin of some of these rock types are not unequivocal, with petrogenetic models ranging from pure incipient rift-related sources (e.g., Thompson et al., 2005), to 'hotspot' or 'plume' related origins (e.g., Haggerty, 1999). Finding a likely source for these volcanic rocks is not made any less ambiguous when experimental and geochemical data are considered as many of these lavas are thought to derive from close to the boundary layer that separates the convecting and conducting mantle (e.g., Foley, 1992; Day et al., 2005), i.e. both the asthenosphere and SCLM can be implicated in the genesis of these magmas. Re-Os isotope data are limited for these types of lavas, and instances where this is combined with HSE abundance data are comparatively rare. Examples from the literature when HSE and / or Re-Os isotope data are available are summarized in Day (2013).

When elevated osmium contents in basalts clearly exclude the influence of crustal contamination, radiogenic $^{187}Os/^{188}Os$ (e.g., >0.15) is often interpreted as being derived from olivine-poor mantle heterogeneities, such as clinopyroxenites (Carlson et al., 1996; Carlson and Nowell, 2001; Janney et al., 2002), primarily as a result of their time-integrated ingrowths to high $^{187}Os/^{188}Os$ (Reisberg et al., 1991; Reisberg and Lorand, 1995; Kumar et al., 1996). At the onset of S-saturated melting at depth, these fertile heterogeneities with radiogenic Os isotopic compositions melt preferentially (Hirschmann et al., 2003; Rosenthal et al., 2009). Combined with the Os isotope and HSE signature associated with pyroxenite-dominated melts, high NiO and low MnO concentrations in olivine phenocrysts are also diagnostic of olivine-poor mantle domains such as phlogopite-rich pyroxenites (Prelević et al., 2013). These phlogopite-bearing pyroxenites can be derived from the reaction of peridotitic mantle wedge with melts derived from terrigenous sediments, possibly from the uppermost regions of the subducting slab (Prelević et al., 2015). As such, many CIAV appear to have non-peridotitic sources, with some sodic mafic-alkali magmas possessing radiogenic $^{187}Os/^{188}Os$ compositions, but moderately high Os contents (>0.5 ng g^{-1} Os). Extreme Os isotopic compositions could reflect low degrees of partial melting and preferential sampling of more fusible mafic components, such as pyroxenite, in the asthenospheric mantle (cf. CFB above). Alternatively, melting of metasomatised lithosphere during rifting events (e.g., Carlson and Nowell, 2001; Thompson et al., 2005) may also be responsible for the PGE abundances and Re-Os systematics of some CIAV, such as the Newer volcanic rocks, Australia (Vogel and Keays, 1997). Similarly, carbonatites may also ultimately originate from mafic as opposed to ultramafic sources due to their close association with other ultrapotassic rocks (e.g., Gudfinnsson and Presnall, 2005). For example, young (>20 Ma) carbonatites from Fuerteventura, Canary Islands, possess low Os abundances (5 to 15 pg g^{-1}) and highly radiogenic $^{187}Os/^{188}Os$ that extend to values in excess of 0.6 (Widom et al., 1999). Conversely, the high Os abundance and unradiogenic Os isotope signatures of some kimberlites and katungites are consistent with a petrogenesis involving the assimilation or derivation from the SCLM (Pearson et al., 1995; Carlson et al., 1996; Araujo et al., 2001; Carlson and Nowell, 2001; Pearson et al., 2008). More recently, Chalapathi Rao et al (2013) provided strong evidence for contrasting mantle sources for kimberlites and lamproites in the Eastern Dharwar craton, southern India. Re–Os isotope of orangeites from the Bastar craton and Mesoproterozoic kimberlites and lamproites contrasted with an unradiogenic Re-depleted kimberlite sample with present-day $^{187}Os/^{188}Os$ (0.1109) and a Re-Os isotopic fingerprint characteristic of Proterozoic lithosphere, with the positive γOs (2.9 to 3.6) of two kimberlites from Raichur and Narayanpet (Eastern Dharwar craton) that retained both both plume and subduction-related source signatures (cf. Heinonen et al. 2014 for the petrogenesis of continental flood basalts from the Antarctic province of the Karoo). The enriched Re–Os mantle sources for the

nearby Kodomali orangeite (γOs = +3) and the Krishna lamproites, with very radiogenic (γOs 56 + 355), similar to those displayed by the lamproites of the Italian peninsula (Conticelli et al., 2007), suggest a subducted component for the latter ultra-potassic rocks, demonstrating the complex interplay of likely sources contributing to magma genesis around the Eastern Dharwar craton in both time and space (Chalapathi Rao et al., 2013).

The low Os concentrations of primary low-degree potassic and sodic mafic-alkali volcanic rocks, combined with the high Os abundance of mantle and crustal xenoliths in some kimberlites, alnoites and melnoites make these volcanic rocks highly susceptible to contamination as they pass through and interact with the SCLM and overlying crust. Evolved magmas of this type may also be susceptible to the effects of S-saturation prior to eruption (Vogel and Keays, 1997), i.e. they may have experienced the prior precipitation of sulfide and concomitant harvesting of HSE from the S-saturated magma. Despite these caveats, some continental intraplate magmas still retain unique information on the composition of their mantle source. In particular, early Cretaceous alkaline picrites and basalts from the North China craton have petrological and Os-Sr-Nd isotope compositions consistent with contributions from recycled and foundered eclogitic lower continental crust (Gao et al., 2008). More recently, Chu et al. (2013) examined a suite of highly potassic basalts from Wudalianchi-Erkeshan, NE China and, despite the incorporation of modest amounts of continental crust and the potential of sulfide contamination derived from the SCLM, traced the source of the basalts back to the asthenosphere. Their findings suggested a complex interaction between crust and SCLM with highly potassic melts generated at least partly from SCLM containing phlogopite, itself with an ancient terrigenous sediment signature (Sun et al., 2014). In contrast to a predominantly peridotitic phlogopite-bearing source for continental volcanism reported by Sun et al. (2014), Miocene ultrapotassic rocks within the Sailipu area of the western Lhasa terrane, southern Tibet, were variously attributed to the interaction of both spinel- and garnet-lherzolite derived melt with a phlogopite-bearing pyroxenite source (Wang et al. 2014). Although the latter study postulated that the observed chemistry of the ultramafic melts could be attributed to crustal contamination, unfeasibly large-scale assimilation of continental crust would be necessary to account for the nature of the Sailipu basalts. While the lithophile element-based isotope systems are relatively insensitive to crustal contamination, mixing calculations using HSE concentrations and $^{187}Os/^{188}Os$ of primitive arc compositions (Os = 0.2 ng g^{-1}; $^{187}Os/^{188}Os$ = 0.125; Shirey and Walker, 1998; Suzuki et al., 2011), continental crust (Os = 0.01 ng g^{-1}; $^{187}Os/^{188}Os$ =1.10; Shirey and Walker, 1998) and depleted mantle material (Os =0.405 ng g^{-1}; $^{187}Os/^{188}Os$ = 0.108; Shirey and Walker, 1998) demonstrated that the composition of the samples from western Lhasa (Wang et al., 2014) would require an unreasonably high degree of crustal contamination (>80%) (**Figure 32**). Two other studies of ultrapotassic rocks

from Italy and the Balkans (Conticelli et al., 2007; Prelević et al., 2015, respectively) attributed a similar combination of mantle sources (as opposed to crustal contamination) as being primarily responsible for the observed chemical and isotopic compositions.

The recent study of Chu et al. (2013) also discussed the complex chemical and isotopic signatures preserved in the Wudalianchi-Erkeshan highly potassic basalts in the context of crustal and lithospheric contamination. Here, the range of $^{187}Os/^{188}Os$ in basalts ($^{187}Os/^{188}Os$ =0.1187–0.17) was partially attributed to 2–8 % crustal contamination; a degree of assimilation that otherwise would be difficult to detect using lithophile element isotope systems. In fact, Gannoun et al. (2015a) suggested that degrees of crustal assimilation of up to 15 % would have no measureable effect on Nd and Pb isotope ratios of basalts, while Li et al. (2014) commented that lithophile element-based isotope systems may be opaque to as much as 18 % crustal contamination. In the latter study, high NiO and SiO_2 contents, but low MnO, CaO, MgO and Pb contents, in addition to radiogenic $^{187}Os/^{188}Os$, low Os abundances (5 to 43 ng g^{-1}) and high, but variable, Re/Os (3 to 126) of intra-continental OIB-like basalts from West Qinling, central China, were attributed to crustal contamination on the strength of the sensitivity of Os isotope systematics to the incorporation of continental crust.

In contrast, the most unradiogenic Os isotope signatures observed in continental alkaline intraplate volcanism may have been affected by the assimilation of xenocryst-hosted primary sulfide. The often unradiogenic $^{187}Os/^{188}Os$ and high (> µg g^{-1}) Os content of sulfides enclosed within olivine xenocrysts (Alard et al., 2002) are prime candidates for the source of a possible "nugget effect". For example, a 20 µg mantle sulfide with an Os concentration of 20 µg g^{-1} (see Alard et al., 2000, 2002; Pearson et al., 2002; Harvey et al., 2006, 2010, 2011; Lorand et al., 2013; Harvey et al., 2015, this volume for typical sulfides) contains twice as much Os as 2 g of basalt with an Os concentration of 100 pg g^{-1}. This type of nugget effect was attributed by Chu et al. (2013) as being responsible for the poor reproducibility of $^{187}Os/^{188}Os$ in two Wudalianchi-Erkeshan basalts (LHS-6 and HSS-6). In this instance, the heterogeneous distribution of a component that contains anomalously high Os (+ PGE) abundances throughout the sampled rock powder could account for the observed heterogeneities in replicate basalt analyses. A similar source of heterogeneity was suggested by Gannoun et al. (2015a) to account for comparable unradiogenic $^{187}Os/^{188}Os$ signatures in some Cameroon Line basalts.

Processes affecting the HSE compositions of sub-aerial volcanism

The previous sections demonstrate that it is essential to consider the many possible source and contamination factors that may influence the ultimate composition of intraplate magmas. Irrespective of the tectonic setting in which an erupted magma was generated, sub-aerially erupted lavas may be

subject to an additional group of processes whose affects need to be assessed prior to interpretations concerning magma sources and potential contaminants. These processes, including post-emplacement alteration and magmatic degassing, were reviewed comprehensively in Day (2013). While there has been a dearth of new data in the intervening period, one study in particular merits attention; the recent examination of Os loss through magmatic degassing at Piton de la Fournaise, Réunion Island (Gannoun et al., 2015b).

Oceanic island basalts have lower Re concentrations than MORB. This is anomalous considering the incompatible behavior of Re during basalt petrogenesis (Hauri and Hart, 1997). This apparent quirk has been attributed to two possible causes; (i) the presence of garnet and/or sulfide in their mantle source (Righter and Hauri, 1998), or (ii) magmatic degassing of Re (Bennett et al., 2000; Lassiter, 2003; Norman et al., 2004). Several lines of evidence support the idea that Re loss is a late and shallow stage process, which favors process (i) above. For example, an increase in oxygen fugacity promotes the loss of Re from Re metal (Borisov and Jones, 1999), suggesting that at the oxidation state relevant to OIB (FMQ), the rate of Re loss from a magma will increase by an order of magnitude per log unit of fO_2 increase. Sub-aerial eruptions from Réunion and Hawaii preserve evidence for an increase in fO_2 in the lavas during emplacement, from FMQ -1.8 close to eruption vents, to up to FMQ +3 in lava samples that have travelled several km and cooled slowly (Rhodes and Vollinger, 2005; Boivin and Bachélery, 2009).

Although Re and Os have the highest elemental condensation temperature (1821 and 1812 K, respectively; Lodders, 2003), these elements are commonly enriched in volcanic gas sublimates and aerosols (Crocket, 2000; Yudovskaya et al., 2008; Mather et al., 2012). However, the relative and absolute volatilities of Re and Os, and hence the degree of degassing from sub-aerial lavas, are not well constrained. The propensity for an elemental species to be volatilized post-eruption can be described in terms of an emanation coefficient, (E_x), where $E_x = (C_i - C_f) / C_i$, (C_i = concentration of element x in the magma and C_f = concentration of element x in the magma after degassing; Gill et al., 1985; Lambert et al., 1986). The emanation coefficient of Re ranges from 0.12 (Rubin, 1997) to as high as 0.74 (Norman et al. 2004). The difficulties associated with the analysis of pg g^{-1} quantities of Os in basalts make the emanation coefficient of Os even less well known.

In their recent study, Gannoun et al. (2015b) investigated the Re–Os isotope and elemental systematics of basaltic lavas and gas condensates (a range of Na-K-Ca-Cu sulfates, Ca-Mg-Al-Fe fluorides, and native sulfur) produced during eruption and degassing at Piton de la Fournaise, Réunion Island, in order to examine the geochemical behavior of these two elements during magma degassing. High temperature (>350 °C) deposits were enriched in Re (24 to 79 ng g^{-1}), almost two order of magnitude higher than the corresponding lavas (0.2 to 0.8 ng g^{-1}), while the Os abundances

of the high temperature condensates were similar to those of the lavas (14 to 132 pg g^{-1}). The highest temperature condensates (Na–K sulfates; 384 to 400 °C), yielded $^{187}Os/^{188}Os$ that were significantly lower (i.e. 0.124–0.129) than their corresponding lava. These unradiogenic osmium isotope ratios were attributed by Gannoun et al. (2015b) to the volatilization of Os originally contained in old, unradiogenic mantle sulfides. Sulfides associated with earlier volcanic eruptions at Réunion Island (<7 Ma) were deemed too young to provide the distinctive unradiogenic Os fingerprint of the volcanic gas, leading Gannoun et al. (2015b) to infer that the observed unradiogenic Os was ultimately derived from a mantle source. In the context of osmium mantle geochemistry, loss of unradiogenic Os during magmas degassing could help to explain osmium isotope disequilibrium between lavas and melting residues.

This contrasted with the Re-Os systematics of the low-to-medium temperature condensates, which contained the highest Os abundances (13 to 77 ng g^{-1}) with unfractionated $^{187}Os/^{188}Os$ (0.130 to 0.135), which are indistinguishable from the April 2007 lava flow and the historical lavas of Piton de la Fournaise (i.e. $^{187}Os/^{188}Os$ = 0.130 to 0.137; Schiano et al., 2012). In addition, very high concentrations of iridium (1 to 8 ng g^{-1}) reported for hieratite condensates (K_2SiF_6) suggested that Ir was also transported in volatile emissions as gaseous IrF_6 (cf. Toutain and Meyer, 1989). The selective enrichment of HSE demonstrates their potential for transport as metallic hexafluorides (Molski and Seppelt 2009; Craciun et al., 2010; Gannoun et al., 2015b; see also review in Day, 2013). The absence of isotopic fractionation between gas deposits and lavas also indicates that external components (such as seawater, rainwater or air), which all possess particularly radiogenic $^{187}Os/^{188}Os$ (Levasseur et al., 1998, 1999; Gannoun et al., 2006; Chen et al., 2009) have no significant influence on the Os budget of volcanic gases.

HIGHLY SIDEROPHILE ELEMENT SYSTEMATICS OF ARCS

Highly siderophile element abundance studies have been applied to arc volcanism to understand both subduction processes and the generation of economic deposits of precious metals within arc settings. A critical question has regarded the potential mobility of the HSE in subduction zone environments and the collateral effects such processes have regarding the siderophile element budget of the mantle. Fractionation of Re and Pt from Os in subduction zone environments could have a potentially significant effect both on Os isotope signatures at arcs (e.g., Brandon et al., 1996), but also on the long-term Re/Os and Pt/Os fractionations observed in OIB, MORB and mantle rocks. In addition, the potential mobility of HSE in subduction zone environments has important

implications regarding the formation of economic PGE ore deposits such as major epithermal gold deposits associated with some volcanic arcs (e.g., McInnes et al., 1999). For the purpose of this review, we focus on the petrogenetic implications of arc volcanism.

Arc magmatism includes tholeiitic to calc-alkaline compositions and dominantly involves the generation of basalt-andesites, andesites and more evolved magma-types. Only a limited number of arc volcanoes are known to erupt lavas approaching basaltic or picritic compositions. Because the HSE are typically compatible during mantle melting, as well as during fractional crystallization, this means that Os concentrations in arc volcanic rocks are typically very low, resulting in increased susceptibility of arc lavas to crustal contamination (e.g., Righter et al., 2002; Hart et al., 2002; Lassiter & Luhr, 2001; Turner et al., 2009; Bezard et al., 2015). High $^{187}Os/^{188}Os$ in arc lavas has therefore been attributed to assimilation of arc crust during magmatic ascent, but also due to enrichment in radiogenic Os due to contamination of the mantle wedge by slab-derived fluids/melts (e.g., Borg et al., 2000; Alves et al., 1999; 2002), or a combination of these processes (Suzuki et al., 2011). In this section, we review the work done so far in arcs, using both lavas, as well as mantle-derived xenoliths erupted in association with active arcs. Since the behavior of the HSE are reviewed extensively elsewhere in this volume, the focus of this section is largely on the information that can be obtained from the HSE regarding arc processes.

HSE and $^{187}Os/^{188}Os$ in arc lavas

The majority of arc related volcanism is located around the Pacific 'Ring of Fire', extending from the southern tip of Chile, up much of South and North America, into the Aleutians and Kamchatka, through Japan and down as far as the Tonga Trench and New Zealand. Other significant arcs include the Lesser Antilles Arc and the Scotia Arc (**Figure 33**). Despite the extensive distribution of arc volcanoes, limited work has been conducted on Re-Os isotopes in arc volcanic rocks, primarily due to the limited availability of high MgO lavas, which are normally favored for study by Os isotope and HSE abundance studies. High MgO lavas do occur in some arc settings, most notably Grenada, south Lesser Antilles Arc, Tonga, and as boninite occurrences. These lavas are discussed in detail, below.

Work on arcs has shown that arc volcanic rocks typically contain between 0.0001 and 1 ng g^{-1} Os and 0.01 to 1 ng g^{-1} Re (**Figure 34**). Rhenium concentrations generally increase with decreasing MgO in arc lavas, consistent with moderate incompatibility of Re. However, Re can also behave as a volatile element during oxidizing conditions in arc lavas, and for this reason it is likely that low concentrations could reflect loss of Re by this process (e.g., Righter et al., 2008). Positive correlation

between Os and MgO is consistent with strong compatibility of Os during fractional crystallization of arc lavas. The low MgO and HSE contents in arc lavas can make them potentially highly susceptible to crustal contamination effects (cf. Lassiter & Luhr, 2001). Osmium isotopic ratios in recently erupted arc lavas can span an extreme range, from high MgO lavas with $^{187}Os/^{188}Os$ (~0.127-0.128) similar to typical mantle estimates, to andesites, rhyolites and dacites with $^{187}Os/^{188}Os$ >1. There is an overall relationship of increasing $^{187}Os/^{188}Os$ with decreasing Os content, although more than one trend has been recognized in plots of reciprocal Os versus $^{187}Os/^{188}Os$ (**Figure 35**). Alves et al. (2002) pointed out that initial Os isotopic ratios are positively and systematically correlated on $^{187}Os/^{188}Os$ versus reciprocal Os plots, reflecting binary mixing processes, with a common end-member represented by upper mantle peridotite compositions.

To date, no study has found clear associations of Re or Os contents and $^{187}Os/^{188}Os$ with arc basement type, convergence rate or sediment supply. This may be partly due to the lack of available high MgO rocks with which to make cross-comparison of 'primary magmatic composition'. For example, Lassen Peak lavas with 8 to 11.1 wt.% MgO have up to 0.37 ng g^{-1} Os and span a range of $^{187}Os/^{188}Os$ from 0.1289-0.235 (Borg et al., 2002). It has been suggested that these lavas contain a contribution of radiogenic Os from the subducting slab. Conversely, Grenada picrites and basalts (10.5-17.4 wt.% MgO) contain up to 0.36 ng g^{-1} Os and have a slightly more restricted range of $^{187}Os/^{188}Os$ (0.1268-0.1644), yet these lavas are not considered to have a contribution from the slab, but instead have experienced various levels of crustal assimilation (Woodland et al., 2002; Bezard et al., 2015). Likewise, boninite (13 wt. %) and some low MgO lavas (<1.5 wt. %) from the Tonga-Kermadec arc have $^{187}Os/^{188}Os$ of 0.1275-0.1283, indicating that more radiogenic values for lavas in this arc are consistent with localized arc contamination (Turner et al., 2009). Unique to that study is that the sample with the least radiogenic Os signature is a dacite, suggesting that evolved magmas can develop by fractionation from mantle-derived magma with minimal interaction with high Re/Os arc crust. High MgO (≥10 wt.%) volcanics from the central and northern Tonga arc, including some with boninitic affinity, possess a greater range of $^{187}Os/^{188}Os$ from 0.131-0.156, while lower MgO samples range up to $^{187}Os/^{188}Os$ = 0.4, again largely illustrating the potential effects of localized arc contamination (Dale et al., 2012b).

Contents of the HSE in arc-related lavas have been reported for Grenada basalts and picrites, Izu-Bonin lavas (Woodland et al., 2002) and Lihir lavas (McInnes et al., 1999) (**Figure 36**). These generally high MgO lavas show similar Re and PPGE enrichment over the IPGE, to many intraplate tholeiites and alkali basalts (e.g., Day, 2013). However, despite the picritic (MgO >13·5 wt. %) nature of Grenada lavas, they contain low concentrations of the HSE (<0·2 ng g^{-1} Ir, 1–4 ng g^{-1} Pd) compared with other lavas of similar MgO content. Woodland et al. (2002) argued that this was

probably due to a combination of lower degrees of partial mantle melting and early removal of PGE with cumulus phases such as olivine, magnetite and sulfide. Comparison of alkali Grenada lavas with boninitic Izu–Bonin lavas illustrates that although the major element chemistries of Grenada and Izu–Bonin are different, relative and absolute abundances of the IPGE and PPGE are similar. Rhenium, however, is markedly depleted in the Grenada picrites compared with the Izu–Bonin boninites, suggesting either retention of Re by residual garnet in the Grenada sub-arc mantle wedge (Woodland et al., 2002) or volatile-loss of Re. In some of these cases, their generation above a subduction zone did not appear to have any significant systematic effect on the HSE signatures of resultant lavas. However, Grenada samples possess markedly high Pt/Ru ratios and significant PPGE/IPGE fractionation in general. This feature has also been observed in Tongan arc lavas and associated lavas from the Fonualei rifts (Dale et al. 2012b), which possess amongst the most extreme Pt/Ru ratios yet observed in terrestrial mantle-derived magmas (up to 300 in rocks with MgO >8 wt. %). This was attributed by Dale et al. (2012b) to the retention of IPGE in the mantle source by chromitite and/or IPGE-rich PGM, despite sulfide exhaustion. Sulfide exhaustion is consistent with the sulfide-undersaturated nature of the magmas and led to very high PPGE concentrations in the melts.

HSE and $^{187}Os/^{188}Os$ in arc xenoliths

HSE studies of mantle xenoliths from arc settings have provided the opportunity to document the behavior of these HSE during slab fluid-induced metasomatism of the mantle wedge, with spinel harzburgite, websterite and pyroxenite mantle xenoliths occuring in back-arc environments in a number of arcs. Relatively radiogenic Os isotope signatures in mantle xenoliths and mantle rocks from arc settings, including the Cascades, Canadian Cordillera, Japan, Lihir, Papua New Guinea, Kamchatka, and the Catalina Schist have been documented, and attributed to the mobility of Os in slab fluids (Brandon et al., 1996; 1999; McInnes et al., 1999; Peslier et al., 2000; Widom et al., 2003). For example Simcoe xenoliths, which represent fragments of mantle lithosphere from the back-arc of the Cascade arc front, have been metasomatised by silica-rich fluids or hydrous melts leading to higher fO_2 leading to radiogenic Os isotopic compositions being imparted to these peridotites (Brandon et al., 1996; 1999). These features are consistent with part or the entire metasomatic agent being derived from the Juan de Fuca slab. Studies of Kamchatka peridotites also indicate metasomatism of the Kamchatka sub-arc mantle wedge by radiogenic slab-derived fluids and melts (Widom et al., 2003).

HSE patterns of the arc-related mantle xenoliths are broadly similar to typical oceanic mantle xenoliths (**Figure 36**), but the xenoliths can often exhibit elevated $^{187}Os/^{188}Os$, with Simcoe xenoliths

ranging from 0.123-0.157 and Kamchatka xenoliths ranging from 0.123-0.148. The regional variations in Re–Os isotope signatures are consistent with previous petrographic and geochemical studies of the Kamchatka mantle xenoliths that reveal multistage metasomatic histories resulting from interaction of the mantle wedge with a variety of slab-derived fluids and melts, including silicic slab-melt metasomatism associated with subduction of relatively hot, young (~15–25 Ma) oceanic crust in the northern arc front, hydrous slab-fluid metasomatism associated with subduction of colder, old (~100 Ma) oceanic crust in the southern arc front, and carbonate-rich slab-melt metasomatism in the southern segment behind the arc front, where the slab is deeper. Similar ranges of Re–Os isotope signatures in peridotites from Avachinsky, Japan and Lihir, and from Valovayam and the Cascades, respectively, suggest that the age (temperature) and depth of subducting oceanic crust influences the Re–Os composition of metasomatized sub-arc mantle.

Radiogenic Os from slab components or from crustal contamination

A continuing debate exists over the influence of slab-derived $^{187}Os/^{188}Os$ to arcs, versus the potential for crustal or seawater contamination of magmas with low Os abundances. From Lassen lavas, Borg et al. (2000) showed that crustal contamination could only explain the Re-Os isotope systematics if distribution coefficients for Re in sulfide were ~40-1100 times higher than published estimates, and instead argued for contributions from a highly radiogenic Os slab component ($^{187}Os/^{188}Os$ up to 1.4). Alves et al. (2002) also favoured slab components adding radiogenic Os to arcs, citing evidence from arcs worldwide for different mixing systematics between mantle peridotite and variably radiogenic Os slab contributions. Conversely, Bezard et al. (2015) have shown that Grenada picrites with radiogenic $^{87}Sr/^{86}Sr$ (0.705) have $^{187}Os/^{188}Os$ (0.127) that overlap with the mantle range and that assimilation and fractional crystallization can explain compositions of Lesser Antilles lavas, without the requirement of a slab input (**Figure 37**). Dreher et al. (2005) studied Os isotopes in Mindanao adakites, showing that the majority of these rocks had unradiogenic Os isotopes, inconsistent with the idea that adakites with high Sr/Y and low Y and heavy rare earth element concentrations, reflect melting of young subducted crust in subduction zones.

On the other hand, the range in Os isotopes in Mexican Volcanic Belt rocks, which represent subduction-related calc-alkaline and lamprophyric rocks in which high fO_2 precludes sulfide fractionation, could be explained up to 12% assimilation and fractional crystallization (Lassiter & Luhr, 2001). To obviate potential issues of shallow-level crustal contamination, Suzuki et al. (2011) examined Cr-spinel from beach sands in the Bonin Islands, reasoning that Cr-spinel is an early-formed mineral in most magmas and an indicator of primitive magma Os compositions. They found

unradiogenic Os in Cr-spinel with boninitic affinity, versus a potential slab component reflected in spinel with tholeiitic affinity. These authors also argued that oxidative conditions in the mantle can lead to radiogenic Os mobilization in the arc. Ultimately, the most convincing arguments for or against radiogenic Os from the slab comes from high-MgO Grenada picrites. These samples have been shown to have less-radiogenic Os signatures in more mafic lavas, with an increasing influence of crustal contamination in more evolved melts (Woodland et al., 2002; Bezard et al., 2015). Combined with evidence for the potential influence of subduction zone fluids on the composition of arc xenoliths, these results suggest that some contribution from the slab can be exhibited in arc lavas, but that the role of crustal contamination of melts within the arc itself can obfuscate original mantle-derived signatures.

Mechanical mixing processes

The debate as to whether slab-derived signatures are evident in HSE and Os isotopes within arc volcanic rocks has recently been enhanced by the recognition that mechanical mixing between peridotite mantle and recycled ocean rocks is likely an important process in modifying HSE contents at subduction zones. Studies of HSE contents and Os isotope compositions of mélange mafic metamorphic blocks at Catalina Island and the Franciscan Complex (California) and at the Samana Metamorphic Complex (Dominican Republic) have shown significant differences between block cores and block rims (Penniston-Dorland et al., 2012; 2014). In particular, while the cores of the blocks have enhanced PPGE compared with IPGE and radiogenic $^{187}Os/^{188}Os$, mimicking patterns for evolved basaltic rocks, or some sedimentary protoliths, the rims approach HSE contents expected in some mantle peridotites, with less radiogenic $^{187}Os/^{188}Os$ (**Figure 38**). Penniston-Dorland et al. (2014) have demonstrated that mèlange mechanical mixing occurs across a range of temperatures (≤200˚C to ~600˚C) during subduction leading to a hybrid rock composition of peridotite, basaltic materials and sediments. Measurements of the HSE in arc volcanics suggest variable amounts of peridotitic mantle with radiogenic Os components (e.g., Alves et al., 1999; 2002; Borg et al., 2000) and mechanical mixing may play a major role in this process.

CONCLUSIONS AND PERSPECTIVES

The highly siderophile elements are expected to be strongly incorporated into Earth's metallic core, but their abundance in the upper mantle appears to have been set by the late addition of meteoritic material after core formation was complete. Partial melting of the mantle since that time has resulted in a significant fractionation of the HSE. The platinum-PGE, Re and Au, can behave as moderately compatible or incompatible elements during melting, and may be variably enriched in melts, whereas the iridium-PGE behave as highly compatible elements. Sulfide is a major host for HSE in mantle rocks, despite its relatively low abundance (between 0.04 and 0.08%). However, sulfide cannot account for the fractionation of HSE that occurs during the melting that generates MORB, which generally possess very low Os-Ir-Ru contents, and relatively high Re-Pd and Pt. Rather this fractionation appears to result from the crystallisation of Os-Ir-Ru alloy phases in refractory mantle rocks, accompanying the exhaustion of sulfide by melting. The HSE content of MORB is further modified by the segregation of sulfide during fractional crystallisation in the magmatic environment, where the HSE are quantitatively removed into sulfide, leaving the residual melt depleted in these elements.

The fractionation of Re and Os accompanying the generation of MORB, intraplate lavas and those produced at convergent margins is one of the key processes controlling the distribution of these elements between Earth's mantle and crust. Therefore, decay of ^{187}Re to ^{187}Os provides a potentially exceptional tracer of recycled crustal materials in Earth's mantle. This is because both oceanic and continental crust possess high Re/Os ratios, and develop radiogenic Os isotope compositions over time, which in turn can be readily traced as recycled material if mixed back into the convective mantle. However, while MORB glass commonly preserves a radiogenic ^{187}Os/^{188}Os isotope composition, this is most readily explained by seawater-derived contamination of the melt that occurs during magma ascent through the oceanic crust. Although reliable data for MORB glass remain limited these observations suggest that to a greater or lesser extent all MORB glass has been affected by seawater-derived contamination. This then also implies that other elements may have been affected by such contamination, most likely dependent upon their relative concentration in MORB glass and seawater. Sulfide, although demonstrably affected by the same seawater contamination, provides a more reliable record of the primary ^{187}Os/^{188}Os isotope composition of MORB, particularly those sulfides with high Os concentrations (i.e. > 100 ng g^{-1}). These high-Os sulfides preserve relatively unradiogenic ^{187}Os/^{188}Os isotope compositions pointing to a mantle source that

has experienced long term depletion of Re, similar to abyssal peridotites, with no evidence for the presence of recycled crust.

In addition to the effects of seawater contamination observed in MORB, intraplate lavas and those generated at convergent margins may interact with sub-continental lithospheric mantle, itself variably contaminated by multiple metasomatic events since it became isolated from the convecting mantle, and incorporate additional complications from the overlying crust. At convergent margins there is the additional complication of fluxes generated as a result of the subduction of the down-going slab with the potential for overprinting pre-existing Re-Os isotope and HSE fingerprints. While the HSE and its isotope systems offer some unique perspecives on mantle processes and the generation of a wide range of magmas, their application needs to be exercised with care – the geochemical context provided by other isotope systems and trace element signatures should be considered and the specific set of local conditions, both physical and chemical, taken into account in addition to the use of these invaluable tools.

ACKNOWLEDGMENTS

We thank Jean-Louis Birck, Olivier Alard, Christian Pin, Ivan Vlastélic, Anthony Cohen, Ali Bouhifd for valuable insight and discussions over the years. AG would like to thank Jean-Luc Devidal for assistance with the electron microprobe measurements at Blaise Pascal University. The authors wish to thank Chris W. Dale for review that greatly improved the manuscript. This research was partially financed by the French Government Laboratory of Excellence initiative n°ANR-10-LABX-0006, the Région Auvergne and the European Regional Development Fund. This is Laboratory of Excellence ClerVolc contribution number 178.

1792 **REFERENCES**
1793

1794 Agranier A et al. (2005) The spectra of isotopic heterogeneities along the Mid-Atlantic Ridge. Earth
1795 Planet Sci Lett 238:96-109
1796 Ahmed AH and Arai S (2002) Unexpectedly high-PGE chromitite from the deeper mantle section of
1797 the northern Oman ophiolite and its tectonic implications. Contrib Mineral Petrol 143:263-278
1798 Ahmed AH, Hanghoj K, Kelemen PB, Hart SR and Arai S (2006) Osmium isotope systematics of the
1799 Proterozoic and Phanerozoic ophiolite chromites: In situ ion probe analysis of primary Or-rich
1800 PGM. Earth Planet Sci Lett 245:777-791
1801 Alard O, Griffin WL, Lorand JP, Jackson SE, O'Reilly SY (2000) Non-chondritic distribution of the
1802 highly siderophile elements in mantle sulfides. Nature 407:891-894
1803 Alard O, Griffin WL, Pearson NJ, Lorand J-P, O'Reilly SY (2002) New insights into the Re–Os
1804 systematics of subcontinental lithospheric mantle from in-situ analysis of sulfides. Earth Planet
1805 Sci Lett 203:651-663
1806 Alard O, Luguet A, Pearson NJ, Griffin WL, Lorand JP, Gannoun A, Burton KW, O'Reilly SY
1807 (2005) In situ Os isotopes in abyssal peridotites bridge the isotopic gap between MORBs and
1808 their source mantle. Nature 436:1005-1008
1809 Allègre CJ, Turcotte DL (1986) Implications of a two-component marble-caked mantle. Nature
1810 323:123-127
1811 Alves S, Schiano P, Allègre CJ (1999) Rhenium-osmium isotopic investigation of Java subduction
1812 zone lavas. Earth Planet Sci Lett 168:65-77
1813 Alves S, Schiano P, Capmas F, Allègre CJ (2002) Osmium isotope binary mixing arrays in arc
1814 volcanism. Earth Planet Sci Lett 198:355-369
1815 Anbar AD, Creaser CR, Papanastassiou DA, Wasserburg GJ (1992) Rhenium in seawater:
1816 Confirmation of generally conservative behaviour. Geochim Cosmochim Acta 56:4099-4103
1817 Andrews DA, Brenan JM (2002a) The solubility of ruthenium in sulfide liquid: Implications for
1818 platinum-group mineral (PGM) stability and sulfide melt/silicate melt partitioning. Chem Geol
1819 192:163-181
1820 Andrews DA, Brenan JM (2002b) Phase Equilibrium Constraints on the Magmatic Origin of Laurite
1821 + Ru-Os-Ir Alloy. Can Mineral 40:1705-1716
1822 Anguita F, Hernan F (1975) A propagating fracture model versus a hot spot origin for the Canary
1823 Islands. Earth Planet Sci Lett 27:11-19
1824 Araujo AJN, Carlson RW, Gaspar JC, Bizzi LA (2001) Petrology of kamfugites and kimberlites from
1825 the Alto Paranaiba alkaline province, Minas Gerais, Brazil. Contrib Mineral Petrol 142:163-177
1826 Argus DF, Gordon RG, DeMets C (2011) Geologically current motion of 56 plates relative to the no-
1827 net-rotation reference frame. Geochem Geophys Geosyst 12.
1828 http://dx.doi.org/10.1029/2011GC003751
1829 Arndt NT (2012) Plates vs. Plumes: a Geological Controversy (2010) Wiley-Blackwell, Chichester,
1830 UK, 364p
1831 Arndt N, Christensen U (1992) The role of lithospheric mantle in continental flood volcanism;
1832 thermal and geochemical constraints. J Geophys Res 97:10967-10981
1833 Arndt NT, Czamanske GK, Wooden JL, Fedorenko VA (1993) Mantle and crustal contributions to
1834 continental flood volcanism. Tectonophysics 223:39-52
1835 Augé T (1985) Platinum-group-mineral inclusions in ophiolitic chromitite from the Vourinos
1836 Complex, Greece. Can Mineral 23:163-171
1837 Augé T (1988) Platinum-group minerals in the Tiebaghi and Vourinos ophiolitic complexes: genetic
1838 implications. Can Mineral 26:177-192
1839 Bach W, Peucker-Ehrenbrink B, Hart SR and Blusztajn JS (2003) Geochemistry of hydrothermally
1840 altered oceanic crust: DSDP/ODP Hole 504B-Implications for sea water-crust exchange

1841 budgets and Sr- and Pb-isotopic evolution of the mantle. Geochem Geophys Geosyst 3.
1842 http://dx.doi.org/10.1029/2002GC000419
1843 Baker JA, Jensen KK (2004) Coupled 186Os–187Os enrichments in the Earth's mantle – core–
1844 mantle interaction or recycling of ferromanganese crusts and nodules? Earth Planet Sci Lett
1845 220:277-286
1846 Ballhaus C, Bockrath C, Wohlgemuth-Ueberwasser C, Laurenz V, Berndt J (2006) Fractionation of
1847 the noble metals by physical processes. Contrib Mineral Petrol 152:667-684
1848 Barfod, DN (1999) Noble Gas Geochemistry of the Cameroon Line Volcanic Chain. (PhD thesis).
1849 Michigan Univ
1850 Barnes SJ, Fiorentini ML (2008) Iridium, ruthenium and rhodium in komatiites: evidence for iridium
1851 alloy saturation. Chem Geol 257:44-58
1852 Barnes S-J, Naldrett AJ, Gorton MP (1985) The origin of the fractionation of platinum-group
1853 elements in terrestrial magmas. Chemical Geology 53:302-323
1854 Bebout GE, Ryan JG, Leeman WP (1993) B-Be systematics in subduction-related metamorphic
1855 rocks: Characterization of the subducted component. Geochim Cosmochim Acta 57:2227-2237
1856 Becker H (2000) Re-Os fractionation in eclogites and blueschists and the implications for recycling
1857 of oceanic crust into the mantle. Earth Planet Sci Lett 177:287-300
1858 Becker H, Jochum KP, Carlson RW (2000) Trace element fractionation during dehydration of
1859 eclogites from high-pressure terranes and the implications for element fluxes in subduction
1860 zones. Chem Geol 163:65-99
1861 Becker H, Horan MF, Walker RJ, Gao S, Lorand JP, Rudnick RL (2006) Highly siderophile element
1862 composition of the Earth's primitive upper mantle: constraints from new data on peridotite
1863 massifs and xenoliths. Geochim Cosmochim Acta 70:4528-4550
1864 Becker H, Dale CW (2015) Re–Pt–Os isotopic and highly siderophile element behavior in oceanic
1865 and continental mantle tectonites. Rev Mineral Geochem 81 xxxxxx
1866 Bennett VC, Norman MD, Garcia MO (2000) Rhenium and platinum group element abundances
1867 correlated with mantle source components in Hawaiian picrites: sulfides in the plume. Earth
1868 Planet Sci Lett 183:513-526
1869 Bezard R, Schaefer BF, Turner S, Davidson JP, Selby D (2015) Lower crustal assimilation in oceanic
1870 arcs: insights from an osmium isotopic study of the Lesser Antilles. Geochim Cosmochim Acta
1871 150:330-344
1872 Bezos A et al. (2005) Platinum-group element systematics in Mid-Oceanic Ridge basaltic glasses
1873 from the Pacific, Atlantic, and Indian Oceans. Geochim Cosmochim Acta 69:2613-2627
1874 Birck JL (2001) The precision and sensitivity of Thermal Ionisation Mass Spectrometry (TIMS): an
1875 overview of the present status. Geostand Geoanal Res 25:253-259
1876 Birck JL, Roy Barman M, Capmas F (1997) Re-Os isotopic measurements at the femtomole level in
1877 natural samples. Geostandards Newsletter 20:9-27
1878 Bird JM, Weathers MS (1975) Josephinite: specimens from the Earth's core?. Earth Planet Sci Lett
1879 28:51-64
1880 Bird JM, Bassett WA (1980) Evidence of a deep mantle history in terrestrial osmium–iridium–
1881 ruthenium alloys. J Geophys Res 85:5461-5470
1882 Bird JM, Meibomb A, Frei R, Nägler TF (1999) Osmium and lead isotopes of rare OsIrRu minerals:
1883 derivation from the core–mantle boundary region?. Earth Planet Sci Lett 170:83-92
1884 Blusztajn J, Hart SR, Ravizza G and Dick HJB (2000) Platinum-group elements and Os isotopic
1885 characteristics of the lower oceanic crust. Chem Geol 168:113-122
1886 Bockrath C, Ballhaus C, Holzheid A (2004a) Fractionation of the platinum-group elements during
1887 mantle melting. Science 305:1951-1953
1888 Bockrath C, Ballhaus C, Holzheid A (2004b) Stabilities of laurite RuS2 and monosulfide liquid
1889 solution at magmatic temperature. Chem Geol 208:265-271

Boivin P, Bachélery P (2009) Petrology of 1977 to 1998 eruptions of Piton de la Fournaise, La Réunion Island. J Volcanol Geotherm Res 184:109-105

Borg LE, Brandon AD, Clynne MA, Walker RJ (2000) Re-Os isotopic systematics of primitive lavas from the Lassen region of the Cascade arc, California. Earth Planet Sci Lett 177:301-317

Borisov A, Jones JH (1999) An evaluation of Re, as an alternative to Pt, for the 1 bar loop technique: an experimental study at 1400 °C. Am Mineral 84:1528-1534

Borisov A, Palme H, Spettel B (1994) Solubility of palladium in silicate melts: implications for core formation in the Earth. Geochim Cosmochim Acta 58:705-716

Borisov A, Palme H (1995) The solubility of iridium in silicate melts: new data from experiments with $Ir_{10}Pt_{90}$ alloys. Geochim Cosmochim Acta 59:481-485

Borisov A, Palme H (1997) Experimental determination of the solubility of platinum in silicate melts. Geochim Cosmochim Acta 61:4349-4357

Borisov A, Palme H (2000) Solubilities of noble metals in Fe containing silicate melts as derived from experiments in Fe-free systems. Am Mineral 85:1665-1673

Botcharnikov RE, Holtz F, Mungall JE, Beermann O, Linnen RL, Garbe-Schoenberg D (2013) Behavior of gold in a magma at sulfide-sulfate transition: Revisited. Amer Mineral 98:1459-1464

Brandl PA, Beier C, Regelous M, Abouchami W, Haase KM, Garbe-Schönberg D, Galer SJG (2012) Volcanism on the flanks of the East Pacific Rise: Quantitative constraints on mantle heterogeneity and melting processes. Chem Geol 298-299:41-56

Brandon AD, Creaser RA, Shirey SB, Carlson RW (1996) Osmium recycling in subduction zones. Science 272:861-864

Brandon AD, Graham DW, Waight T, Gautason B (2007) ^{186}Os and ^{187}Os enrichments and high-3He/4He sources in the Earth's mantle: evidence from Icelandic picrites. Geochim Cosmochim Acta 71:4570-4591

Brandon AD, Norman MD, Walker RJ, Morgan JW (1999) ^{186}Os-^{187}Os systematics of Hawaiian picrites. Earth Planet Sci Lett 174: 25-42

Brandon AD, Snow JE, Walker RJ, Morgan JW, Mock TD (2000) ^{190}Pt-^{186}Os and ^{187}Re-^{187}Os systematics of abyssal peridotites. Earth Planet Sci Lett 177:319-355

Brandon AD, Puchtel IS, Walker RJ, Day JMD, Irving AJ, Taylor LA (2012) Evolution of the martian mantle inferred from the ^{187}Re-^{187}Os isotope and highly siderophile element abundance systematics of shergottite meteorites. Geochim Cosmochim Acta 76:206-235

Brandon AD, Walker RJ, Morgan JW, Norman MD, Prichard HM (1998) Coupled ^{186}Os and ^{187}Os evidence for core-mantle interaction. Science 280:1570-1573

Brandon AD, Walker RJ, Puchtel IS, Becker H, Humayun N, Revillon S (2003) ^{186}Os-^{187}Os systematics of Gorgona Island komatiites: implications for early growth of the inner core. Earth Planet Sci Lett 206:411-426

Brandon AD, Walker RJ, Puchtel IS (2006) Platinum–osmium isotope evolution of the Earth's mantle: constraints from chondrites and Os-rich alloys. Geochim Cosmochim Acta 70:2093-2103

Brenan JM (2008) Re–Os fractionation by sulfide–silicate partitioning: a new spin. Chem Geol 248:140-165

Brenan JM, Andrews D (2001) High Temperature Stability of Laurite and Ru-Os-Ir Alloy and their Role in PGE Fractionation in Mafic Magmas. Can Mineral 39:573-592

Brenan JM, Cherniak DJ, Rose LA (2000) Diffusion of osmium in pyrrhotite and pyrite: implications for closure of the Re-Os isotopic system. Earth Planet Sci Lett 188:399-413

Brenan JM, McDonough WF, Dalpé C (2003) Experimental constraints on the partitioning of rhenium and some platinum-group elements between olivine and silicate melt. Earth Planet Sci Lett 212:135-150

1940 Brenan JM, McDonough WF, Ash R (2005) An experimental study of the solubility and partitioning
1941 of iridium, osmium and gold between olivine and silicate melt. Earth Planet Sci Lett 237:855-
1942 872
1943 Brenan JM and McDonough WF (2009) Core formation and metal-silicate fractionation of osmium
1944 and iridium from gold. Nat Geosci 2:798-801
1945 Brenan JM, Finnegan CF, McDonough WF (2012) Experimental constraints on the partitioning of
1946 Ru, Rh, Ir, Pt and Pd between chromite and silicate melt: the importance of ferric iron. Chem
1947 Geol 302-303:16-32
1948 Brenan JM, Bennett N, Zajacz Z (2015) Fractionation of the highly siderophile elements (HSE)
1949 during planetary differentiation: An overview of results from experiments done at high pressure
1950 and temperature. Rev Mineral Geochem 81:1-74
1951 Brügmann GE, Arndt NT, Hofmann AW, Tobschall HJ (1987) Noble metal abundances in komatite
1952 suites from Alexo, Ontario and Gorgona Island, Columbia. Geochim Cosmochim Acta
1953 51:2159-2169
1954 Burton KW, Schiano P, Birck JL, Allègre CJ (1999) Osmium isotope disequilibrium between mantle
1955 minerals in a spinel-lherzolite. Earth Planet Sci Lett 172:311-322
1956 Burton KW, Schiano P, Birck JL, Allègre CJ, Rehkamper M, Halliday AN, Dawson JB (2000) The
1957 distribution and behaviour of rhenium and osmium amongst mantle minerals and the age of the
1958 lithospheric mantle beneath Tanzania. Earth Planet Sci Lett 183:93-106
1959 Burton KW, Gannoun A, Birck JL, Allègre CJ, Schiano P, Clocchiatti R, Alard O (2002) The
1960 compatibility of rhenium and osmium in natural olivine and their behaviour during mantle
1961 melting and basalt genesis. Earth Planet Sci Lett 198:63-76
1962 Burton KW, Gannoun A, Parkinson, IJ, Schiano, P (2015) No evidence for radiogenic osmium in the
1963 source of mid-ocean ridge basalts from the Indian Ocean. Submitted to Geochim Cosmochim
1964 Acta
1965 Capobianco CJ, Drake MJ (1990) Partitioning of ruthenium, rhodium, and palladium between spinel
1966 and silicate melt and implications for platinum-group element fractionation trends. Geochim
1967 Cosmochim Acta 54:869-874
1968 Capobianco CJ, Hervig RL, Drake MJ (1994) Experiments on crystal/liquid partitioning of Ru, Rh
1969 and Pd for magnetite and hematite solid solutions crystallized from silicate melt. Chem Geol
1970 113:23-43
1971 Carlson RW (2005) Application of the Pt-Re-Os isotopic systems to mantle geochemistry and
1972 geochronology. Lithos 82:249–272
1973 Carlson RW, Nowell GM (2001) Olivine-poor sources for mantle-derived magmas: Os and Hf
1974 isotopic evidence from potassic magmas of the Colorado plateau. Geochem Geophys Geosys 2
1975 (2000GC000128)
1976 Carlson RW, Esperance S, Svisero DP (1996) Chemical and Os isotopic study of Cretaceous potassic
1977 rocks from southern Brazil. Contrib Mineral Petrol 125:393-405
1978 Cebria JM, Lopez-Ruiz J, Doblas M, Martins LT, Munha J (2003) Geochemistry of the Early Jurassic
1979 Messejana-Plasencia dyke (Portugal-Spain); implications on the origin of the Central Atlantic
1980 Magmatic Province. J Petrol 44:547-568
1981 Chalapathi Rao NV, Creaser RA, Lehmann B, Panwar BK (2013) Re–Os isotope study of Indian
1982 kimberlites and lamproites: implications for mantle source regions and cratonic evolution.
1983 Chem Geol 353:36-47
1984 Chaussidon M, Jambon A (1994) Boron content and isotopic composition of oceanic basalts:
1985 geochemical and cosmochemical implications. Earth Planet Sci Lett 121:277–291
1986 Chaussidon M, Marty B (1995) Primitive isotope composition of the mantle. Science 269:383-386
1987 Chatterjee R, Lassiter JC (2015) High precision Os isotopic measurement using N-TIMS:
1988 Quantification of various sources of error in $^{186}Os/^{188}Os$ measurements. Chem Geol 396:112-
1989 123

Chazey WJ, Neal CR (2005) Platinum-group element constraints on source composition and magma evolution of the Kerguelen Plateau using basalts from ODP Leg 183. Geochim Cosmochim Acta 19:4685-4701

Chen C, Sedwick PN, Sharma M (2009) Anthropogenic osmium in rain and snow reveals global-scale atmospheric contamination. P Nat Acad Sci USA 106:7724-7728

Chesley JT, Ruiz J (1998) Crust–mantle interaction in large igneous provinces: implications from Re-Os isotope systematics of the Columbia River flood basalts. Earth Planet Sci Lett 154:1-11

Chesley J, Ruiz J, Righter K, Ferrari L, Gomez-Tuena A (2002) Source contamination versus assimilation: an example from the Trans-Mexican Volcanic Arc. Earth Planet Sci Lett 195:211-221

Chou CL (1978) Fractionation of siderophile elements in the Earth's upper mantle. Proc Lunar Planet Sci Conf. 9:219-230

Chu ZY, Harvey J, Liu CZ, Guo JH, Wu FY, Tian W, Zhang YL, Yang YH (2013) Source of highly potassic basalts in northeast China: evidence from Re-Os, Sr-Nd-Hf isotopes and PGE geochemistry. Chem Geol 357:52-66

Class C, Goldstein SL, Shirey SB (2009) Osmium isotopes in Grand Comore lavas: A new extreme among a spectrum of EM-type mantle endmembers. Earth Planet Sci Lett 284:219-227

Clocchiatti R (1977) Les inclusions vitreuses des phenocristaux d'olivine et de chromite d'un 'basalte picritique' de la ride medio-atlantique: témoins de la contamination mécanique d'un basalte a olivine. C R Acad Sci Paris 285:1155-1158

Colodner D, Sachs J, Ravizza G, Turekian K, Edmond J, Boyle E (1993) The geochemical cycle of rhenium: a reconnaissance. Earth Planet Sci Lett 117:205-221

Coltice N, Bertrand H, Rey P, Jourdan F, Philipps BR, Ricard Y (2009). Global warming of the mantle beneath continents back to the Archean. Gondwana Res 15:254-266

Condomines M, Morand P, Allègre CJ (1981) ^{230}Th-^{238}U radioactive disequilibria in tholeiites from the Famous zone (Mid Atlantic Ridge, 36°50'N: Th and Sr isotopic geochemistry. Earth Planet Sci Lett 121:247-256

Connolly BD, Puchtel IS, Walker RJ, Arevalo R, Piccoli PM, Byerly G, Robin-Popieul C, Arndt N (2011) Highly siderophile element systematics of the 3.3 Ga Weltevreden komatiites, South Africa: implications for early Earth history. Earth Planet Sci Lett 311:253-263

Conticelli S, Carlson RW, Widom E, Serri G (2007) Chemical and isotopic composition (Os, Pb, Nd, and Sr) of Neogene to Quaternary calc-alkalic, shoshonitic, and ultrapotassic mafic rocks from the Italian peninsula: inferences on the nature of their mantle sources. Geol Soc Am Special Paper 418:171-202

Coogan LA (2014) The lower oceanic crust. In Treatise on Geochemistry (eds. K. Turekian and H. D. Holland). Elsevier, pp. 497-541

Cottrell E, Walker D (2006) Constraints on core formation from Pt partitioning in mafic silicate liquids at high temperatures. Geochim Cosmochim Acta 70:1565–1580

Courtillot V, Jaupart C, Manighetti I, Tapponnier P, Besse J (1999) On causal links between flood basalts and continental breakup. Earth Planet Sci Lett 166:177-195

Courtillot V, Davaille A, Besse J, Stock J (2003) Three distinct types of hotspots in the Earth's mantle. Earth Planet Sci Lett 205:295-308

Craciun R, Picone D, Long RT, Li S, Dixon DA (2010) Third row transition metal hexafluorides, extraordinary oxidizers, and Lewis acids: electron affinities, fluoride affinities, and heats of formation of WF_6, ReF_6, OsF_6, IrF_6, PtF_6, and AuF_6. Inorg Chem 49:1056-1070

Crank J (1975) The Mathematics of Diffusion. Oxford University Press, New York

Creaser RA, Papanastassiou DA, Wasserburg GJ (1991) Negative thermal ion mass spectrometry of osmium, rhenium, and iridium. Geochim Cosmochim Acta 55:397-401

Crocket JH (2000) PGE in fresh basalt, hydrothermal alteration products, and volcanic incrustations of Kilauea volcano, Hawaii. Geochim Cosmochim Acta 64:1791-1807

2040 Crocket JH (2002) Platinum-group elements in basalts from Maui, Hawai'i: low abundances in alkali
2041 basalts. Can Mineral 40:595-609
2042 Crockett JH, Fleet ME, Stone WE (1997) Implications of composition for experimental partitioning
2043 of platinum-group elements and gold between sulfide liquid and basalt melt: The significance
2044 of nickel content. Geochim Cosmochim Acta 61:4139-4149
2045 Czamanske GK, Moore JG (1977) Composition and phase chemistry of sulfide globules in basalt in
2046 the Mid-Atlantic Ridge rift valley near 37°N lat. Geol Soc Am Bull 88:587-599
2047 Dale CW, Gannoun A, Burton KW, Argles TW, Parkinson IJ (2007) Rhenium-osmium isotope and
2048 elemental behaviour during subduction of oceanic crust and the implications for mantle
2049 recycling. Earth Planet Sci Lett 177:211-225
2050 Dale CW, Burton KW, Pearson DG, Gannoun A, Alard O, Argles TW, Parkinson IJ (2009a) Highly
2051 siderophile element behaviour accompanying subduction of oceanic crust: whole rock and
2052 mineral-scale insights from a high-pressure terrain. Geochim Cosmochim Acta 73:1394-1416
2053 Dale CW, Pearson DG, Starkey NA, Stuart FM, Ellam RM, Larsen LM, Fitton JG, Macpherson CG
2054 (2009b) Osmium isotopes in Baffin Island and West Greenland picrites: implications for the
2055 187Os/188Os composition of the convecting mantle and the nature of the high 3He/4He mantle.
2056 Earth Planet Sci Lett 278:267-277
2057 Dale CW, Burton KW, Greenwood RC, Gannoun A, Wade J, Wood BJ, Pearson DG (2012a) Late
2058 accretion on the earliest planetesimals revealed by the highly siderophile elements. Science
2059 336:72-75
2060 Dale CW, Macpherson CG, Pearson DG, Hammond SJ, Arculus RJ (2012b) Inter-element
2061 fractionation of highly siderophile elements in the Tonga Arc due to flux melting of a depleted
2062 source. Geochim Cosmochim Acta 89:202–225
2063 Day JMD (2013) Hotspot volcanism and highly siderophile elements. Chem Geol 341:50-74
2064 Day JMD, Walker RJ (2015) Highly siderophile element depletion in the Moon. Earth Planet Sci Lett
2065 423:114-124
2066 Day JMD, Hilton DR, Pearson, DG, Macpherson CG, Kjarsgaard BA, Janney PE (2005) Absence of
2067 a high time-integrated ^{3}He/(U+Th) source in the mantle beneath continents. Geology 33, 733-
2068 736
2069 Day JMD, Pearson DG, Taylor LA (2007) Highly siderophile element constraints on accretion and
2070 differentiation of the Earth–Moon system. Science 315:217-219
2071 Day JMD, Pearson DG, Macpherson CG, Lowry D, Carracedo J-C (2009). Pyroxenite-rich mantle
2072 formed by recycled oceanic lithosphere: oxygen–osmium isotope evidence from Canary Island
2073 lavas. Geology 37:555-558
2074 Day JMD, Walker RJ, James OB, Puchtel IS (2010a) Osmium isotope and highly siderophile element
2075 systematics of the lunar crust. Earth Planet Sci Lett 289:595-605
2076 Day JMD, Pearson DG, Macpherson CG, Lowry D, Carracedo J-C (2010b) Evidence for distinct
2077 proportions of subducted oceanic crust and lithosphere in HIMU-type mantle beneath El Hierro
2078 and La Palma, Canary Islands. Geochim Cosmochim Acta 74:6565-6589
2079 Day JMD, Walker RJ, Qin L, Rumble D (2012) Late accretion as a natural consequence of planetary
2080 growth. Nat Geosci 5:614-617
2081 Day JMD, Brandon AD, Walker RJ (2015) Highly siderophile elements in terrestrial bodies. Rev
2082 Mineral Geochem 81:161-227
2083 Day JMD, Waters CL, Schaefer BF, Walker RJ, Turner S (2015) Use of hydrofluoric acid
2084 desilicification in the determination of highly siderophile element abundances and Re-Pt-Os
2085 isotope systematics in mafic-ultramafic rocks. Geostandard and Geoanalytical Research doi:
2086 10.1111/j.1751-908X.2015.00367.x
2087 Debaille V, Trønnes RG, Brandon AD, Waight TE, Graham DW, Lee C-TA (2009) Primitive off-rift
2088 basalts from Iceland and Jan Mayen: Os-isotopic evidence for a mantle source containing
2089 enriched subcontinental lithosphere. Geochim Cosmochim Acta 73:3423-3449

2090 Deckart K, Bertrand H, Liegeois J-P (2005) Geochemistry and Sr, Nd, Pb isotopic composition of the
2091 Central Atlantic Magmatic Province (CAMP) in Guyana and Guinea. Lithos 82:289-314
2092 DeMets C, Gordon RG, Argus DF (2010) Geologically current plate motions. Geophys J Internat
2093 181:1-80
2094 De Min A, Piccirillo EM, Marzoli A, Bellieni G, Renne PR, Ernesto M, Marques L (2003) The
2095 Central Atlantic Magmatic Province (CAMP) in Brazil: Petrology, Geochemistry, $^{40}Ar/^{39}Ar$
2096 ages, paleomagnetism and geodynamic implications. In: Hames WE, McHone JG, Renne PR,
2097 Ruppel C (eds) The Central Atlantic Magmatic Province: Insights from Fragments of Pangea.
2098 Geophysical Monograph, Am Geophys Union 136:209-226
2099 DePaulo DJ (1981) Trace element and isotopic effects of combined wallrock assimilation and
2100 fractional crystallization. Earth Planet Sci Lett 53:189-202
2101 DePaolo DJ, Wasserburg GJ (1976) Nd isotopic variations and petrogenetic models. Geophys Res
2102 Lett 3:249-252
2103 Dick HJB, Fisher RL, Bryan WB (1984) Mineralogic variability of the uppermost mantle along mid-
2104 ocean ridge. Earth Planet Sci Lett 69:88-106
2105 Dick HJB and 27 others (2000) A long in situ section of the lower ocean crust: Results of ODP Leg
2106 176 drilling at the Southwest Indian Ridge. Earth Planet Sci Lett 179:31-51
2107 Dorais MJ, Tubrett M (2008) Identification of a subduction zone component in the Higganum dyke,
2108 Central Atlantic Magmatic province: a LA-ICP-MS study of clinopyroxenes with implication
2109 for flood basalt petrogenesis. Geochem Geophys Geosys 9:Q10005,
2110 doi:10.1029/2008GC002079
2111 Dosso L, Bougault H, Beuzart P, Calvez JY, Joron JL (1988) The geochemical structure of the
2112 South-East Indian ridge. Earth Planet Sci Lett 88:47-59
2113 Dosso L, Bougault H, Joron JL (1993) Geochemical morphology of the North Mid-Atlantic Ridge,
2114 IO'-24"N: Trace element-isotope complementarity. Earth Planet Sci Lett 120:443-462
2115 Drake M, Righter K (2002) Determining the composition of the Earth. Nature 416:39-44
2116 Dungan MA, Rhodes JM (1978) Residual glasses and melt inclusions in basalts from DSDP Legs 45
2117 and 46: evidence for magma mixing. Contrib. Mineral. Petrol. 67: 417-431.
2118 Dupré B, Allègre CJ (1983) Pb–Sr isotope variation in Indian Ocean basalts and mixing phenomena.
2119 Nature 303:142-146
2120 Ebel DS, Naldrett AJ (1997) Crystallization of sulfide liquids and the interpretation of ore
2121 composition. Can J Earth Sci 34:352-365
2122 Eisele J, Sharma M, Galer SJG, Blichert-Toft J, Devey CW, Hofmann AW (2002) The role of
2123 sediment recycling in EM-1 inferred from Os, Pb, Hf, Nd, Sr isotopes and trace element
2124 systematics of the Pitcairn hotspot. Earth Planet Sci Lett 196:197-212
2125 Ellam RM, Carlson RW, Shirey SB (1992) Evidence from Re-Os isotopes for plume lithosphere
2126 mixing in Karoo flood basalt genesis. Nature 359:718–721
2127 Ernst RE, Buchan KL (2002). Maximum size and distribution in time and space of mantle plumes:
2128 evidence from large igneous provinces. J Geodyn 31:309-342
2129 Ertel W, O'Neill HStC, Sylvester PJ and Dingwell DB (1999) Solubilities of Pt and Rh in
2130 haplobasaltic silicate melt at 1300 °C. Geochim Cosmochim Acta 63:2439-2449
2131 Ertel W, O'Neill HStC, Sylvester PJ, Dingwell DB, Spettel B (2001) The solubility of rhenium in
2132 silicate melts: implications for the geochemical properties of rhenium at high temperatures.
2133 Geochim Cosmochim Acta 65:2161-2170
2134 Ertel W, Drake MJ, Walter MJ, Sylvester PJ (2006) Experimental study of platinum solubility in
2135 silicate melt to 14 GPa and 2273 K: implications for accretion and core formation in Earth.
2136 Geochim Cosmochim Acta 70:2591-2602
2137 Escrig S, Capmas F, Dupré B, Allègre CJ (2004) Osmium isotopic constraints on the nature of the
2138 DUPAL anomaly from Indian mid-ocean-ridge basalts. Nature 431:59-63

2139 Escrig S, Schiano P, Schilling J-G, Allègre CJ (2005a) Rhenium–osmium isotope systematics in
2140 MORB from the Southern Mid-Atlantic Ridge (40–50°S). Earth Planet Sci Lett 235:528-548
2141 Escrig S, Doucelance R, Moriera M, Allègre CJ (2005b) Os isotope systematics in Fogo Island:
2142 evidence for lower continental crust fragments under the Cape Verde Southern Islands. Chem
2143 Geol 219:93-113
2144 Falloon TJ, Danyushevsky LV, Ariskin A, Green DH, Ford CE (2007) The application of olivine
2145 geothermometry to infer crystallisation temperatures of parental liquids: implications for the
2146 temperature of MORB magmas. Chem Geol 241:207-233
2147 Fischer-Gödde M, Becker H, Wombacher F (2011) Rhodium, gold and other highly siderophile
2148 elements in orogenic peridotites and peridotite xenoliths. Chem Geol 280:365-383
2149 Fischer-Gödde M, Becker H (2012) Osmium isotope and highly siderophile element constraints on
2150 ages and nature of meteoritic components in ancient lunar impact rocks. Geochim Cosmochim
2151 Acta, 77:135-156
2152 Fleet ME, Stone WE, Crocket JH (1991) Partitioning of palladium, iridium, and platinum between
2153 sulfide liquid and basalt melt: effects of melt composition, concentration and oxygen fugacity.
2154 Geochim Cosmochim Acta 55:2545-2554
2155 Fleet ME, Crocket JH, Stone WE (1996) Partitioning of platinum group elements (Os, Ir, Ru, Pt, Pd)
2156 and gold between sulfide liquid and basalt melt. Geochim Cosmochim Acta 60:2397–2412
2157 Foley S (1992) Petrological characterization of the source components of potassic magmas:
2158 geochemical and experimental constraints. Lithos 28:187-204
2159 Fonseca ROC, Campbell IH, O'Neill HStC, Allen C,M (2009) Solubility of Pt in sulfide mattes:
2160 Implications for the genesis of PGE-rich horizons in layered intrusions. Geochim Cosmochim
2161 Acta 73:5764-5777
2162 Fonseca ROC, Mallmann G, O'Neill HStC, Campbell IH, Laurenz V (2011) Solubility of Os and Ir
2163 in sulfide melt: Implications for Re/Os fractionation during mantle melting. Earth Planet Sci
2164 Lett 311-339-350
2165 Fonseca ROC, Laurenz V, Mallmann G, Luguet A, Hoehne N, Jochum KP (2012) New constraints
2166 on the genesis and long-term stability of Os-rich alloys in the Earth's mantle. Geochim
2167 Cosmochim Acta 87:227-242
2168 Fortenfant SS, Gunther D, Dingwell DB, Rubie DC (2003) Temperature dependence of Pt and Rh
2169 solubilities in a haplobasaltic melt. Geochim Cosmochim Acta 67:123-131
2170 Fortenfant SS, Dingwell DB, Ertel-Ingrisch W, Capmas F, Birck JL, Dalpe C (2006) Oxygen
2171 fugacity dependence of Os solubility in haplobasaltic melt. Geochim Cosmochim Acta 70:742-
2172 756
2173 Gaetani GA, Grove TL (1997) Partitioning of moderately siderophile elements among olivine,
2174 silicate melt, and sulfide melt: Constraints on core formation in the Earth and Mars. Geochim
2175 Cosmochim Acta 61:1829-1846
2176 Gaffney AM, Nelson BK, Reisberg L, Eiler J (2005) Oxygen-osmium isotope systematics of West
2177 Maui lavas: a record of shallow-level magmatic processes. Earth Planet Sci Lett 239:122-139
2178 Gannoun A, Burton KW, Thomas LH, Parkinson IJ, Calsteren PV, Schiano P (2004) Osmium isotope
2179 heterogeneity in the constituent phases of mid-ocean ridge basalts. Science 303:70-72
2180 Gannoun A, Burton KW, Vigier N, Gíslason S, Rogers NW, Mokadem M, Sigfússon B (2006) The
2181 influence of weathering process on riverine osmium isotopes in a basaltic terrain. Earth Planet
2182 Sci Lett 243:732-748
2183 Gannoun A, Burton KW, Parkinson IJ, Alard O, Schiano P, Thomas LE (2007) The scale and origin
2184 of the osmium isotope variations in mid-ocean ridge basalts. Earth Planet Sci Lett 259:541–556
2185 Gannoun A, Burton KW (2014) High precision osmium elemental and isotope measurements of
2186 North Atlantic seawater. J Anal At Spectrom 29:2330-2342

2187 Gannoun A, Burton KW, Barfod DN, Schiano P, Vlastélic I, Halliday AN (2015a) Resolving mantle
2188 and magmatic processes in basalts from the Cameroon volcanic line using the Re-Os isotope
2189 system. Lithos 224-225:1-12
2190 Gannoun A, Vlastélic I, Schiano P (2015b) Escape of unradiogenic osmium during sub-aerial lava
2191 degassing: Evidence from fumarolic deposits, Piton de la Fournaise, Réunion Island. Geochim
2192 Cosmochim Acta 166:312-326
2193 Gao S, Rudnick RL, Xu WL, Yuan HL, Liu YS, Walker RJ, Puchtel IS, Liu X, Huang H, Wang XR,
2194 Yang J (2008) Recycling deep cratonic lithosphere and generation of intraplate magmatism in
2195 the North China Craton. Earth Planet Sci Lett 270:41-53
2196 Gibson SA, Thompson RN, Day JA (2006) Timescales and mechanisms of plume-lithosphere
2197 interactions: 40Ar/39Ar geochronology and geochemistry of alkaline igneous rocks from the
2198 Paraná-Etendeka large igneous province. Earth Planet Sci Lett 251:1-17
2199 Gill J, Williams R, Bruland K (1985) Eruption of basalt and andesite lava degasses ^{222}Rn and ^{210}Po.
2200 Geophys Res Lett 12:17-20
2201 Godard M, Lagabrielle Y, Alard O, Harvey J (2008) Geochemistry of the highly depleted peridotites
2202 drilled at ODP Sites 1272 and 1274 (Fifteen-Twenty Fracture Zone, Mid-Atlantic Ridge):
2203 Implications for mantle dynamics beneath a slow spreading ridge. Earth Planet Sci Lett
2204 267:410-425
2205 González-Jiménez JM, Gervilla F, Proenza JA, Kerestedjian T, Augé T, Bailly L (2009) Zoning of
2206 laurite (RuS_2)–erlichmanite (OsS_2): implications for the origin of PGM in ophiolite chromitites.
2207 Eur J Mineral 21:419-432
2208 González-Jiménez JM, Proenza JA, Gervilla F, Melgarejo JC, Blanco-Moreno JA, Ruiz-Sánchez R,
2209 Griffin WL (2011) High-Cr and high-Al chromitites from the Sagua de Tánamo district,
2210 Mayarí-Cristal ophiolitic massif (eastern Cuba): Constraints on their origin from mineralogy
2211 and geochemistry of chromian spinel and platinum-group elements. Lithos 125:101-121
2212 Green DH (1971) Compositions of basaltic magmas as indicators of conditions of origin: application
2213 to oceanic volcanism. Phil Trans R Soc Lond Ser A 268:707-725
2214 Grimes CB, John BE, Cheadle MJ, Wooden JL (2008) Protracted construction of gabbroic crust at a
2215 slow spreading ridge: Constraints from 206Pb238U zircon ages from Atlantis Massif and IODP
2216 Hole U1309D (30°N, MAR). Geochem Geophys Geosyst 9.
2217 http://dx.doi.org/10.1029/2008GC002063
2218 Grove TL, Kinzler, RJ, Bryan, WB (1993) Fractionation of mid-ocean ridge basalt (MORB). *In*:
2219 Mantle Flow and Melt Migration at Mid-Ocean Ridges, Phipps-Morgan J. et al. (ed) American
2220 Geophysical Monograph 71:281-311
2221 Gudfinnsson GH, Presnall DC (2005) Continuous gradations among primary carbonatitic,
2222 kimberlitic, melilititic, basaltic, picritic, and komatiitic melts in equilibrium with garnet
2223 lherzolite at 3–8 GPa. J Petrol 46:1645-1659
2224 Haggerty SE (1999) A diamond trilogy: superplumes, supercontinents and supernovae. Science
2225 285:851-860
2226 Hamelin B, Allègre CJ (1985) Large-scale units in the depleted upper mantle revealed by an isotope
2227 study of the Southwest Indian Ridge. Nature 315:196-199
2228 Hamelin B, Dupre D, Allègre CJ (1984) Lead-strontium isotopic variations along the East Pacific
2229 Rise and the Mid-Atlantic Ridge: a comparative study. Earth Planet Sci Lett 67:340-350
2230 Hamelin B, Dupre D, Allègre CJ (1986) Pb-Sr-Nd isotopic data of Indian Ocean ridges: new
2231 evidence of large-scale mapping of mantle heterogeneities. Earth Planet Sci Lett 76:286-296
2232 Hanyu T, Tatsumi Y, Senda R, Miyazaki T, Chang Q, Hirahara Y, Takahashi T, Kawabata H, Suzuki
2233 K, Kimura J-I (2011), Geochemical characteristics and origin of the HIMU reservoir: A
2234 possible mantle plume source in the lower mantle. Geochem Geophys Geosyst 12: Q0AC09,
2235 doi:10.1029/2010GC003252.

2236 Hart SR (1984) A large-scale isotope anomaly in the southern hemisphere mantle. Nature 309:753-
2237 757
2238 Hart SR, Ravizza G (1996) Os partitioning between phases in lherzolite and basalt. In: Earth
2239 Processes: Reading the isotopic Code. Union Geophys Monogr. Vol 95. Basu A, Hart SR (ed),
2240 p 123-134
2241 Hart SR, Gaetani GA (2006) Mantle Pb paradoxes: the sulfide solution. Contrib Mineral Petrol
2242 152:295-308
2243 Hart SR, Blusztajn J, Dick HJB, Meyer PS, Muehlenbachs K (1999) The fingerprint of seawater
2244 circulation in a 500-meter section of ocean crust gabbro. Geochim Cosmochim Acta 63:4059-
2245 4080
2246 Harvey J, Gannoun A, Burton KW, Rogers NW, Alard O, Parkinson IJ (2006) Ancient melt
2247 extraction from the oceanic upper mantle revealed by Re-Os isotopes in abyssal peridotites
2248 from the Mid-Atlantic ridge. Earth Planet Sci Lett 244:606-621
2249 Harvey J, Gannoun A, Burton KW, Rogers NW, Schiano P, Alard O (2010) Unravelling the effects
2250 of melt depletion and secondary infiltration on mantle Re-Os isotopes beneath the French
2251 Massif Central. Geochim Cosmochim Acta 74:293-320
2252 Harvey J, Dale CW, Gannoun A, Burton KW (2011) Osmium mass balance in peridotite and the
2253 effects of mantle-derived sulfides on basalt petrogenesis. Geochim Cosmochim Acta 75:5574-
2254 5596
2255 Harvey J, Savov IP, Agostini S, Cliff RA, Walshaw RD (2014a) Si-metasomatism in serpentinized
2256 peridotite: the effects of talc-alteration on strontium and boron isotopes in abyssal peridotites
2257 from Hole 1268a, ODP Leg 209. Geochim Cosmochim Acta 126:30-48
2258 Harvey J, Garrido CJ, Savov I, Agostini S, Padrón-Navarta JA, Marchesi C, Lopez Sánchez-Vizcaíno
2259 V, Gómez-Pugnaire MT (2014b). ^{11}B-rich fluids in subduction zones: the role of antigorite
2260 dehydration in subducting slabs and boron isotope heterogeneity in the mantle. Chem Geol
2261 376:20-30
2262 Harvey J, Warren JM, Shirey SB (2015) Mantle sulfides and their role in Re-Os and Pb isotope
2263 geochronology. Rev Mineral Geochem 81:579-635
2264 Hauri EH, (2002) Osmium isotopes and mantle convection. Phil Trans R Soc Lond 360:2371-2382
2265 Hauri EH, Hart SR (1993) Re-Os isotope systematics of HIMU and EMII oceanic island basalts from
2266 the South Pacific Ocean. Earth Planet Sci Lett 114-353-371
2267 Hauri EH, Hart SR (1997) Rhenium abundances and systematics in oceanic basalts. Chem Geol
2268 139:185-205
2269 Hayashi HE, Ohtani E, Terasaki H, Ito Y (2009) The partition of Pt-Re-Os between solid and liquid
2270 metal in the Fe-Ni-S system at high pressure: implications for inner core fractionation. Geochim
2271 Cosmochim Acta 73:4836-4842
2272 Heinonen JS, Carlson RW, Luttinen AV (2010) Isotopic (Sr, Nd, Pb, and Os) composition of highly
2273 magnesian dykes of Vestfjella, western Dronning Maud Land, Antarctica: A key to the origins
2274 of the Jurassic Karoo large igneous province? Chem Geol 277:227-244
2275 Heinonen J, Carlson RW, Riley TR, Luttinen AV, Horan MF (2014) Subduction-modified oceanic
2276 crust mixed with a depleted mantle reservoir in the sources of the Karoo continental flood
2277 basalt province. Earth Planet Sci Lett 394:229-241
2278 Hill RI (1991) Starting plumes and continental break-up. Earth Planet Sci Lett 104:398-416
2279 Hill E, Wood BJ, Blundy JD (2000) The effect of Ca-Tschermaks component on trace element
2280 partitioning between clinopyroxene and silicate melt. Lithos 53:203-215
2281 Hirschmann MM, Stolper EM (1996) A possible role for garnet pyroxenite in the origin of the ‘garnet
2282 signature’ in MORB. Contrib Mineral Petrol 124(2):185-208
2283 Hirschmann MM, Kogiso T, Baker MB, Stolper EM (2003) Alkalic magmas generated by partial
2284 melting of garnet pyroxenite. Geology 31:481-484

Hirt B, Tilton GR, Herr W, Hoffmeister W (1963) The half life of ^{187}Re. In: Geiss, J. and Goldberg, E. (Eds), Earth Science Meteoritics. North Holland Pub., pp. 273-280.

Hirth G, Kohlstedt DL (1996) Water in the oceanic upper mantle: implications for rheology, melt extraction and the evolution of the lithosphere. Earth Planet Sci Lett 144:93-108

Hofmann AW (1997) Mantle geochemistry: the message from oceanic volcanism. Nature 385:219-229

Hofmann AW (2003) Sampling mantle heterogeneity through oceanic basalts: isotopes and trace elements, in: Carlson RW (ed), The Mantle, Treatise on Geochemistry vol. 2 (eds Holland HD, Turekian KK). Elsevier-Pergamon, Oxford, pp. 61-101

Hofmann AW, Hart SR (1978) An assessment of local and regional isotopic equilibrium in the mantle. Earth Planet Sci Lett 38:44-62Holzheid A, Sylvester P, O'Neill HStC, Rubie DC, Palme H (2000) Evidence for a late chondritic veneer in the Earth's mantle from high-pressure partitioning of palladium and platinum. Nature 406:396-399

Holzheid A, Sylvester P, O'Neill HStC, Rubie DC, Palme H (2000) Evidence for a late chondritic veneer in the Earth's mantle from high-pressure partitioning of palladium and platinum. Nature 406:396-399

Horan MF, Walker RJ, Fedorenko VA, Czamanske GK (1995) Osmium and neodymium isotopic constraints on the temporal and spatial evolution of Siberian flood basalt sources. Geochim Cosmochim Acta 59:5159-5168

Horan MF, Walker RJ, Morgan JW, Grossman JN, Rubin A (2003) Highly siderophile elements in chondrites. Chem Geol 196:5-20

Ireland TJ, Walker RJ, Garcia MO (2009) Highly siderophile element and ^{187}Os isotope systematics of Hawaiian picrites: implications for parental melt composition and source heterogeneity. Chem Geol 260:112-128

Ireland TJ, Walker RJ, Brandon AD (2011) ^{186}Os-^{187}Os systematics of Hawaiian picrites revisited: new insights into Os isotopic variations in ocean island basalts. Geochim Cosmochim Acta 75:4456-4475

Ishikawa T, Tera F, Nakazawa T (2001) Boron isotope and trace element systematics of the three volcanic zones in the kamchatka arc. Geochim Cosmochim Acta 65:4523-4537

Ishikawa A, Senda R, Suzuki K, Dale CW, Meisel T (2014) Re-evaluating digestion methods for highly siderophile element and ^{187}Os isotope analysis: Evidence from geological reference materials. Chem Geol 384:27-46

Jackson MG, Shirey SB (2011) Re-Os isotope systematics in Samoan shield lavas and the use of Os-isotopes in olivine phenocrysts to determine primary magmatic compositions. Earth Planet Sci Lett 312:91-101

Jamais M, Lassiter JC, Brügmann G (2008) PGE and Os-isotopic variations in lavas from Kohala Volcano, Hawaii: constraints on PGE behaviour and melt-crust interaction. Chem Geol 250:16-28

Jambon A, Druelle B, Dreibus G, Pineau F (1995) Chlorine and bromine abundance in MORB: the contrasting behaviour of the Mid-Atlantic Ridge and East Pacific Rise and implications for chlorine geodynamic cycle. Chem Geol 126:101-117

Jenner FE, O'Neill HStC (2012) Analysis of 60 elements in 616 ocean floor basaltic glasses. Geochem Geophys Geosys 13. http://dx.doi.org /10.1029/2011/GC004009.

Johnson KTM, Dick HJB (1992) Open system melting and temporal and spatial variation of peridotite and basalt at the Atlantis II fracture zone. J Geophys Res 97:9219-9241

Jones JH, Drake MD (1986) Geochemical constraints on core formation in the Earth. Nature 322:221-228

Katz RF, Weatherley SM (2012) Consequences of mantle heterogeneity for melt extraction at mid-ocean ridges. Earth Planet Sci Lett 335-336:226-237

2334 Kay RW (1985) Island arc processes relevant to crustal and mantle evolution. Tectonophysics 112:1-
2335 15
2336 Keays RR, Lightfoot PC (2007) Siderophile and chalcophile metal variations in Tertiary picrites and
2337 basalts from West Greenland with implications for the sulfide saturation history of continental
2338 flood basalt magmas. Miner Deposita 42:319-336
2339 Kent AJR, Stolper EM, Francis D, Woodhead J, Frei R, Eiler J (2004) Mantle heterogeneity during
2340 the formation of the North Atlantic Igneous Province: constraints from trace elements and Sr-
2341 Nd-Os-O isotope systematics of Baffin Island picrites. Geochem Geophys Geosys 5:Q11004,
2342 http://dx.doi.org/10.1029/2004GC000743
2343 Kerr AC, Mahoney JJ (2007) Oceanic plateaus: problematic plumes, potential paradigms. Chem Geol
2344 241:332-353
2345 Kimura K, Lewis RS, Anders E (1974) Distribution of gold and rhenium between nickel-iron and
2346 silicate melts: implications for the abundance of siderophile elements on the Earth and Moon.
2347 Geochim Cosmochim Acta 38:683-701
2348 Kiseeva ES, Wood BJ (2015) The effects of composition and temperature on chalcophile and
2349 lithophile element partitioning into magmatic sulphides. Earth Planet Sci Lett 424:280-294
2350 Klein EM, Langmuir CH (1987) Global correlations of ocean ridge basalt chemistry with axial depth
2351 and crustal thickness. J Geophys Res 92:8089-8115
2352 Kogiso T, Hirschmann MM, Pertermann M (2004) High-pressure partial melting of mafic lithologies
2353 in the mantle. J Petrol 45:2407-2422
2354 Kogiso T, Suzuki K, Suzuki T, Shinotsuka K, Uesugi K, Takeuchi A, Suzuki Y (2008) Detecting
2355 micrometer-scale platinum-group minerals in mantle peridotite with microbeam synchrotron
2356 radiation X-ray fluorescence analysis. Geochem Geophys Geosys 9.
2357 http://dx.doi.org/10.1029/2007/GC001888.
2358 Kumar N, Reisberg L, Zindler A (1996) A major and trace element and strontium, neodymium, and
2359 osmium isotopic study of a thick pyroxenite layer from the Beni Bousera Ultramafic Complex
2360 of northern Morocco. Geochim Cosmochim Acta 60:1429-1444
2361 Kwékam M, Affaton P, Bruguier B, Liégeois JP, Hartmann G, Njonfang E (2013) The Pan-African
2362 Kekem gabbro-norite (West-Cameroon), U–Pb zircon age, geochemistry and Sr–Nd isotopes:
2363 geodynamical implication for the evolution of the Central African fold belt. J Afr Earth Sci
2364 84:70-88
2365 Lambart S, Laporte D, Provost A, Schiano P (2012) Fate of pyroxenite-derived melts in the
2366 peridotitic mantle: thermodynamic and experimental constraints. J Petrol 53:451-476
2367 Lambart S, Laporte D, Schiano P (2013) Markers of the pyroxenite contribution in the major-element
2368 compositions of oceanic basalts: Review of the experimental constraints. Lithos 160-161:14-36
2369 Lambert G, Le Cloarec MF, Ardouin B, Le Roulley JC (1986) Volcanic emission of radionuclides
2370 and magma dynamics. Earth Planet Sci Lett 76:185-192
2371 Lassiter JC (2003) Rhenium volatility in subaerial lavas: Constraints from subaerial and submarine
2372 portions of the HSDP-2 Mauna Kea drillcore. Earth Planet Sci Lett 214:311-325
2373 Lassiter JC, Hauri EH (1998) Osmium-isotope variations in Hawaiian lavas: evidence for recycled
2374 oceanic lithosphere in the Hawaiian plume. Earth Planet Sci Lett 164:483-496
2375 Lassiter JC, Luhr JF (2001) Osmium abundance and isotope variations in mafic Mexican volcanic
2376 rocks: evidence for crustal contamination and constraints on the geochemical behavior of
2377 osmium during partial melting and fractional crystallization. Geochem Geophys Geosys 2:1027.
2378 http://dx.doi.org/10.1029/2000GC000116
2379 Lassiter JC, Hauri EH, Reiners PW, Garcia MO (2000) Generation of Hawaiian post erosional lavas
2380 by melting of a mixed lherzolite/pyroxenite source. Earth Planet Sci Lett 178:269-284
2381 Lassiter JC, Blichert-Toft J, Hauri EH, Barsczus HG (2003) Isotope and trace element variations in
2382 lavas from Raivavae and Rapa, Cook-Austral Islands: constraints on the nature of HIMU- and

EM-mantle and the origin of mid-plate volcanism in French Polynesia. Chem Geol 202:115-138

Lassiter JC, Byerly BL, Snow JE, Hellebrand E (2014) Constraints from Os-isotope variations on the origin of Lena Trough abyssal peridotites and implications for the composition and evolution of the depleted upper mantle. Earth Planet Sci Lett 403:178-187

Laurenz V, Fonseca ROC, Ballhaus C, Jochum KP, Heuser A, Sylvester PJ (2013) Solubility of palladium and ruthenium in picrite melts: 2. The effect of sulfur. Geochim Cosmochim Acta 108:172-183

Lee D-C, Halliday AN, Davies GR, Essene EJ, Fitton JG, Temdjim R. (1996) Melt enrichment of shallow depleted mantle: a detailed petrological, trace element and isotopic study of mantle-derived xenoliths and megacrysts from the Cameroon line. J Petrol 37: 415-441

Lecuyer C and Reynard B (1996) High-temperature alteration of oceanic gabbros by seawater (Hess Deep, Ocean Drilling Program Leg 147): Evidence from oxygen isotopes and elemental fluxes. J Geophys Res 101:15883-15897

Leeman WP, Tonarini S, Chan LH, Borg LE (2004) Boron and lithium variations in a hot subduction zone, the southern Washington Cascades. Chem Geol 212:101-124

Le Roex AP, Erlank AJ, Needham HD (1981) Geochemical and mineralogical evidence for the occurrence of at least three distinct magma types in the 'famous' region. Contrib Mineral Petrol 77:24-37

Levasseur S, Birk J-L, Allègre CJ (1998) Direct measurement of femtomoles of osmium and the 187Os/186Os in seawater. Science 282:272-274

Levasseur S, Birck JL, Allègre CJ (1999) The osmium riverine flux and the oceanic mass balance of osmium. Earth Planet Sci Lett 174:7-23

Li J, Xu J-F, Suzuki K, He B, Xu Y-G, Ren Z-Y (2010) Os, Nd and Sr isotope and trace element geochemistry of the Muli picrites: insights into the mantle source of the Emeishan large igneous province. Lithos 119:108-122

Li J, Wang XC, Ren ZY, Xu JF, He B, Xu YG (2014) Chemical heterogeneity of the Emeishan mantle plume: evidence from highly siderophile element abundances in picrites. J Asian Earth Sciences 79:191–205

Lissenburg CJ, Rioux M, Shimizu N, Bowring SA, Mével, C (2009) Zircon dating of oceanic crustal accretion. Science 323:1048-1050

Liu CZ, Snow JE, Hellebrand E, Brügmann, G, von der Handt A, Büchl A, Hofmann AW (2008) Ancient, highly heterogeneous mantle beneath Gakkel ridge, Arctic Ocean. Nature 452:311-316

Lodders K. (2003) Solar system abundances and condensation temperatures of the elements. Astrophys J 591:1220-1247

Lodders K, Palme H, Gail HP (2009) Abundances of the elements in the solar system. *In*: Landolt-Börnstein, New Series, Vol VI/4B. J.E. Trümper JE (ed), Springer-Verlag, Berlin, p 560-630

Lorand J-P (1990) Are spinel lherzolite xenoliths representative of the sulfur content of the upper mantle. Geochim Cosmochim Acta 54:1487-1492

Lorand J-P, Luguet A (2015) Chalcophile and siderophile elements in mantle rocks : trace elements controlled by trace minerals. Rev Geochem Mineral 81:441-481

Lorand J-P, Alard O (2001) Platinum-group element abundances in the upper mantle: new constraints from in situ and whole-rock analyses of Massif Central xenoliths (France). Geochim Cosmochim Acta 65: 2789-2806

Lorand J-P, Alard O, Luguet A (2010) Platinum-group element micronuggets and refertilization process in Lherz orogenic massif (northeastern Pyrenees, France). Earth Planet Sci Lett 289:298-310

Lorand J-P, Luguet A, Alard O (2013) Platinum-group element systematics and petrogenetic processing of the continental upper mantle: A review. Lithos 164-167:1-21

Luck JM, Allègre CJ (1982) The study of molybdenites through the ^{187}Re-^{187}Os chronometer. Earth Planet Sci Lett 61:291-296

Luguet A, Lorand JP, Seyler M (2003) Sulfide petrology and highly siderophile element geochemistry of abyssal peridotites: A coupled study of samples from the Kane Fracture Zone (45°W 23°20N, MARK area, Atlantic Ocean). Geochim Cosmochim Acta 67:1553-1570

Luguet A, Shirey SB, Lorand JP, Horan MF, Carlson RW (2007) Residual platinum group minerals from highly depleted harzburgites of the Lherz massif (France) and their role in HSE fractionation in the mantle. Geochim Cosmochim Acta 71:3082-3097

Luguet A, Pearson DG, Nowell GM, Dreher ST, Coggon JA, Spetsius ZV, Parman SW (2008) Enriched Pt-Re-Os isotope systematics in plume lavas explained by metasomatic sulfides. Science 319:453-456

Mahoney JJ, Natland JH, White WM, Poreda R, Bloomer SH, Fisher RL, Baxter AN (1989) Isotopic and geochemical provinces of the Western Indian Ocean spreading centers. J Geophys Res 94:4033-4052

Mahoney JJ, LeRoex AP, Peng Z, Fisher RL, Natland JH (1992) Southwestern limits of Indian Ocean ridge mantle and the origin of low $^{206}Pb/^{204}Pb$ mid-ocean ridge basalt: isotope systematics of the central Southwest Indian Ridge (178-508E). J Geophys Res 97:19771-19790

Mallmann G, O'Neill HStC (2007) The effect of oxygen fugacity on the partitioning of Re between crystals and silicate melt during mantle melting. Geochim Cosmochim Acta 71:2837-2857

Mann U, Frost DJ, Rubie DC, Becker H, Audétat A (2012) Partitioning of Ru, Rh, Pd, Re, Ir and Pt between liquid metal and silicate at high pressures and temperatures- implications for the origin of highly siderophile element concentrations in the Earth's mantle. Geochim Cosmochim Acta 84:593-613

Marcantonio F, Zindler A, Elliott T, Staudigel H (1995) Os isotope systematics of La Palma, Canary Islands: evidence for recycled crust in the mantle source of HIMU ocean islands. Earth Planet Sci Lett 133:397-410

Marchesi C, Dale CW, Garrido CJ, Pearson DG, Bosch D, Bodinier J-L, Gervilla F, Hidas K (2014) Fractionation of highly siderophile elements in refertilized mantle: Implications for the Os isotope composition of basalts. Earth Planet Sci Lett 400:33-44

Martin CE (1991) Osmium isotopic characteristics of mantle-derived rocks. Geochim Cosmochim Acta 55:1421-34

Mathez EA (1976) Sulfur solubility and magmatic sulfides in sub-marine basalt glasses. J Geophys Res 81:4269-4276

Mathez EA, Yeats RS (1976) Magmatic sulfides in basalt glass from DSDP hole 319a and site 320, Nazca plate. Initial Reports of the Deep-Sea Drilling Project 34:363-373

Mather TA, Witt MLI, Pyle DM, Quayle BM, Aiuppa A, Bagnato E, Martin RS, Sims KWW, Edmonds M, Sutton AJ, Ilyinskaya E (2012) Halogens and trace metal emissions from the ongoing 2008 summit eruption of Kılauea volcano, Hawaii. Geochim Cosmochim Acta 83:292-323

Mavrogenes JA, O'Neill HStC (1999) The relative effects of pressure, temperature and oxygen fugacity on the solubility of sulfide in mafic magmas. Geochim Cosmochim Acta 63:1173-1180

May PR (1971) Pattern of Triassic diabase dykes around the North Atlantic in the context of predrift position of the continents. Geol Soc Am Bull 82:1285-1292

McHone JG (2000). Non-plume magmatism and rifting during the opening of the Central Atlantic Ocean. Tectonophysics 316:287-296

McHone JG, Anderson DL, Beutel EK, Fialko YA (2005) Giant dikes, rifts, flood basalts, and plate tectonics: A contention of mantle models. In: Foulger GR, Natlund JH, Presnall DC, Anderson DL (eds) In: Plates, Plumes, and Paradigms, Geol Soc Am Special Paper 388:401-420

McInnes BIA, McBride JS, Evans NJ,Lambert DD, Andrew AS (1999) Osmium isotope constraints on ore metal recycling in subduction zones. Science 286:512-516

2482 McDonough WF, Sun SS (1995) The chemical composition of the Earth. Chem Geol 120:223-253
2483 Meisel T, Walker RJ, Morgan JW (1996) The osmium isotopic composition of the Earth's primitive
2484 upper mantle. Nature 383:517-520
2485 Meisel T, Walker RJ, Irving AJ, Lorand JP (2001) Osmium isotopic compositions of mantle
2486 xenoliths: a global perspective. Geochim Cosmochim Acta 65:1311-1323
2487 Meisel T, Reisberg L, Moser J, Carignan J, Melcher F, Brügmann G (2003) Re-Os systematics of
2488 UB-N, a serpentinized peridotite reference material. Chem Geol 201:161-179
2489 Merle R, Marzoli A, Reisberg L, Bertrand H, Nemchin A, Chiaradia M, Callegaro S, Jourdan F,
2490 Bellieni G, Kontak D, Puffer J, McHone JG (2014) Sr, Nd, Pb and Os isotope systematics of
2491 CAMP tholeiites from eastern North America (ENA): evidence of a subduction-enriched
2492 mantle source. J Petrol 55:133-180
2493 Michael PJ, Schilling JG (1989) Chlorine in mid-ocean ridge magmas: Evidence for assimilation of
2494 seawater-influenced components. Geochim Cosmochim Acta 53:3131-3143
2495 Michael PJ, Cornell WC (1998) Influence of spreading rate and magma supply on crystallization and
2496 assimilation beneath mid-ocean ridges: Evidence from chlorine and major element chemistry of
2497 mid-ocean ridge basalts. J Geophys Res 103:18325-18356
2498 Michard A, Montigny R, Schlich R (1986) Geochemistry of the mantle beneath the Rodriguez Triple
2499 Junction and the South-East Indian Ridge. Earth Planet Sci Lett 78:104-114
2500 Mitchell RH, Keays RR (1981) Abundance and distribution of gold, palladium and iridium in some
2501 spinel and garnet lherzolites: implications for the nature and origin of precious metal-rich
2502 intergranular components in the upper mantle. Geochim Cosmochim Acta 45:2425-2442
2503 Molski MJ, Seppelt K (2009) The transition metal hexafluorides. Dalton Trans 3379:3379-3383.
2504 Molzahn M, Reisberg L, Worner G (1996) Os, Sr, Nd, Pb, O isotope and trace element data from the
2505 Ferrar flood basalts, Antarctica: evidence for an enriched subcontinental lithospheric source.
2506 Earth Planet Sci Lett 144:529-546
2507 Momme P, Oskarsson N, Keays RR (2003) Platinum-group elements in the Icelandic rift system:
2508 melting processes and mantle sources beneath Iceland. Chem Geol 196:209-234
2509 Momme P, Tegner C, Brooks CK, Keays RR (2006) Two melting regimes during Paleogene flood
2510 basalt generation in East Greenland: combined REE and PGE modeling. Contrib Mineral Petrol
2511 151:88-100
2512 Moore JG, Calk LC (1971) Sulfide spherules in vesicles of dredge pillow basalt. Am Mineral 56.476-
2513 488
2514 Moore JG Schilling JG (1973) Vesicles, water, and sulfur in Reykjanes Ridge basalt. Contrib Mineral
2515 Petrol 41:105-118
2516 Moore A., Coogan L. A., Costa F. and Perfit M. R. (2014) Primitive melt replenishment and crystal-
2517 mush disaggregation in the weeks preceding the 2005–2006 eruption 9°50N, EPR. Earth Planet
2518 Sci Lett 403:15-26
2519 Moran AE, Sisson VB, Leeman WP (1992) Boron depletion during progressive metamorphism:
2520 Implications for subduction processes. Earth Planet Sci Lett 111:331-349
2521 Morgan WJ (1971) Convection plumes in the lower mantle. Nature 230:42-43
2522 Morgan WJ (1983). Hotspot tracks and the early rifting of the Atlantic. Tectonophysics 94:123-139
2523 Mungall JE (2002) Roasting the mantle: slab melting and the genesis of major Au and Au-rich Cu
2524 deposits. Geology 30:915-918
2525 Mungall JE, Brenan JM (2014) Partitioning of platinum-group elements and Au between sulfide
2526 liquid and basalt and the origins of mantle-crust fractionation of the chalcophile elements.
2527 Geochim Cosmochim Acta 125:265-289
2528 Mungall JE, Hanley JJ, Arndt NT, Debecdelievre A (2006) Evidence from meimechites and other
2529 low-degree mantle melts for redox controls on mantle-crust fractionation of platinum group
2530 elements. Proc Natl Acad Sci 103:12695-12700
2531 Murthy V (1991) Early differentiation of the Earth and the problem of mantle siderophile

elements: a new approach. Science 253:303-306
Nakagawa M, Franco HEA (1997) Placer Os–Ir–Ru alloys and sulfides: indicators of sulfur fugacity in an ophiolite? Can Mineral 35:1441-1452
Nakano N, Nakamura E (2001) Boron isotope chemistry of metasedimentary rocks and toumalines in a subduction zone metamorphic suite. Phys Earth Planet Inter 127:233-252
Niu Y (2004) Bulk-rock major and trace element compositions of abyssal peridotites: implications for mantle melting, melt extraction and post melting processes beneath mid-ocean ridges. J. Petrol. 45(12):2423-2458
Norman MD, Garcia MO, Bennett VC (2004) Rhenium and chalcophile elements in basaltic glasses from Ko'olau and Moloka'i volcanoes: magmatic outgassing and composition of the Hawaiian plume. Geochim Cosmochim Acta 68:3761-3777
O'Driscoll B, González-Jiménez J-M (2015) An inventory and overview of natural occurrences of the platinum-group minerals (PGM) in extraterrestrial and terrestrial rocks. Rev Mineral Geochem 81:489-576
O'Driscoll B, Day JMD, Daly JS, Walker RJ, McDonough WF (2009) Rhenium-osmium isotope and platinum-group elements in the Rum Layered Suite, Scotland: implications for Cr-spinel seam formation and the composition of the Iceland mantle anomaly. Earth Planet Sci Lett 286:41-51
Ohtani E, Yurimoto H (1996) Element partitioning between metallic liquid, magnesiowustite, and silicate liquid at 20 GPa and 2500^{o}C: A secondary ion mass spectroscopic study. Geophys Res, Lett 23:1993-1996
O'Neill HStC (1991) The origin of the Moon and early history of the Earth—a chemical model: Part 2. The Earth. Geochim Cosmochim Acta 55:1159-1172
O'Neill HStC, Mavrogenes J (2002) The sulfide capacity and the sulfur content at sulfide saturation of silicate melts at 1400°C and 1 bar. J Petrol 43:1049-1087
O'Neill HStC, Dingwell DB, Borisov A, Spettel B, Palme H (1995) Experimental petrochemistry of some highly siderophile elements at high temperatures, and some implications for core formation and the mantle's early history. Chem Geol 120:255-273
O'Nions RK, Hamilton PJ, Evenson AM (1977) Variations in $^{143}Nd/^{144}Nd$ and $^{87}Sr/^{86}Sr$ ratios in oceanic basalts. Earth Planet Sci Lett 34:13-22
Palme H, O'Neill HStC (2003) Cosmochemical estimates of mantle composition. In: Treatise on Geochemistry, The Mantle and Core (ed) Carlson RW. Elsevier, Amsterdam. p 1-38
Patten C, Barnes SJ, Mathez EA (2012) Textural variations in MORB sulfide droplets due to differences in crystallization history. Can Mineral 50:675-692
Patten C, Barnes SJ, Mathez EA, Jenner FE (2013) Partition coefficients of chalcophile elements between sulfide and silicate melts and the early crystallization history of sulfide liquid: LA-ICP-MS analysis of MORB sulfide droplets. Chem Geol 358:170-188
Peach CL, Mathez EA, Keays RR (1990) Sulfide melt-silicate melt distribution coefficients for noble metals and other chalcophile elements as deduced from MORB: implications for partial melting. Geochim Cosmochim Acta 54:3379-3389
Peach CL, Mathez EA, Keays RR, Reeves SJ (1994) Experimentally determined sulfide melt-silicate melt partition coefficient for iridium and palladium. Chem Geol 117:361-377
Peacock SM, Hervig RL (1999) Boron isotopic composition of subduction-zone metamorphic rocks. Chem Geol 160:281-290
Pearson DG, Carlson RW, Shirey SB, Boyd FR, Nixon PH (1995) The Stabilisation of Archean lithospheric mantle: a Re-Os isotope study of peridotite xenoliths from the Kaapvaal craton. Earth Planet Sci Lett 134:341-357
Pearson DG, Davies GR, Nixon PH, Greenwood PB, Mattey DP (1991) Oxygen isotope evidence for the origin of pyroxenites in the Beni Bousera peridotite massif N. Morocco: derivation from subducted oceanic lithosphere. Earth Planet Sci Lett 102:289-301

Pearson DG, Shirey SB,Harris JW,Carlson RW (1998) Sulfide inclusions in diamonds from the Koffiefontein kimberlite, S. Africa: Constraints on diamond ages and mantle Re-Os systematics. Earth Planet Sci Lett 160:311-326

Pearson DG, Shirey SB, Bulanova GP, Carlson RW, Milledge HJ (1999) Re–Os isotope measurements of single sulfide inclusions in a Siberian diamond and its nitrogen aggregation systematics. Geochim Cosmochim Acta 63:703–711

Pearson DG, Irvine GJ, Ionov DA, Boyd FR, Dreibus GE (2004) Re–Os isotope systematics and platinum group element fractionation during mantle melt extraction: A study of massif and xenolith peridotite suites. Chem Geol 208:29-59

Pearson DG, Nowell GM, Kjarsgaard BA, Dowall DP (2008) The genesis of kimberlite: geochemical constraints. Ext Abs 9th Int Kimb Conf Frankfurt (No.9IKC-A-00149)

Pearson NJ, Alard O, Griffin WL, Jackson SE, O'Reilly SY (2002) In situ measurement of Re–Os isotopes in mantle sulfides by laser ablation multicollector-inductively coupled plasma mass spectrometry: analytical methods and preliminary results. Geochim Cosmochim Acta 66:1037-1050

Pegram BJ, Allègre CJ (1992) Osmium isotopic compositions from oceanic basalts. Earth Planet Sci Lett 111:59-68

Penniston-Dorland SC, Walker RJ, Pitcher L, Sorensen SS (2012) Mantle-crust interactions in a paleosubduction zone: Evidence from highly siderophile element systematics of eclogite and related rocks. Earth Planet Sci Lett 319-320, 295-306

Penniston-Dorland SC, Gorman JK, Bebout GE, Piccoli PM., Walker RJ (2014) Reaction rind formation in the Catalina Schist: Deciphering a history of mechanical mixing and metasomatic alteration. Chem Geol 384:47-61

Peslier AH, Reisberg L, Ludden J, Francis D (2000) Os isotopic systematics in mantle xenoliths; age constraints on the Canadian Cordillera lithosphere. Chem Geol 166:85-101

Peucker-Ehrenbrink B, Ravizza G, Hofmann AW (1995) The marine $^{187}Os/^{186}Os$ record of the past 80 million years. Earth Planet Sci Lett 130:155-167

Peucker-Ehrenbrink B, Bach W, Hart SR, Blusztajn J, Abbruzzese T (2003) Rhenium–osmium isotope systematics and platinum group element concentrations in oceanic crust from DSDP/ODP Sites 504 and 417/418. Geochem Geophys Geosyst 4. http://dx.doi.org/10.1029/2002GC000414

Peucker-Ehrenbrink B, Hanghoj K, Atwood T and Kelemen PB (2012) Rhenium-osmium isotope systematics and platinum group element concentrations in oceanic crust. Geology 40:199-202

Pitcher L, Helz RT, Walker RJ, Piccoli P (2009) Fractionation of the platinum-group elements and Re during crystallization of basalt in Kilauea Iki Lava Lake, Hawaii. Chem Geol 260:196-210

Plank T, Langmuir CH (1992) Effects of the melting regime on the composition of the oceanic crust. J Geophys Res 97:19749-19770

Prelević D, Jacob DE, Foley SF (2013) Recycling plus: a new recipe for the formation of Alpine-Himalayan orogenic mantle lithosphere. Earth Planet Sci Lett 362:187-197

Prelević D, Brügmann G, Barth M, Božovic M, Cvetković V, Foley SF, Maksimović Z (2015) Os-isotope constraints on the dynamics of orogenic mantle: The case of the Central Balkans. Gondwana Res 27:1560-1573

Price RC, Kennedy AK, Riggs-Sneerginger M, Frey FA (1986) Geochemistry of basalts from the Indian Ocean triple junction: implications for the generation and evolution of Indian Ocean ridge basalts. Earth Planet Sci Lett 78:379-396

Prinzhofer A, Lewin E, Allègre CJ (1989) Stochastic melting of the marble cake mantle: evidence from local study of the East Pacific Rise at 12"50'N. Earth Planet Sci Lett 92:189-206

Puchtel IS, Humayun M (2000) Platinum group elements in Kostomuksha komatiites and basalts: Implications for oceanic crust recycling and core-mantle interaction. Geochim Cosmochim Acta 64:4227-4242

2631 Puchtel IS, Humayun M (2001) Platinum group element fractionation in a komatiitic basalt lava lake.
2632 Geochim Cosmochim Acta 65:2979-2993
2633 Puchtel IS, Brandon AD, Humayan M (2004) Precise Pt-Re-Os isotope systematics of the mantle
2634 from 2.7-Ga komatiites. Earth Planet Sci Lett 224:157-174
2635 Puchtel IS, Brandon AD, Humayan M, Walker RJ (2005) Evidence for the early differentiation of the
2636 core from Pt/Re/Os isotope systematics of 2.8-Ga komatiites. Earth Planet Sci Lett 237:118-134
2637 Puchtel IS, Walker RJ, Brandon AD, Nisbet EG (2009) Pt-Re-Os and Sm-Nd isotope and HSE and
2638 REE systematics of the 2.7 Ga Belingwe and Abitibi komatiites. Geochim Cosmochim Acta
2639 73:6367-6389
2640 Puffer JH (2001) Contrasting HFSE contents of plume sourced and reactivated arc-sourced
2641 continental flood basalts. Geology 29:675-678
2642 Puffer JH (2003) A reactivated back-arc source for CAMP magma. In: Hames WE, McHone JG,
2643 Renne PR, Ruppel C (eds) The Central Atlantic Magmatic Province: Insights from Fragments
2644 of Pangea. Geophysical Monograph, Am Geophys Union 136:151-162
2645 Putirka KD, Perfit M, Ryerson FJ, Jackson MG (2007) Ambient and excess mantle temperatures,
2646 olivine thermometry, and active vs. passive upwelling. Chem Geol 241:177-206
2647 Rehkämper M, Hofmann AW (1997) Recycled ocean crust and sediment in Indian Ocean MORB.
2648 Earth Planet Sci Lett 147:93-106
2649 Rehkämper M, Halliday AN, Fitton JG, Lee DC, Wieneke M, Arndt NT (1999) Ir, Ru, Pt, and Pd in
2650 basalts and komatiites: new constraints for the geochemical behaviour of the platinum-group
2651 elements in the mantle. Geochim Cosmochim Acta 63: 3915-3934
2652 Reisberg L, Lorand J-P (1995) Longevity of sub-continental mantle lithosphere from osmium isotope
2653 systematics in orogenic peridotite massifs. Nature 376:159-162
2654 Reisberg L, Allègre CJ, Luck J-M (1991) The Re-Os systematics of the Ronda ultramafic complex of
2655 Southern Spain. Earth Planet Sci Lett 105:196-213
2656 Reisberg L, Zindler A, Marcantonio F, White W, Wyman D, Weaver B (1993) Os isotope
2657 systematics in ocean island basalts. Earth Planet Sci Lett 120:149-167
2658 Reisberg L, Rouxel O, Ludden J, Staudigel H and Zimmermann C (2008) Re-Os results from ODP
2659 Site 801: Evidence for extensive Re uptake during alteration of oceanic crust. Chem Geol
2660 248:256-271
2661 Rhodes JM, Vollinger MJ (2005) Ferric/ferrous ratios in 1984 Mauna Loa lavas: a contribution to
2662 understanding the oxidation state of Hawaiian magmas. Contrib Mineral Petrol 149:666-674
2663 Rhyzenko B, Kennedy GC (1973) The effect of pressure on the eutectic in the system Fe–FeS. Am J
2664 Sci 273:803-810
2665 Riches AJV, Day JMD, Walker RJ, Simonetti A, Liu Y, Neal CR, Taylor LA (2012) Rhenium–
2666 osmium isotope and highly siderophile element abundance systematics of angrite meteorites.
2667 Earth Planet Sci Lett 353–354:208-218
2668 Righter K, Hauri EH (1998) Compatibility of Re in garnet during mantle melting and magma genesis.
2669 Science 280:1737-1741
2670 Righter K, Chesley JT, Ruiz J (2002) Genesis of primitive arc basalt: constraints from Re, Os and Cl
2671 on the depth of melting and role of fluids. Geology 30:619-622
2672 Righter K, Campbell AJ, Humayun M, Hervig MRL (2004) Partitioning of Ru, Rh, Pd, Re, Ir, and
2673 Au between Cr-bearing spinel, olivine, pyroxene and silicate melts. Geochim Cosmochim Acta
2674 68:867-880
2675 Righter K, Humayun M, Danielson L (2008) Partitioning of palladium at high pressures and
2676 temperatures during core formation. Nat Geosci 1:321-323
2677 Rocha-Júnior ERV, Puchtel IS, Marques LS, Walker RJ, Machado FB, Nardy AJR, Babinski M,
2678 Figueiredo AMG (2012) Re–Os isotope and highly siderophile element systematics of the
2679 Parana continental flood basalts (Brazil). Earth Planet Sci Lett 337-338:164-173

Rogers NW, Davies MK, Parkinson IJ, Yirgu G (2010) Osmium isotopes and Fe/Mn ratios in Ti-rich picrites from the Ethiopian flood basalt province: no evidence for core contribution to the Afar plume. Earth Planet Sci Lett 296:413-422

Rosenthal A, Foley SF, Pearson DG, Nowell GM, Tappe S (2009) Petrogenesis of strongly alkaline primitive volcanic rocks at the propagating tip of the western branch of the East African Rift. Earth Planet Sci Lett 284:236-248

Roy-Barman M, Allègre CJ (1994) ^{187}Os-^{186}Os ratios of mid-ocean ridge basalts and abyssal peridotites. Geochim Cosmochim Acta 58:5043-54

Roy-Barman M, Allègre CJ (1995) 187Os/186Os in oceanic island basalts: Tracing oceanic crust recycling in the mantle. Earth Planet Sci Lett 129:145-161

Roy-Barman M, Wasserburg GJ, Papanastassiou DA, Chaussidon M (1998) Osmium isotope composition and Re-Os concentrations in sulfide globules from basaltic glasses. Earth Planet Sci Lett 154:331-347

Rubin K (1997) Degassing of metals and metalloids from erupting seamount and midocean ridge volcanoes: observations and predictions. Geochim Cosmochim Acta 61:3525-3542

Rudnick RL, Fountain DM (1995) Nature and composition of the continental crust: a lower crustal perspective. Rev Geophys 33:267-309

Saal AE, Rudnick RL, Ravizza GE, Hart SR (1998) Re–Os isotope evidence for the composition, formation and age of the lower continental crust. Nature 393:58-61

Salters VJM, Stracke A (2004) Composition of the depleted mantle. Geochem Geophys Geosys 5. http://dx.doi.org/10.1029/2003GC000597

Schaefer BF, Parkinson IJ, Hawkesworth CJ (2000) Deep mantle plume osmium isotope signature from West Greenland Tertiary picrites. Earth Planet Sci Lett 175:105-118

Schaefer BF, Turner S, Parkinson I, Rogers N, Hawkesworth C (2002) Evidence for recycled Archaean oceanic mantle lithosphere in the Azores plume. Nature 420:304-307

Scherstén A, Elliott T, Hawkesworth CJ, Norman M (2004) Tungsten isotope evidence that mantle plumes contain no contribution from the Earth's core. Nature 427:234-237

Schiano P, Birck JL, Allègre CJ (1997) Osmium-strontium-neodymium-lead isotopic covariations in mid-ocean ridge basalt glasses and the heterogeneity of the upper mantle. Earth Planet Sci Lett 150:363-379

Schiano P, Burton KW, Dupré B, Birck JL, Guille G, Allègre CJ (2001) Correlated Os-Pb-Nd-Sr isotopes in the Austral–Cook chain basalts: the nature of mantle components in plume sources. Earth Planet Sci Lett 186:527-537

Schiano P, David K, Vlastelic I, Gannoun A, Klein M, Nauret F, Bonnand P (2012) Osmium isotope systematics of historical lavas from Piton de la Fournaise (Réunion Island, Indian Ocean). Contrib Mineral Petrol 164:805-820

Schwartz JJ, John BE, Cheadle MJ, Miranda EA, Grimes, CB, Wooden JL, Dick HJB (2005) Dating the growth of oceanic crust at a slow-spreading ridge. Science 310:654-657

Selo M, Storzer D (1979) Chrolnologie des événements volcaniques de la zone Famous. C R Acad Sci Paris 289:1125-1128

Sen IS, Bizimis M, Sen G, Huang S (2011) A radiogenic Os component in the oceanic lithosphere? Constraints from Hawaiian pyroxenite xenoliths. Geochim Cosmochim Acta 75:4899-4916

Sharma M, Chen C, Blazina T (2012) Osmium contamination of seawater samples stored in polyethylene bottles. Limnol Oceanogr Methods 10:618-630

Shimizu N (1998) The geochemistry of olivine-hosted melt inclusions in a FAMOUS basalt ALV519-4-1. Phys Earth Planet Inter 107:183-201

Shirey SB (1997) Re-Os isotopic composition of Mid-continent rift system picrites: implications for plume-lithosphere interaction and enriched mantle sources. Can J Earth Sci 34:489-503

Shirey SB, Walker RJ (1995) Carius tube digestion for low-blank Re–Os analyses. Anal Chem 67:2136-2141

Shirey SB, Walker RJ (1998) The Re-Os isotope system in cosmochemistry and high-temperature geochemistry. Ann Rev Earth Planet Sci 26:423-500

Sigurdsson H, Schilling JG (1976) Spinels in Mid-Atlantic Ridge basalts: Chemistry and occurrence. Earth Planet Sci Lett 29:7-20

Skovgaard AC, Storey M, Baker J, Blusztajn J, Hart SR (2001) Osmium-oxygen isotope evidence for a recycled and strongly depleted component in the Icelandic mantle plume. Earth Planet Sci Lett 194:259-275

Smith HJ, Spivak AJ, Staudigel H, Hart SR (1995) The boron isotopic composition of altered oceanic crust. Chem Geol 126:119-135

Snow JE, Reisberg L (1995) Os isotopic systematics of the MORB mantle: results from altered abyssal peridotites. Earth Planet Sci Lett 133:411-421

Sobolev AV, Hofmann AW, Kuzmin DV, Yaxley GM, Arndt NT, Chung SL, Danyushevsky LV, Elliott T, Frey FA, Garcia MO, Gurenko AA, Kamenetsky VS, Kerr AC, Krivolutskaya NA, Matvienkov VV, Nikogosian IK, Rocholl A, Sigurdsson IA, Sushchevskaya NM, Teklay M (2007) The amount of recycled crust in sources of mantle-derived melts. Science 316:412-417

Spera FJ, Bohrson WA (2001) Energy-constrained open-system magmatic processes I: General model and energy-constrained assimilation and fractional crystallization (EC-AFC) formulation. J Petrol 42:999-1018.

Spivak AJ, Edmond JM (1987) Boron isotope exchange between seawater and the oceanic crust. Geochim Cosmochim Acta 51:1033-1043

Standish JJ, Hart SR, Blusztajn J, Dick HJB, Lee KL (2002) Abyssal peridotite osmium isotopic compositions from Cr-spinel. Geochem Geophys Geosyst 3. http://dx.doi.org/10.1029/2001GC000161

Su Y, Langmuir CH (2003) Global MORB chemistry compilation at the segment scale. Ph.D. thesis, Department of Earth and Environmental Sciences, Columbia University. http://petdb.ldeo.columbia.edu/documentation/morbcompilation/

Sun Y, Ying J, Zhou X, Shao J, Chu Z, Su B (2014) Geochemistry of ultrapotassic volcanic rocks in Xiaogulihe NE China: Implications for the role of ancient subducted sediments. Lithos 208-209:53-66

Suzuki K, Senda R, Shimizu K (2011) Osmium behavior in a subduction system elucidated from chromian spinel in Bonin Island beach sands. Geology 39:999-1002

Tatsumoto M (1966) Genetic relations of oceanic basalts as indicated by lead isotopes. Science 153:1094-1101

Tejada MLG, Suzuki K, Hanyu T, Mahoney JJ, Ishikawa A, Tatsumi Y, Chang Q, Nakai S (2013) Cryptic lower crustal signature in the source of the Ontong Java Plateau revealed by Os and Hf isotopes. Earth Planet Sci Lett 377–378:84-96

Tejada MLG, Hanyu T, Ishikawa A, Senda R, Suzuki K, Fitton G, Williams R (2015) Re-Os isotope and platinum group elements of a FOcal ZOne mantle source, Louisville Seamounts Chain, Pacific ocean. Geochem Geophys Geosys 16:486-504 doi:10.1002/2014GC005629

Thompson RN, Ottley CJ, Smith PM, Pearson DG, Dickin AP, Morrison MA, Leat PT, Gibson SA (2005) Source of the quaternary alkalic basalts, picrites, and basanites of the Potrillo volcanic field, New Mexico, USA: lithospheric or convecting mantle? J Petrol 46: 1603-1643

Toutain JP, Meyer G (1989) Iridium-bearing sublimates at hot-spot volcano (Piton de la Fournaise, Indian Ocean). Geophys Res Lett 16:1391-1394

Tredoux M, Lindsay NM, Davies G, McDonald I (1995) The fractionation of platinum group elements in magmatic systems, with the suggestion of a novel causation mechanism. S Afr J Geol 98:157-167

Turner S, Handler M, Bindeman I, Suzuki K (2009) New insights into the origin of O–Hf–Os isotope signatures in arc lavas from Tonga–Kermadec. Chem Geol 266:187-193

van Acken D, Becker H, Walker RJ,McDonough WF, Wombacher F, Ash RD, Piccoli PM (2010) Formation of pyroxenite layers in the Totalp ultramafic massif (Swiss Alps) — insights from highly siderophile elements and Os isotopes. Geochim Cosmochim Acta 74: 661-683

Van Orman JA, Keshav S, Fei Y (2008) High pressure solid-metal/liquid-metal partitioning of Os, Re and Pt in the Fe/S system. Earth Planet Sci Lett 274:250-257

Verati C, Bertrand H, Fe¤raud G (2005) The farthest record of the Central Atlantic Magmatic Province into West Africa craton: Precise $^{40}Ar/^{39}Ar$ dating and geochemistry of Taoudenni basin intrusives (northern Mali). Earth Planet Sci Lett 235:391-407

Vidal P, Clauer N (1981) Pb and Sr isotopic systematics of some basalts and sulfides from the East Pacific Rise at 21”N (project RITA). Earth Planet Sci Lett 55:237-246

Vils F, Tonarini S, Kalt A, Seitz H-M (2009) Boron, lithium and strontium isotopes as tracers of seawater–serpentinite interaction at Mid-Atlantic ridge, ODP Leg 209. Earth Planet Sci Lett 286:414-425

Vogel DC, Keays RR (1997) The application of platinum group geochemistry in constraining the source of basalt magmas: results from the Newer Volcanic Province, Victoria, Australia. Chem Geol 136:181-204

Volkening J, Walczyk T, Heumann KG (1991). Osmium isotope ratio determinations by negative thermal ionization mass spectrometry. Int J Mass Spectrom Ion Proc 105:147-159

Walczyk T, Hebeda EH, Heumann KG (1991) Osmium isotope ratio measurements by negative thermal ionization mass spectrometry (NTI-MS) improvement in precision and enhancement in emission by introducing oxygen or freons into the ion source. Fresenius’ J Anal Chem 341:537-541

Walker RJ (2009) Highly siderophile elements in the Earth, Moon and Mars: update and implications for planetary accretion and differentiation. Chemie der Erde - Geochem 69:101-125

Walker RJ, Fassett JD (1986) Isotopic measurement of sub-nanogram quantities of rhenium and osmium by resonance ionization mass spectrometry. Anal Chem 58:2923-2927

Walker RJ, Carlson RW, Shirey SB, Boyd FR (1989) Os, Sr, Nd, and Pb isotope systematics of Southern African peridotite xenoliths; implications for the chemical evolution of subcontinental mantle. Geochim Cosmochim Acta 53:1583-95

Walker RJ, Morgan JW, Beary E, Smoliar MI, Czamanske GK, Horan MF (1997) Applications of the 190Pt-186Os isotope system to geochemistry and cosmochemistry. Geochim Cosmochim Acta 61:4799-4808

Walker RJ, Storey M, Kerr AC, Tarney J, Arndt NT (1999) Implications of 187Os isotopic heterogeneities in a mantle plume: evidence from Gorgona Island and Curaçao. Geochim Cosmochim Acta 63:713-728

Wallace P, Carmichael ISE (1992) Sulfur in basaltic magmas. Geochim Cosmochim Acta 56:1863-1874

Wang BD, Chen JL, Xu JF, Wang LQ (2014) Geochemical and Sr–Nd–Pb–Os isotopic compositions of Miocene ultrapotassic rocks in southern Tibet: Petrogenesis and implications for the regional tectonic history. Lithos 208-209:237-250

Warren JM, Shirey SB (2012) Lead and osmium isotopic constraints on the oceanic mantle from single abyssal peridotite sulfides. Earth Planet Sci Lett 359-360:279-293

Watson EB, Ben Othman D, Luck JM, Hofmann AW (1987) Partitioning of U, Pb, Cs, Yb, Hf, Re and Os between chromian diopsidic pyroxene and haplobasaltic liquid. Chem Geol 62:191-208

Watson EB, Baker DR (1985) Chemical diffusion in magmas: an overview of experimental results and geochemical applications. Adv Phys Geochim 9:120-151

White R, McKenzie D (1989) Magmatism at rift zones: the generation of volcanic continental margins and flood basalts. J Geophys Res 94:7685-7729

White WM (2010) Oceanic island basalts and mantle plumes: the geochemical perspective. Annu Rev Earth Planet Sci 38:133-160

White WM, Schilling JG (1978) The nature and origin of geochemical variation in Mid-Atlantic Ridge basalts from the Central North Atlantic. Geochim Cosmochim Acta 42:1501-1516
Widom E (1997) Sources of ocean island basalts: a review of the osmium isotope evidence. Physica A 244:484-496
Widom E, Shirey SB (1996) Os isotope systematics in the Azores: implications for mantle plume sources. Earth Planet Sci Lett 142:451-465
Widom E, Hoernle KA, Shirey SB, Schmincke H-U (1999) Os isotope systematics in the Canary Islands and Madiera: lithospheric contamination and mantle plume signatures. J Petrol 40:279-296
Widom E, Kepezhinskas P, Defant M (2003) The nature of metasomatism in the sub-arc mantle wedge: evidence from Re–Os isotopes in Kamchatka peridotite xenoliths. Chem Geol 196:282-306
Wilson JT (1963) A possible origin of the Hawaiian Islands. Can J Phys 41:863-870
Wilson M (1997) Thermal evolution of the Central Atlantic passive margins: continental break-up above a Mesozoic superplume. J Geol Soc, London 154:491-495
Wilson AH, Shirey SB, Carlson RW (2003) Archaean ultra-depleted Komatiites formed by hydrous melting of cratonic mantle. Nature 423:858-860
Woodhead JD, McCulloch MT (1998) Ancient seafloor signals in Pitcairn Island lavas and evidence for large amplitude, small length-scale mantle heterogeneities Earth and Planetary Science Letters 94(3-4):257-273
Woodhead J, Brauns M (2004) Current limitations to the understanding of Re–Os behaviour in subduction systems, with an example from New Britain. Earth Planet Sci Lett 221:309-323
Woodland SJ (2000) Development of ICP MS isotope dilution preconcentration techniques for determination of platinum group elements in volcanic rocks. PhD thesis University of Durham
Woodland SJ, Pearson DG, Thirlwall MF (2002) A platinum group element and Re–Os isotope investigation of siderophile element recycling in subduction zones: comparison of Grenada, Lesser Antilles Arc, and the Izu-Bonin arc. J Petrol 43:171-198
Workman RK, Hart SR, Jackson MG, Regelous M, Farley KA, Blusztajn J, Kurz M (2004) Recycled metasomatised lithosphere as the origin of the Enriched Mantle II (EM2) end-member: evidence from the Samoan Volcanic Chain. Geochem Geophys Geosys 5:Q04008 http://dx.doi.org/10.1029/2003GC000623
Workman RK, Hart SR (2005) Major and trace element composition of the depleted MORB mantle (DMM). Earth Planet Sci Lett 231:53-72
Wright E, White WM (1987) The origin of Samoa: new evidence from Sr, Nd and Pb isotopes. Earth Planet Sci Lett 81:151-162
Xu JF, Suzuki K, Xu YG, Mei HJ, Li J (2007) Os, Pb, and Nd isotope geochemistry of the Permian Emeishan continental flood basalts: insights into the source of a large igneous province. Geochim Cosmochim Acta 71:2104-2119
Yang AY, Zhao TP, Zhou MF, Deng XG, Wange GQ, Li J (2013) Os isotopic compositions of MORBs from the ultra-slow spreading Southwest Indian Ridge: Constraints on the assimilation and fractional crystallization (AFC) processes. Lithos 179:28-35
Yang AY, Zhou MF, Zhao TP, Deng XG, Qi L, Xu JF (2014) Chalcophile elemental compositions of MORBs from the ultraslow-spreading Southwest Indian Ridge and controls of lithospheric structure on S-saturated differentiation. Chem Geol 382:1-13
Yaxley GM (2000) Experimental study of the phase and melting relations of homogeneous basalt + peridotite mixtures and implications for the petrogenesis of flood basalts. Contrib Mineral Petrol139:326-338
Yaxley GM, Green DH (1998) Reactions between eclogite and peridotite: mantle refertilization by subducted oceanic crust. Schweizerische Mineralogische und Petrographische Mitteilungen 78:243-25

Yokoyama T, Walker D, Walker RJ (2009) Low osmium solubility in silicate at high pressures and temperatures. Earth Planet Sci Lett 279:165-173

You CF, Spivack AJ, Gieskes JM, Martin JB, Davisson ML (1996) Boron contents and isotopic compositions in pore waters: a new approach to determine temperature induced artefacts-geochemical implications. Mar Geol 129:351-361

Yudovskaya MA, Tessalini S, Distler VV, Chaplygin IV, Chugaev AV, Dikov YP (2008) Behaviour of highly siderophile elements during magma degassing: a case study at the Kudryavy volcano. Chem Geol 248:318-341

Zhang M, Suddaby P, O'Reilly SY, Norman M, Qiu J (2000) Nature of the lithospheric mantle beneath the eastern part of the Central Asian fold belt: mantle xenolith evidence. Tectonophysics 328:131-156

Zhang YL, Liu CZ, Ge WC, Wu FY, Chu ZY (2011) Ancient sub-continental lithospheric mantle (SCLM) beneath the eastern part of the Central Asian Orogenic Belt (CAOB): implications for crust–mantle decoupling. Lithos 126:233-247

Zhang Z, Zhi X, Chen L, Saunders AD, Reichow MK (2008) Re-Os isotopic compositions of picrites from the Emeishan flood basalt province, China. Earth and Planetary Science Letters 276:30-39

Zindler A, Staudigel H, Batiza R (1984) Isotope and trace element geochemistry of young Pacific seamounts: implications for the scale of upper mantle heterogeneity. Earth Planet Sci Lett 70:175-195

Zindler A, Hart SR (1986) Chemical geodynamics. Chemical geodynamics. Ann Rev Earth Planet Sci 14:493-571

Figure captions

Figure 1. CI-chondrite normalised PGE abundances in (a) mantle derived melts and (b) primitif upper mantle and residual mantle rocks. Due to extraction of the low melting temperature Cu-Ni sulfide melt, which concentrates Pt and Pd, the PGE patterns of residual mantle rocks are depleted in Re, Pd and Pt. The depletion factor increases with the degree of melting (10 to 40%), and therefore with the amount of magma extracted from the mantle column, due to the concentration of the PGE in monosulfide solid solution (mss) and also to the fact that an increase in the degree of melting decreases the amount of mss remaining in the residual mantle. Mantle derived rocks show the opposite behaviour. MORB are IPGE depleted (Ru, Ir, Os) relative to the mantle composition because base-metal sulfides are not exhausted. In contrast the very high degree of partial melting (>35%) needed to generate the archean komatiite melts consumed all the base-metal sulfides in the mantle, generating PGE pattern close to the mantle. Data sources: MORB (Gannoun et al., 2007; Burton et al., 2015; Bézos et al., 2005; Yang et al., 2013; 2014; Jenner et al., 2012; Rehkämper et al., 1999); Komatiites (Connolly et al., 2011; Puchtel et al;, 2004; 2005; 2009); Abyssal peridotites(Harvey et al., 2006; Luguet et al., 2007; Pearson et al., 2004; Reisberg and Lorand, 1995); Primitif mantle (Becker et al., 2006).

Figure 2. Highly siderophile elements concentrations, normalised to CI-chondrite (Lodders et al., 2009). Primitive Earth mantle composition are from Becker et al. (2006) and from McDonough and Sun (1995). Predicted composition of Earth's mantle as a result of metal-silicate partitioning at low pressure (1 atm) are from Borisov et al. (1994; 1995); Borisov and Plame (1997); Fortenfant et al. (2003; 2006); Ertel et al. (1999); Ertel et al. (2001) and at high pressure (20 GPa) are from Brenan & McDonough (2009); Cottrell and Walker (2006); Ertel et al. (2006); Holzheid et al. (2000); Righter et al. (2008); Ohtani and Yurimoto (1996). The Late veneer addition are using the average composition of all chondrite groups (Walker, 2009).

Figure 3. Summary of sulfide/silicate partition coefficients determined by experiment (Andrews and Brenan, 2002; Brenan, 2008; Crocket et al., 1997; Fleet et al., 1996; Mungall and Brenan, 2014) and from natural samples (Gannoun et al., 2004; 2007; Hart end Ravizza, 1996; Patten et al., 2013; Peach et al., 1990; Roy Barman et al., 1998)

Figure 4. Mineral-melt partition coefficients of HSE determined by experiment (Brenan et al., 2003; 2005; 2012; Chazey and Neal, 2005;Mallman and O'Neill, 2007; Righter et al., 2004) and from natural samples (Burton et al., 1999; 2000; 2002; Connolly et al., 2011; Debaille et al., 2009; Gannoun et al., 2004; Gao et al., 2008; Hart and Ravizza; 1996; Harvey et al., 2010; 2011; Jackson end Shirey, 2011; Puchtel and Humayun, 2001; Puchtel et al., 2009).

Figure 5. CI-chondrite-normalized PGE patterns for refractory mantle sulfides and intrergranular Cu-rich sulfides. Reported patterns are a combination of different peridotites (Alard et al., 2000; 2005; Harvey et al., 2006; Lorand et al., 2001). Calculated mixture of residual included sulfide and an appropriate amount of intergranular sulfides produces a primitive mantle-like PGE pattern.

Figure 6. CI-chondrite normalized PGE abundances for Os-Ir-Ru alloys from ophiolite chromitites (Augé, 1985; 1988; González-Jiménez et al., 2009; 2011; Nakagawa and Franco, 1997).

Figure 7. PGE vs. Ni plots of MORBs. The high-F (mostly MORBs from Kolbeinsey Ridge) and low-F fields represent MORB suites produced by high and low degrees of partial melting defined by Bézos et al. (2005). Data sources: Jenner et al., 2012; Yang et al., 2014.

Figure 8. Rhenium ($pg.g^{-1}$) against osmium ($pg.g^{-1}$) for terrestrial basalts. Literature data are from the following references: MORB (Burton et al., 2015; Escrig et al., 2004; Gannoun et al., 2007; Schiano et al., 1997; Yang et al., 2013). OIB (Class et al., 2009; Day et al., 2009; 2010b; Hauri and Hart, 1993; Ireland et al., 2009; 2011; Jackson et al., 2011; Schiano et al., 2001; Widom and Shirey, 1996); Arc lavas (Alves et al., 2002; Chesley et al;, 2002); Komatiites (Connolly et al., 2011; Puchtel et al;, 2004; 2005; 2009); Mantle rocks (Harvey et al., 2006; Pearson et al., 2004; Reisberg and Lorand, 1995); CI-chondrite (Becker et al., 2006).

Figure 9. Re/Os ratio versus Os concentrations for terrestrial basalts. Data are frome the same references as for Figure 8

Figure 10. Rhenium concentrations ($pg.g^{-1}$) in MORB glass shown against (a) Aluminium (wt. % Al_2O_3) and (b) sulfur ($\mu g.g^{-1}$). Plotted data for MORB are from the same references as in Figure 8.

Figure 11. Osmium concentrations ($pg.g^{-1}$) in MORB glass shown against Nickel ($\mu g.g^{-1}$). Plotted data for MORB are from the same references as in Figure 8.

Figure 12. $^{187}Os/^{188}Os$ versus $1/^{188}Os$ ratios for MORB glasses. There is no covariation between Os concentration and Os isotope composition, and hence no evidence for binary mixing (see text for discussion). Plotted data are from Burton et al., 2015; Gannoun et al., 2004; 2007; Yang et al., 2013.

Figure 13. ^{187}Re-^{187}Os isotope evolution diagram for MORB glasses. No covariation is observed between $^{187}Re/^{188}Os$ and $^{187}Os/^{188}Os$. MORB glass possesses high $^{187}Re/^{187}Os$ (parent/daughter) ratios which raises the possibility that radiogenic ^{187}Os could be produced in very short periods of time (Gannoun et al., 2004; 2007). However, those samples with the highest $^{187}Re/^{187}Os$ (>2000) possess $^{187}Os/^{188}Os$ compositions close to the value expected for the primitive upper mantle.

Figure 14. $^{187}Os/^{188}Os$ isotope composition of MORB glasses (Burton et al., 2015; Gannoun et al., 2004; 2007; Yang et al., 2013) shown against (a) $^{87}Sr/^{86}Sr$ (b) $^{143}Nd/^{144}Nd$ and (c) $^{206}Pb/^{204}Pb$ (see text for discussion) (Sr, Nd and Pb data from Dosso et al., 1993; Escrig et al., 2004; Hamelin and Allègre, 1985; Hamelin et al., 1984; 1986; Prinzhofer et al., 1989; Schiano et al., 1997; Vidal and Clauer, 1981).

Figure 15. $^{187}Os/^{188}Os$ isotope composition of MORB glass shown against (a) ridge depth (metres below sea level) and (b) spreading rate (cm/year) (calculated using Argus et al., 2011 and De Mets et al., 2010).

Figure 16. Comparison of $^{187}Os/^{188}Os$ isotope ratios for MORB glass investigated previously (Schiano et al., 1997; Escrig et al., 2004) and re-analyzed in Gannoun et al. (2007) and Burton et al. (2015)

Figure 17. Osmium abundance shown against the deviation of the measured $^{187}Os/^{188}Os$ (in %) between recent studies (Gannoun et al., 2007; Burton et al., 2015) and earlier work (Schiano et al., 1997; Escrig et al., 2004). The highest deviation in the reported $^{187}Os/^{188}Os$ is observed for the glass samples with the lowest Os contents.

Figure 18. $^{187}Re–^{188}Os$ isotope evolution diagram for coexisting phases from the olivine– basalt ARP1974-011-018 (Gannoun et al. 2004) . Olivine, plagioclase, glass, and matrix yield a best-fit line corresponding to an age of 565 ± 336 ky(2σ). Clinopyroxene (not shown) does not lie on this best-fit line, suggesting either an older age or a different and more radiogenic source for this phase.

Figure 19. $^{187}Re–^{188}Os$ isotope evolution diagram for coexisting phases from the picritic basalt ARP1973-010-003 (Gannoun et al. 2004). Olivine, plagioclase, glass, and sulfide lie on a best-fit line corresponding to an age of 2.53 ± 0.15 My (2 σ). Spinel possesses a distinct isotope composition from this best-fit line and is probably the phase responsible for the displacement of the matrix from the same line.

Figure 20. $^{187}Os/^{188}Os$ vs 1/[Os] for heterogeneous Indian MORB. Two samples from the central indian ridge, MD57 D9-1 and D9-6 show high range of $^{187}Os/^{188}Os$ ratios from 0.126 to 0.254 which covaries with Os concentrations (Burton et al., 2015).

Figure 21. $^{187}Os/^{188}Os$ vs (a) Cl and (b) B for MORB glass

Figure 22. $^{187}Os/^{188}Os$ isotope composition of MORB glass shown against $\delta^{11}B$ ratios in the same sample (symbols as in Fig. 2) illustrating a clear positive covariation between both isotope systems. MORB samples with radiogenic $^{187}Os/^{188}Os$ values also possess high $\delta^{11}B$ ratios. Mixing curves between uncontaminated MORB ($^{187}Os/^{188}Os$ of 0.125 and $\delta^{11}B$ of −10‰ with 7 $pg.g^{-1}$ and 1 $\mu g.g^{-1}$ for Os and B concentrations respectively) and other sources are also shown. (1) Direct contamination by seawater with $^{187}Os/^{188}Os$ of 1.06, $\delta^{11}B$ of +40‰, [Os]= 0.01 $pg.g^{-1}$ and [B]= 4.6 $\mu g.g^{-1}$ (Levasseuret al., 1998). (2) Assimilation of Fe–Mn oxyhydroxides or Os-rich sediments. The grey field in the left of the graph encompasses the potential mixing lines $^{187}Os/^{188}Os$ ~1, [Os]= 1 $pg.g^{-1}$, $\delta^{11}B$= +10‰ and [B]= 10 $\mu g.g^{-1}$. (3) Assimilation of relatively old altered oceanic crust with variable $^{187}Os/^{188}Os$ ratios (0.15, 0.20 and 0.25 for a, b and c, respectively), [Os]= 10 $pg.g^{-1}$, [B]= 8 $\mu g.g^{-1}$ and $\delta^{11}B$= +6‰. Marks on the curves denote the weight percentage of assimilated altered oceanic crust (in 1% increments) present in the mixture.

Figure 23. Backscattered-electron (BSE) images and chemical maps of typical MORB sulfides from the picritic basalt ARP1973-010-003 (Famous area, Mid-Atlantic ridge). Chemical maps were produced using a wavelength dispersive spectrometry (WDS) coupled to a CAMECA SX-100

microprobe at Blaise Pascal University (Clermont-Ferrand, France). Shading indicates the relative abundance of a given element. MSS: monosulfide solid solution; ISS: intermediate solid solution; Pn: pentlandite. **a**. spherical sulfide globule inclusion in olivine. **b**. sulfide globule inclusion in basalt matrix. Both grains have coarse grained texture.

Figure 24. Bulk composition of sulfide droplets in the system Fe-Ni-Cu in weight fraction. The grey zone corresponds to the bulk composition of sulfide droplets from Czamanske & Moore (1977). Dashed line represents the composition of sulfide liquid composition at Mss crystallization at 1100, 1050, and 1000 °C from Ebel & Naldrett (1997). Note that texture of sulfide droplets is not dependent on their composition. Droplet liquidus range between more than 1100 to 1050 °C. Modified from Czamanske and Moore (1977) and Patten et al. (2012).

Figure 25. $^{187}Os/^{188}Os$ isotope composition shown against Os concentration (ng g^{-1}) for individual sulfides from MORB. This indicates a negative covariation between $^{187}Os/^{188}Os$ and Os concentration in the sulfides, where low Os sulfides possess more radiogenic Os isotope compositions. These radiogenic values may indicate that such sulfides are more susceptible to seawater derived contamination. Data taken from Burton et al., 2015; Gannoun et al., 2004; 2007; Roy Barman et al., 1998. (see text for discussion).

Figure 26. $^{187}Os/^{188}Os$ isotope composition of individual sulfides shown against the $^{187}Os/^{188}Os$ value of the glass host. In all cases, sulfide grains possess $^{187}Os/^{188}Os$ values that are less radiogenic than their glass host. Sulfides also show a much reduced range of Os isotope compositions compared to the corresponding host glass.

Figure 27. Histogram showing measured $^{187}Os/^{188}Os$ isotope ratios for (a) N-MORB glass data (Burton et al., 2015; Gannoun et al., 2004; 2007; Yang et al., 2013) (b) single grain sulfide data for MORB (Burton et al., 2015; Gannoun et al., 2004; 2007; unpublished data; Roy Barman et al., 1998) (c) abyssal peridotite whole-rock data (Alard et al., 2005; Brandon et al., 2000; Harvey et al., 2006; Martin, 1991; Snow and Reisberg, 1995; Standich et al., 2001) (d) single grain sulfide data for abyssal peridotites (Alard et al., 2005; Harvey et al., 2006; Warren and Shirey, 2012). The estimate for the primitive upper mantle (PUM; Meisel et al., 1996) is also shown. The average $^{187}Os/^{188}Os$ isotope composition of abyssal peridotites is 0.127±0.015 (n = 129) while individual sulfides yield an average $^{187}Os/^{188}Os$ composition of 0.125±0.021 (n = 63). N-MORB analysed thus far show no evidence for a subchondritic source which may reflect local melting of abyssal peridotites (Brandon et al., 2000), resistance of depleted peridotites to remelting (Hirth and Kohlstedt, 1996; Mange, 1996) or that Os from undepleted (fertile) mantle dominates the MORB budget.However, the high-Os (>20 ng g^{-1}) sulfides yield an average composition of 0.129 ± 0.005 (n=31) close to the PUM estimation with values as low as 0.1236. Therefore, these high-Os sulfides show no evidence no evidence for significant Re enrichment in the MORB source, as might be expected from the presence of recycled oceanic crust. Rather they indicate that the upper mantle source of these samples has experienced a long-term depletion of Re, similar to that observed in abyssal peridotites, and consistent with the incompatible nature of this element during mantle melting.

Figure 28. CI-chondrite normalised PGE abundance (Lodders et al., 2009). Open squares: average Deep Sea Drilling Project (DSDP) Sites 417/418; diamends: DSDP Hole 504B (Peucker-Ehrenbrink

et al., 2003); solid squares: Ocean Drilling Program Hole 735B (Blusztajn et al., 2000); open circles: Oman crustal section (Peucker-Ehrenbrink et al., 2012); solid circles: composite ocean crust (Peucker-Ehrenbrink et al., 2012). The pattern of average MORB (This chapter) and abyssal peridotites (Harvey et al., 2006; Luguet et al., 2007; Pearson et al., 2004; Reisberg and Lorand, 1995) are added for comparison.

Figure 29. Plot of Os concentration versus Os isotope ratios for Louiville Seamount Chain basalts (age-corrected) and olivines (present-day). Pacific ocean island basalts (OIB), mid-ocean ridge basalts (MORB), and Ontong Java Plateau basalts (OJP) basalts are shown for comparison. Osmium abundances and isotopic signatures are limited compared to other Pacific OIB. Data sources: Schiano et al. (1997, 2001); Brandon et al. (1999); Eisele et al. (2002); Jackson and Shirey (2011); Hanyu et al. (2011); Tejada et al. (2013). Modified after Tejada et al. (2015).

Figure 30. $^{187}Os/^{188}Os$ versus (a) $^{206}Pb/^{204}Pb$ and (b) $^{143}Nd/^{144}Nd$ diagrams for Cameroon Volcanic Line (CVL) basalts. Pb and Nd isotope data are from Barfod (1999) and Lee et al. (1996). HIMU, DMM, EM1, and BSE are shown for reference. The average $^{187}Os/^{188}Os$ ratio for sub-continental lithospheric mantle is from Shirey and Walker (1998). Ultramafic xenoliths beneath the continental part of the CVL are also shown. The increments in the curves are 2%. The grey shaded area indicates the possible compositions for crustally contaminated lavas. The most radiogenic samples from the continental sector can be explained by assimilation of 8 to 16% of continental crust. Assuming for the uncontaminated starting point [Os] = 10 pg g-1, $^{187}Os/^{188}Os$ = 0.156, $^{206}Pb/^{204}Pb$ = 20.24, [Pb] = 2 µg g^{-1}; for upper continental crust (UCC) [Os] = 50 pg g^{-1}, $^{187}Os/^{188}Os$ = 1.4, $^{206}Pb/^{204}Pb$ = 19.3, [Pb] = 8 µg g-1; and for lower continental crust (LCC) [Os] = 50 pg g^{-1}, $^{187}Os/^{188}Os$ = 0.8 (Saal et al., 1998), $^{206}Pb/^{204}Pb$ = 17.5, [Pb] = 8 µg g^{-1}. Curves (1) and (2) describe the possible mixing trajectories between HIMU and DMM. (1) Assimilation of mantle xenocrysts and (2) mixing of lavas derived from DMM and HIMU sources. Modelling parameters are as follows: for (1) DMM mantle [Os] = 3 ng g^{-1}, $^{187}Os/^{188}Os$ = 0.125, $^{206}Pb/^{204}Pb$ = 18.5, [Pb] = 0.15 µg g^{-1} and for (2) DMM melt [Os] = 8 pg g^{-1}, $^{187}Os/^{188}Os$ = 0.127, $^{206}Pb/^{204}Pb$ = 18.5, [Pb] = 0.45 µg g^{-1}. For Os–Nd modelling the starting point was chosen to be the closest to HIMU endmember, $^{143}Nd/^{144}Nd$ = 0.513, [Nd] = 40 µg g-1, 187Os/188Os = 0.15, [Os] = 10 pg g^{-1}; for UCC $^{143}Nd/^{144}Nd$ = 0.512, [Nd] = 27 µg g^{-1} (Rudnick and Fountain, 1995), $^{187}Os/^{188}Os$ = 1.4, [Os] = 50 pg g^{-1}; and for LCC $^{143}Nd/^{144}Nd$ = 0.512, [Nd] = 50 µg g^{-1} (Kwékam et al., 2013), $^{187}Os/^{188}Os$=0.8, [Os]=30 pg g^{-1} (Saal et al., 1998). Reproduced with permission of Elsevier BV from Gannoun A, Burton KW, Barfod DN, Schiano P, Vlastélic I, Halliday AN (2015a) Resolving mantle and magmatic processes in basalts from the Cameroon volcanic line using the Re-Os isotope system. Lithos 224-225:1-12.

Figure 31. HSE patterns for 1.27 Ga Coppermine CFB, ~130 Ma Parana basalts and ~61 Ma West Greenland picrites versus fractional crystallization models (grey-lines from 13 wt.% MgO, highest HSE concentrations to 4 wt.% MgO, lowest HSE concentrations) assuming an 'average' West Greenland picrite composition for model starting composition. Explanation of the model is provided in detail in Day et al. (2013). Data sources are: Woodland (2000), Rocha-Junior et al. (2012) and Day et al. (2013). CI-chondrite normalization from Horan et al. (2003).

Figure 32. $^{187}Os/^{188}Os$ vs. 1/Os for the Wudalianchi-Erkeshan highly potassic basalts, NE China. The solid lines represent binary mixing lines modeled as follows: Fields of crust addition to the intraplate basalts of 2%, 3.5% and 8% lower continental crust are calculated using the values of Saal et al. (1988; $^{187}Os/^{188}Os$ = 0.8 and Os concentration = 49 pg g^{-1}). Metasomatic compositions are based upon mean values from Alard et al. (2002) and Sen et al. (2011). Mean primary sulfide compositions

are taken from Alard et al. (2000, 2002), Pearson et al. (2002), Harvey et al. (2006, 2010, 2011), Lorand et al. (2013) – see also the supplementary information from Harvey et al. (2015, this volume). Modified after Chu et al. (2013).

Figure 33. World map showing locations of major convergent margin settings (stippled lines) and divergent boundary settings (grey lines) mentioned in the text.

Figure 34. Plots of Os and Re versus MgO content for convergent margin picrites, basalts and evolved rocks. Data sources: Brandon et al. (1996); Alves et al. (1999; 2002); Borg et al. (2000), Woodland et al. (2002); Woodhead & Brauns (2004); Turner et al. (2009); Bezard et al. (2015).

Figure 35. Plots of Os and reciprocal Os (1/Os) versus $^{187}Os/^{188}Os$ for convergent margin picrites, basalts and evolved rocks. Data sources: Brandon et al. (1996); Alves et al. (1999; 2002); Borg et al. (2000), Woodland et al. (2002); Woodhead & Brauns (2004); Turner et al. (2009); Bezard et al. (2015).

Figure 36. CI-chondrite normalized HSE diagrams for Lihir mantle xenoliths and lavas (McInnes et al., 1999), Grenada picrites and basalts and Izu-Bonin lavas (Woodland et al., 2000), and Kamchatka xenoliths (Widom et al., 2003). Note that PPGE > IPGE lavas from the Izu-Bonin and Grenada. CI chondrite normalization from Horan et al. (2003).

Figure 37. Assimilation accompanied by fractional crystallization (AFC) models of $^{87}Sr/^{86}Sr$ versus $^{187}Os/^{188}Os$ for Lesser Antilles primitive lavas Parameters for Models 1 and 2 are shown in the figure and in Table 3 of Bezard et al. (2015).

Figure 38. Primitive mantle normalized HSE diagram for cores and rinds of Mèlange metamorphic magic blocks from the Catalina Schist, Franciscan Complex and Samana Metamorphic Complex. Cores are consistent with dominantly reflecting basaltic/sedimentary protoliths with radiogenic Os and rinds are can represent as 70% peridotite HSE contributions. Data are from Penniston-Dorland et al., 2012; 2014, with primitive mantle normalization from Becker et al. (2006).

3201 Figure 1
3202

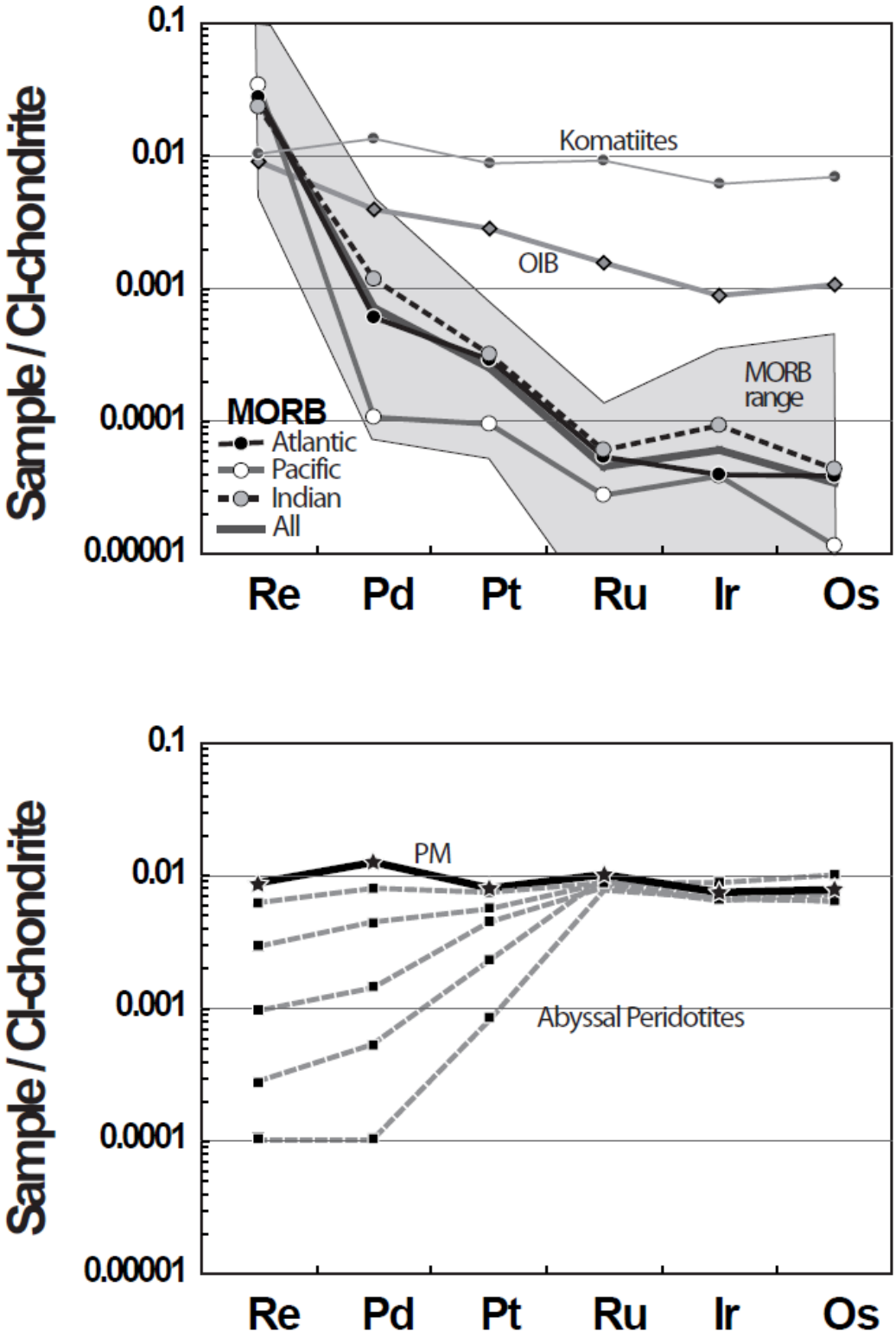

3203
3204
3205

Figure 2

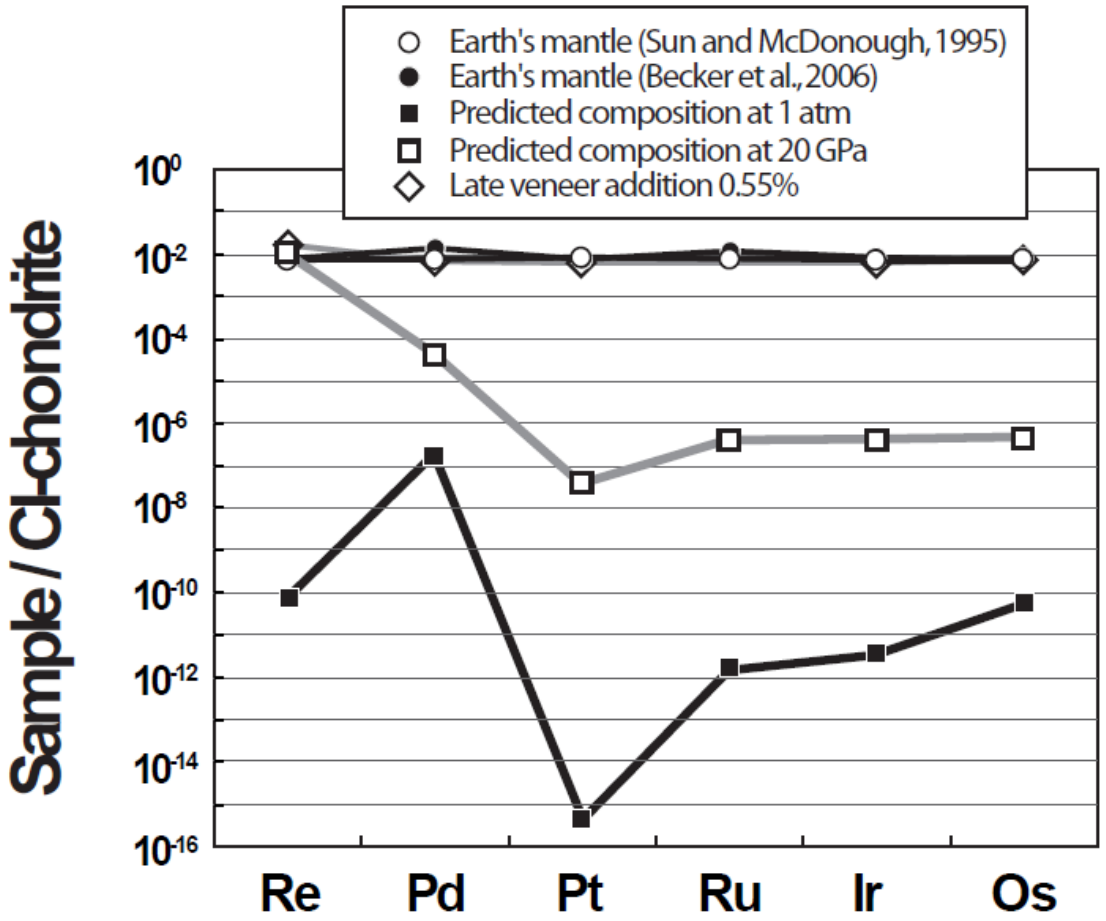
Earth's mantle (Sun and McDonough, 1995)
Earth's mantle (Becker et al., 2006)
Predicted composition at 1 atm
Predicted composition at 20 GPa
Late veneer addition 0.55%
Sample / CI-chondrite
10^0
10^-2
10^-4
10^-6
10^-8
10^-10
10^-12
10^-14
10^-16
Re
Pd
Pt
Ru
Ir
Os

Figure 3

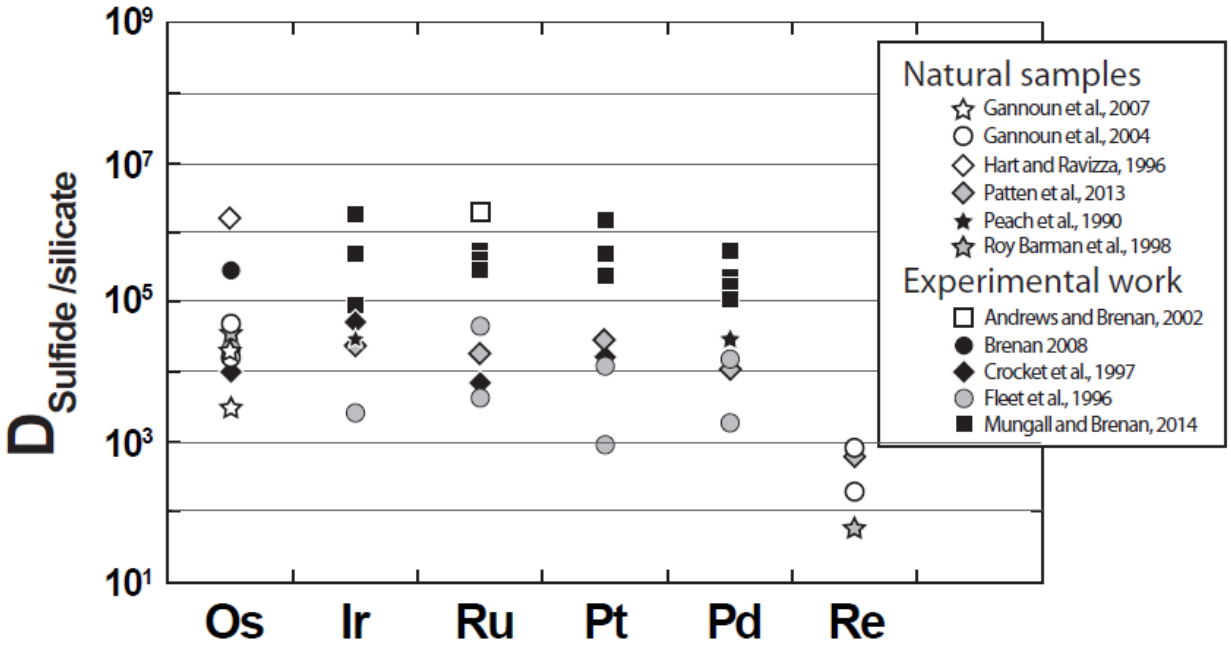
10^9
10^7
10^5
10^3
10^1
$D_{Sulfide/silicate}$
Os
Ir
Ru
Pt
Pd
Re
Natural samples
Gannoun et al., 2007
Gannoun et al., 2004
Hart and Ravizza, 1996
Patten et al., 2013
Peach et al., 1990
Roy Barman et al., 1998
Experimental work
Andrews and Brenan, 2002
Brenan 2008
Crocket et al., 1997
Fleet et al., 1996
Mungall and Brenan, 2014

Figure 4

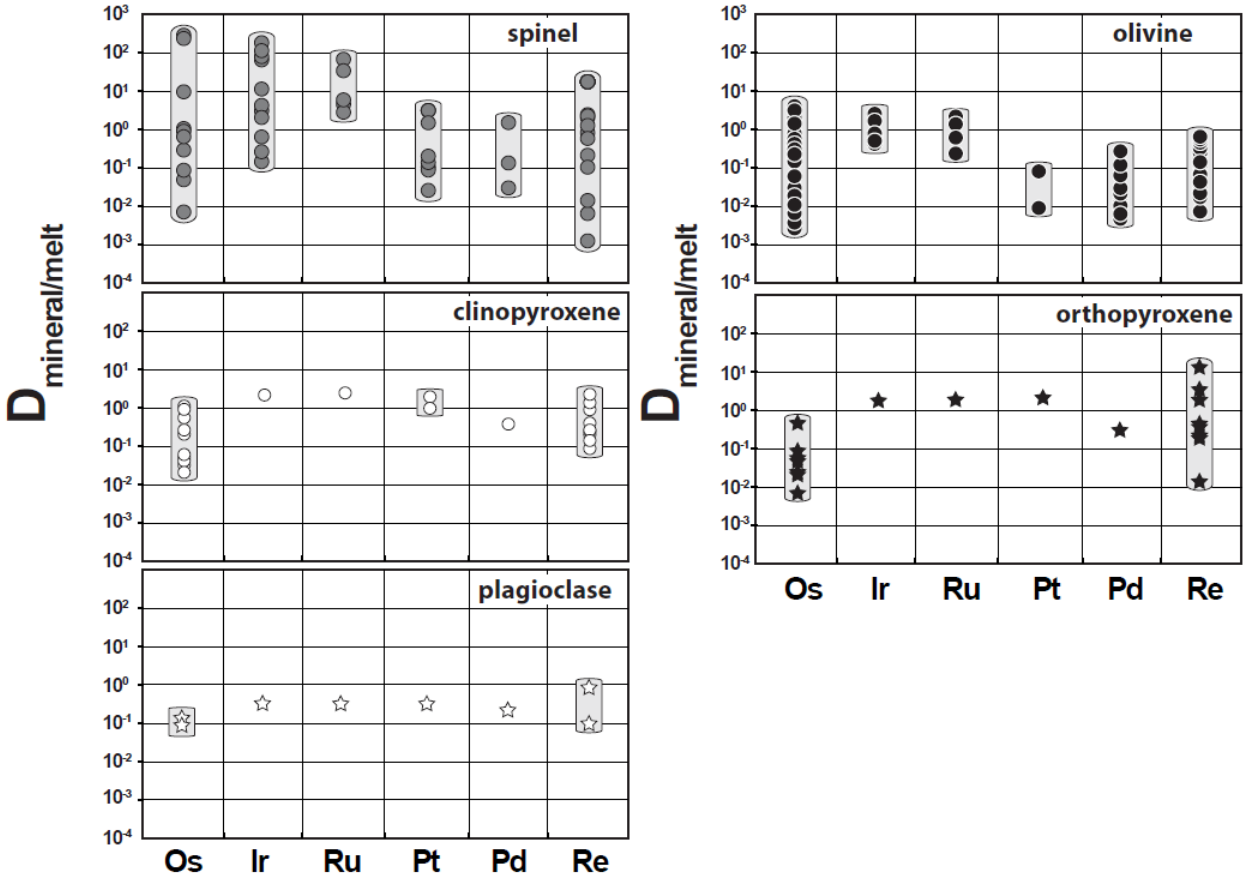
spinel
clinopyroxene
plagioclase
olivine
orthopyroxene
D mineral/melt
Os
Ir
Ru
Pt
Pd
Re

3287 Figure 5

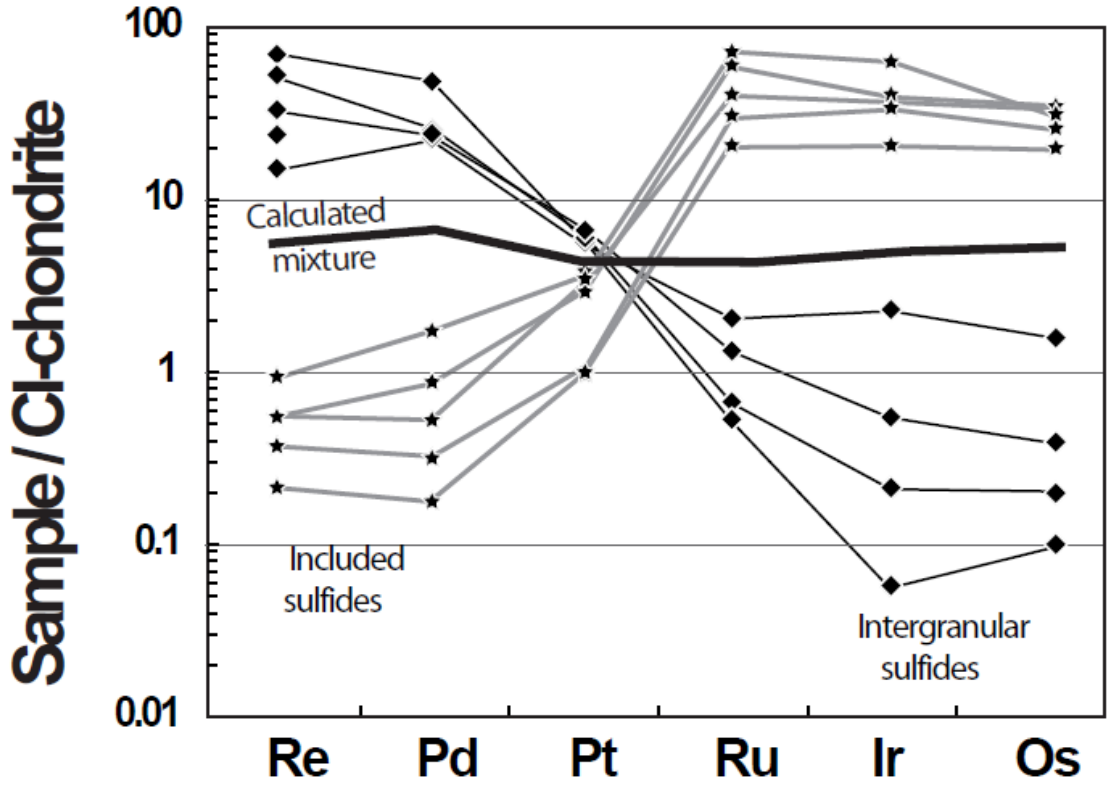

3288
3289
3290
3291
3292
3293
3294
3295
3296
3297
3298
3299
3300
3301
3302
3303
3304
3305
3306
3307
3308
3309
3310
3311
3312

Figure 6

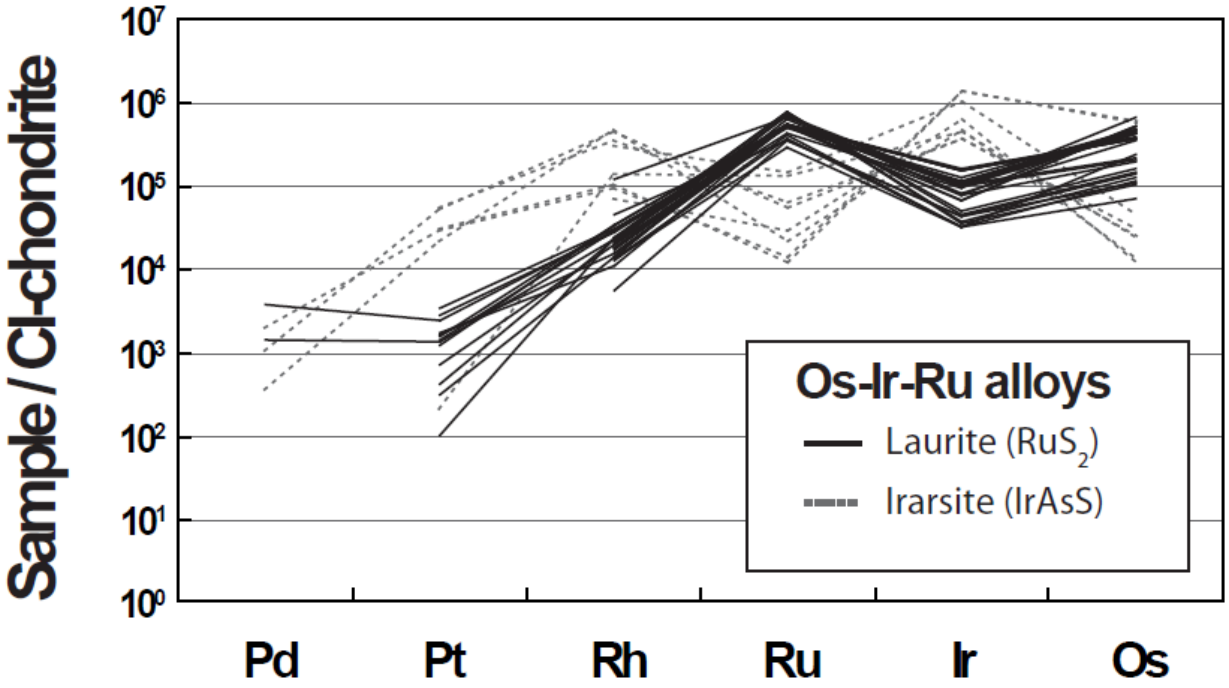
Sample / CI-chondrite
10^7
10^6
10^5
10^4
10^3
10^2
10^1
10^0
Pd
Pt
Rh
Ru
Ir
Os
Os-Ir-Ru alloys
Laurite (RuS2)
Irarsite (IrAsS)

3343
3344 Figure 7
3345

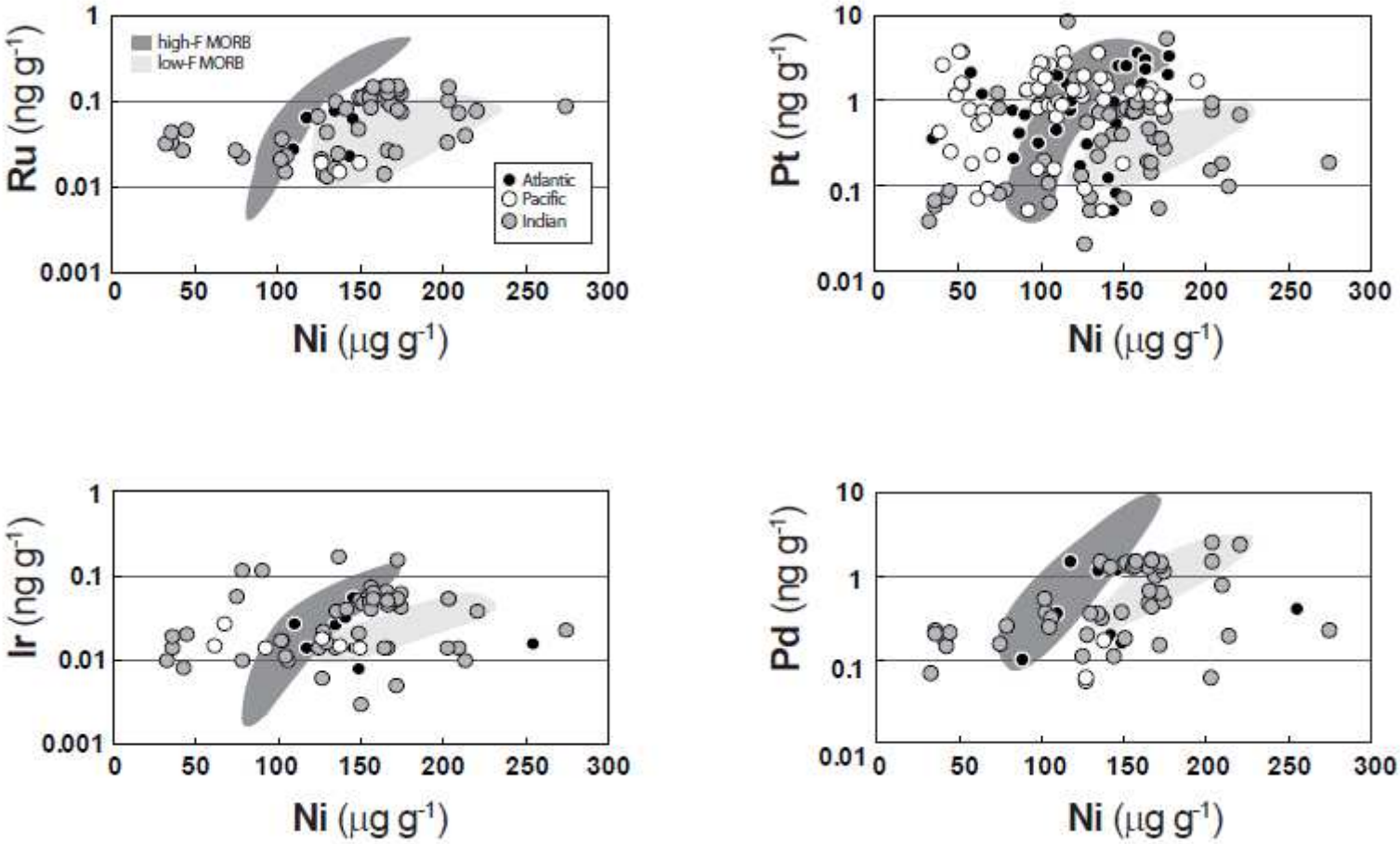

3346
3347
3348

Figure 8

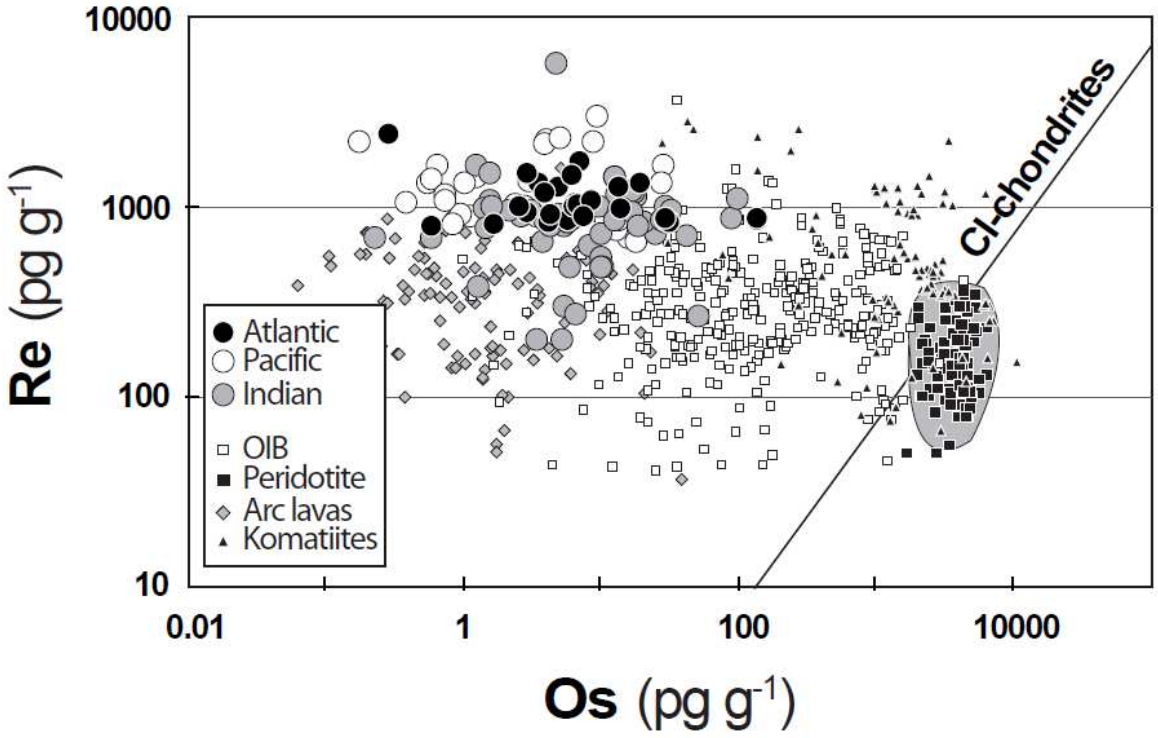
10000
1000
100
10
0.01
1
100
10000
Re (pg g-1)
Os (pg g-1)
Atlantic
Pacific
Indian
OIB
Peridotite
Arc lavas
Komatiites
CI-chondrites

Figure 9

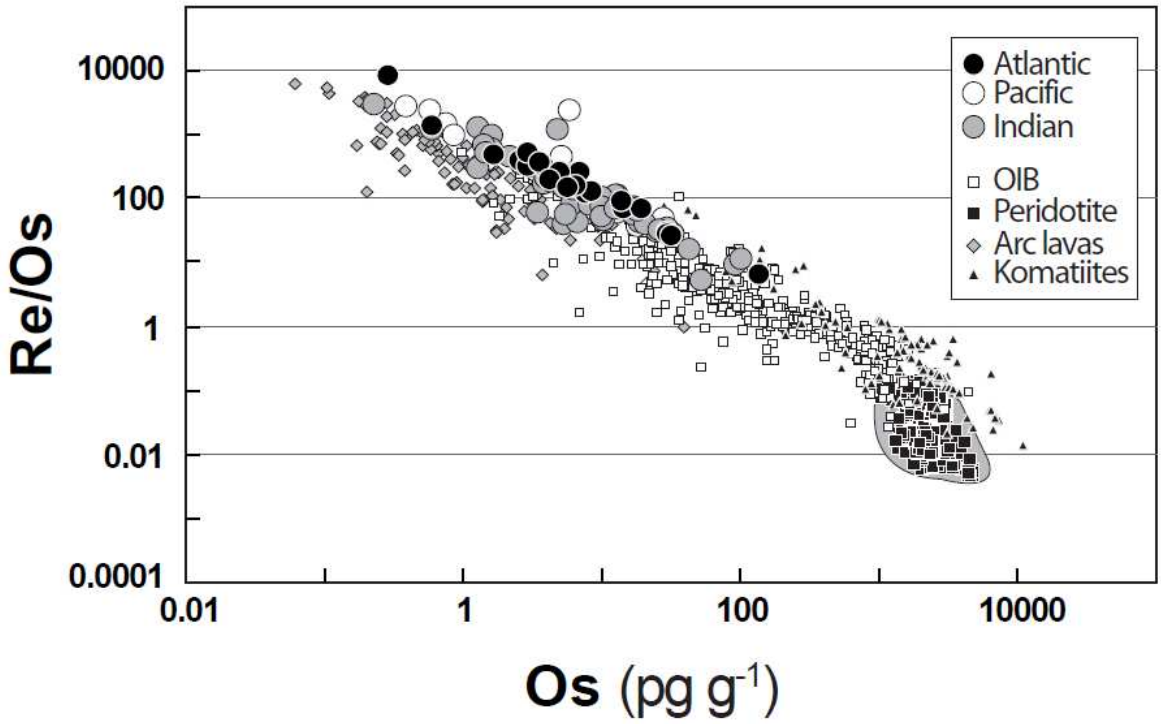
Re/Os
10000
100
1
0.01
0.0001
0.01
1
100
10000
Os (pg g-1)
Atlantic
Pacific
Indian
OIB
Peridotite
Arc lavas
Komatiites

3403 Figure 10
3404

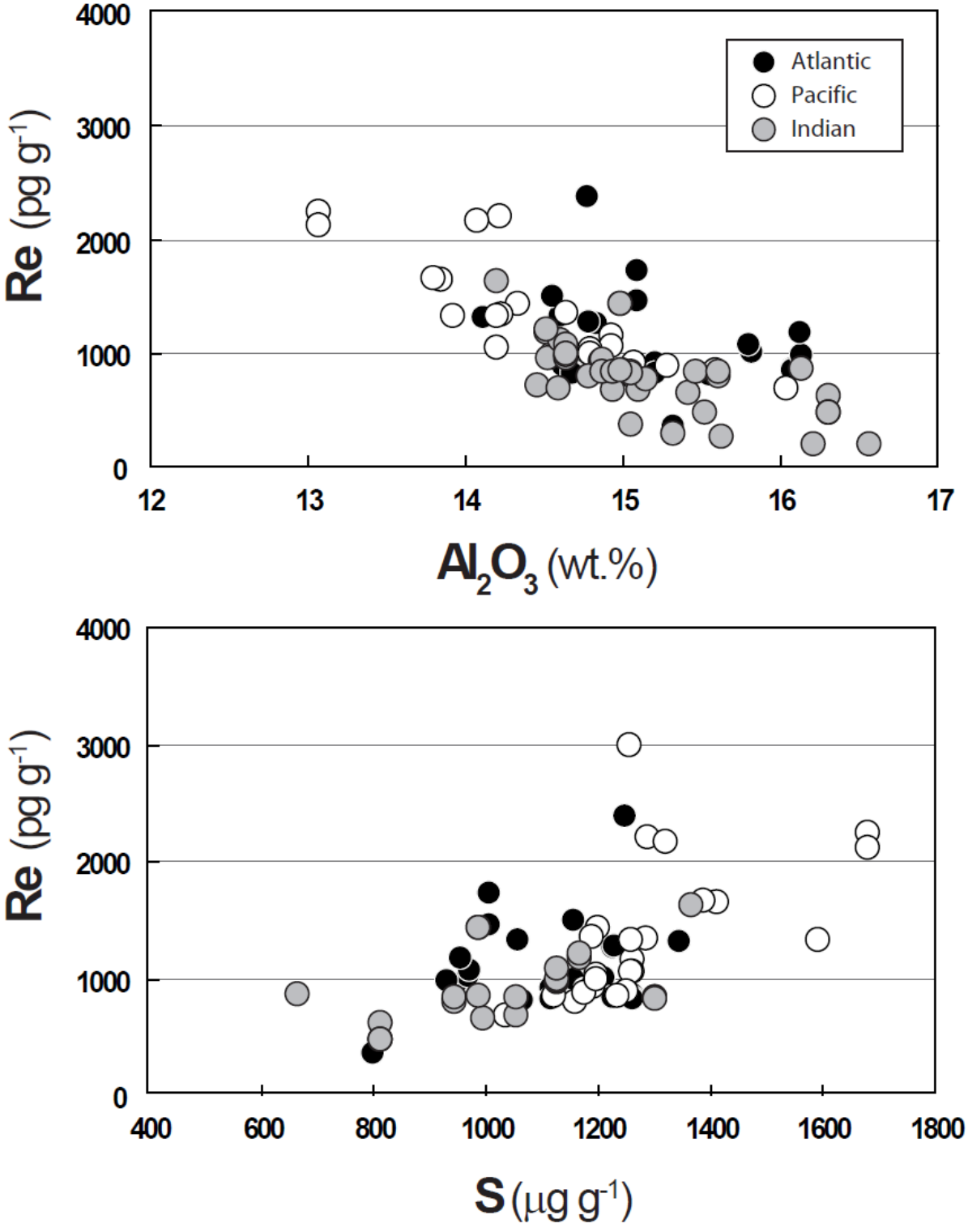

3405
3406
3407
3408
3409

Figure 11

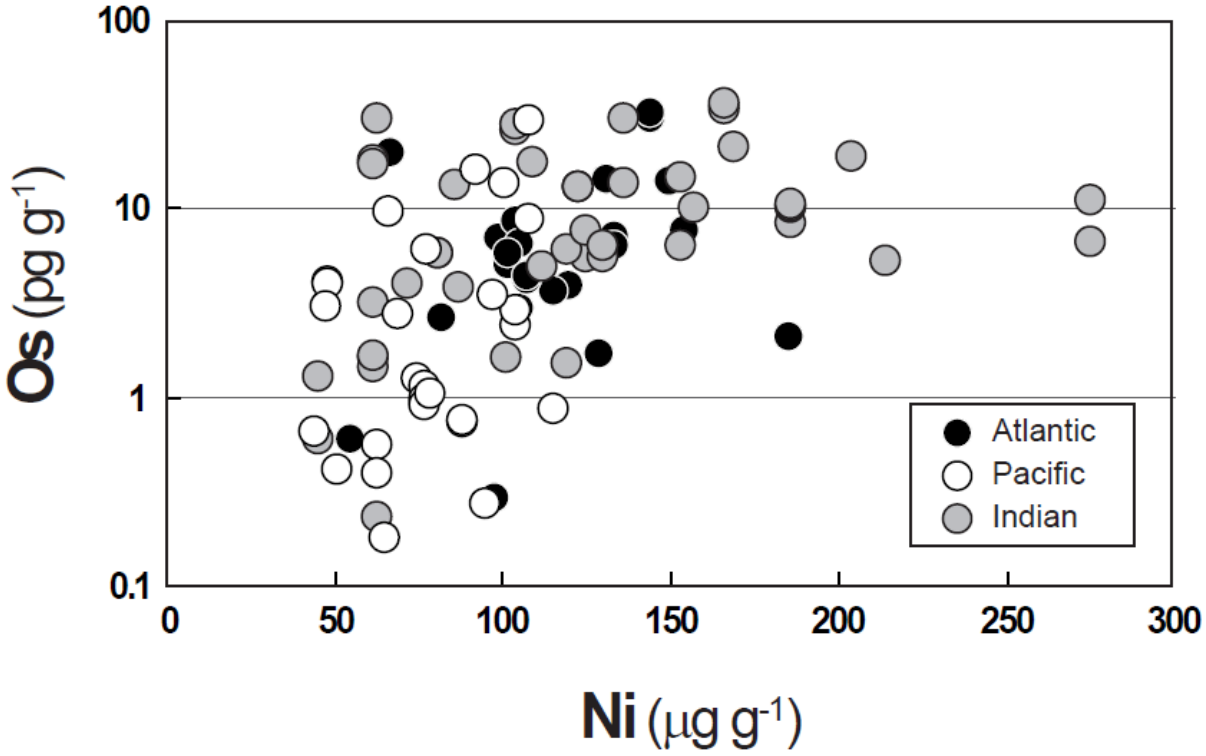
100
10
1
0.1
Os (pg g-1)
0
50
100
150
200
250
300
Ni (µg g-1)
Atlantic
Pacific
Indian

Figure 12

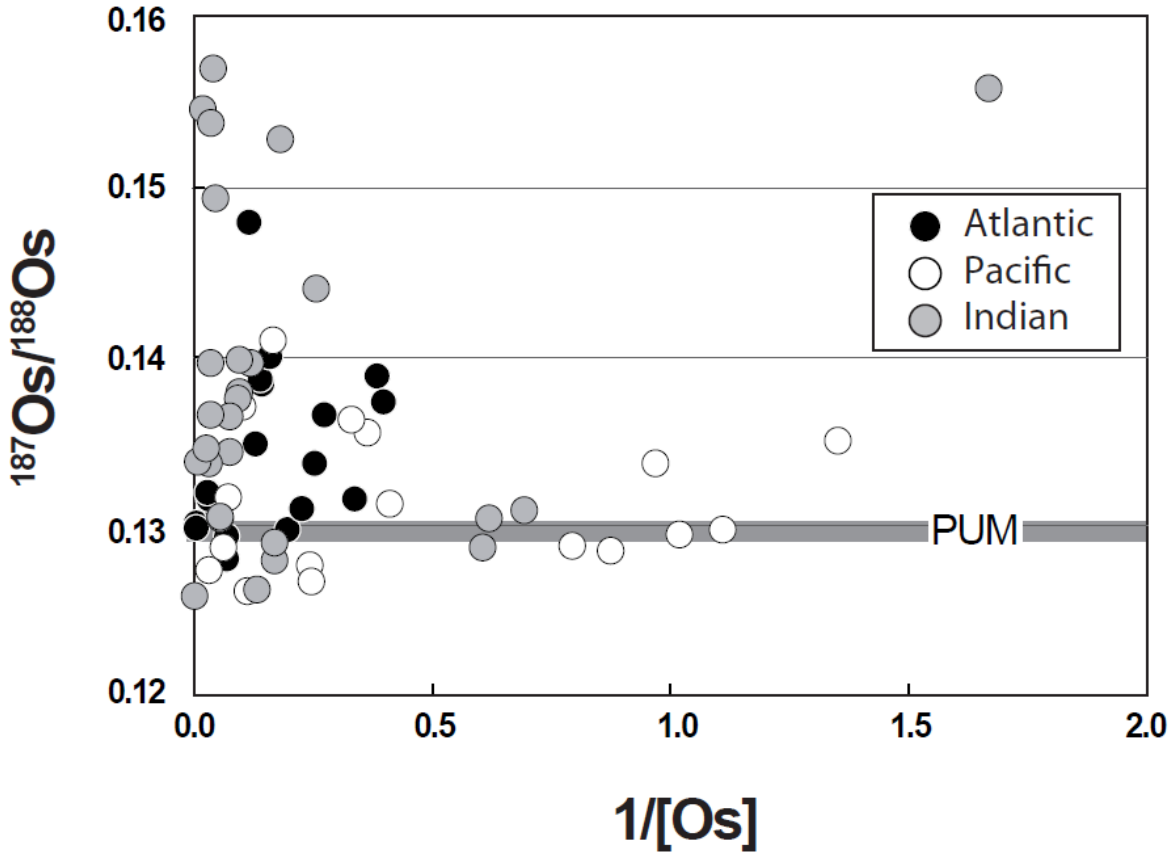
0.16
0.15
0.14
0.13
0.12
0.0
0.5
1.0
1.5
2.0
187Os/188Os
1/[Os]
Atlantic
Pacific
Indian
PUM

Figure 13

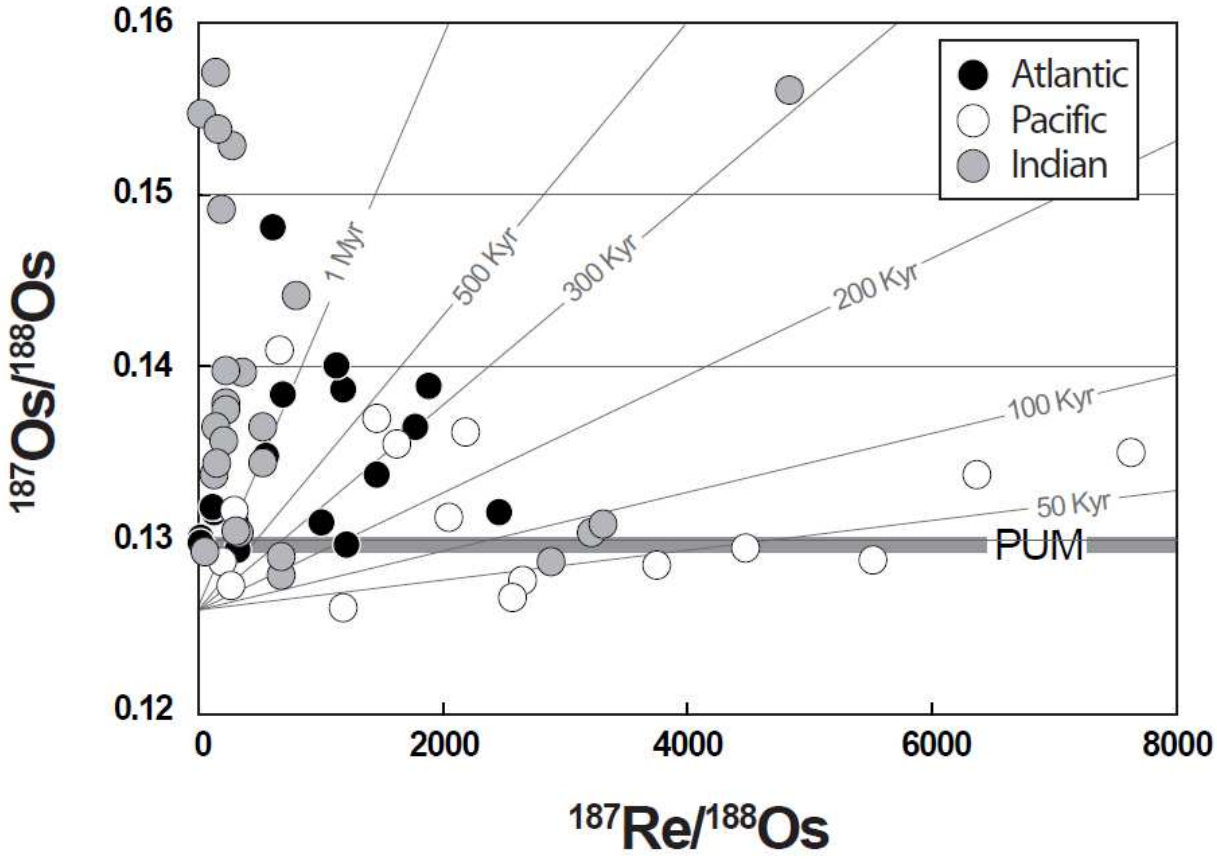
0.16
0.15
0.14
0.13
0.12
0
2000
4000
6000
8000
$^{187}Os/^{188}Os$
$^{187}Re/^{188}Os$
Atlantic
Pacific
Indian
1 Myr
500 Kyr
300 Kyr
200 Kyr
100 Kyr
50 Kyr
PUM

3489 Figure 14
3490

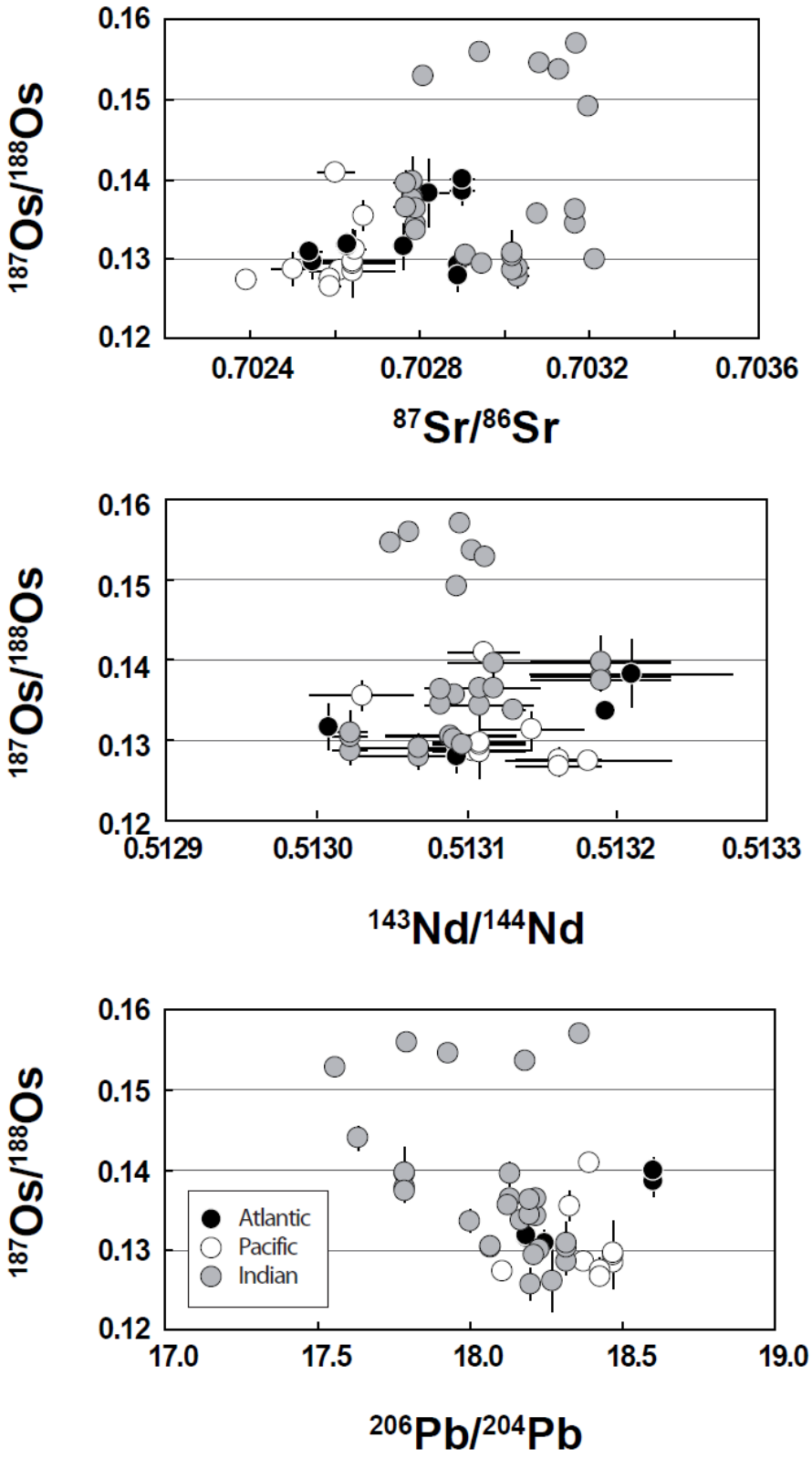

3491
3492
3493
3494

Figure 15

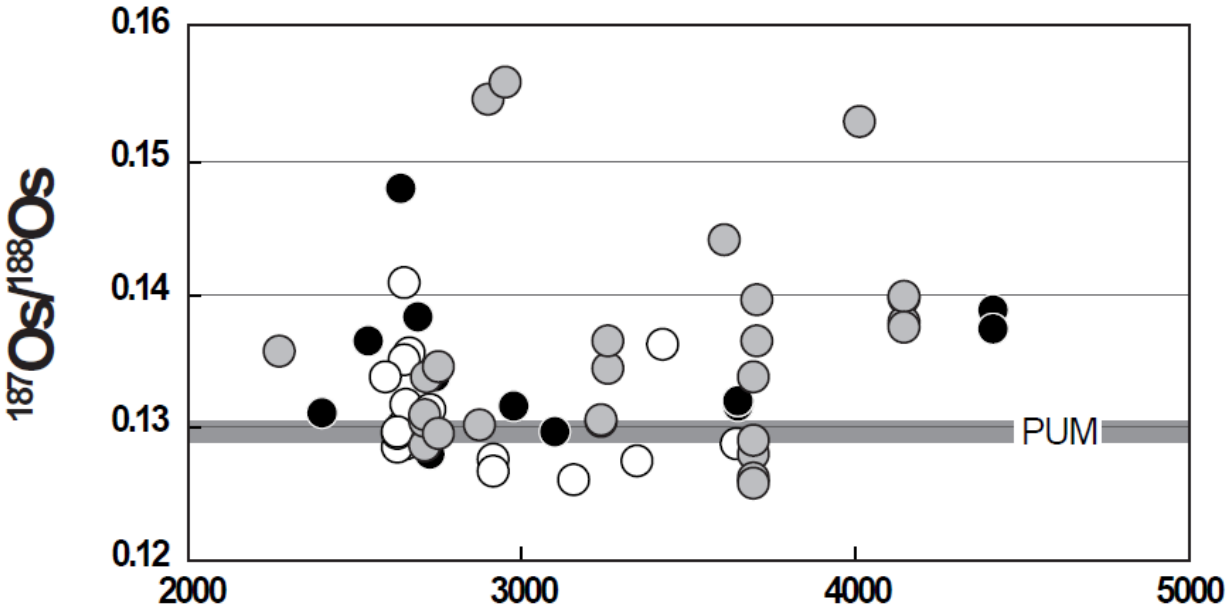

Figure 16

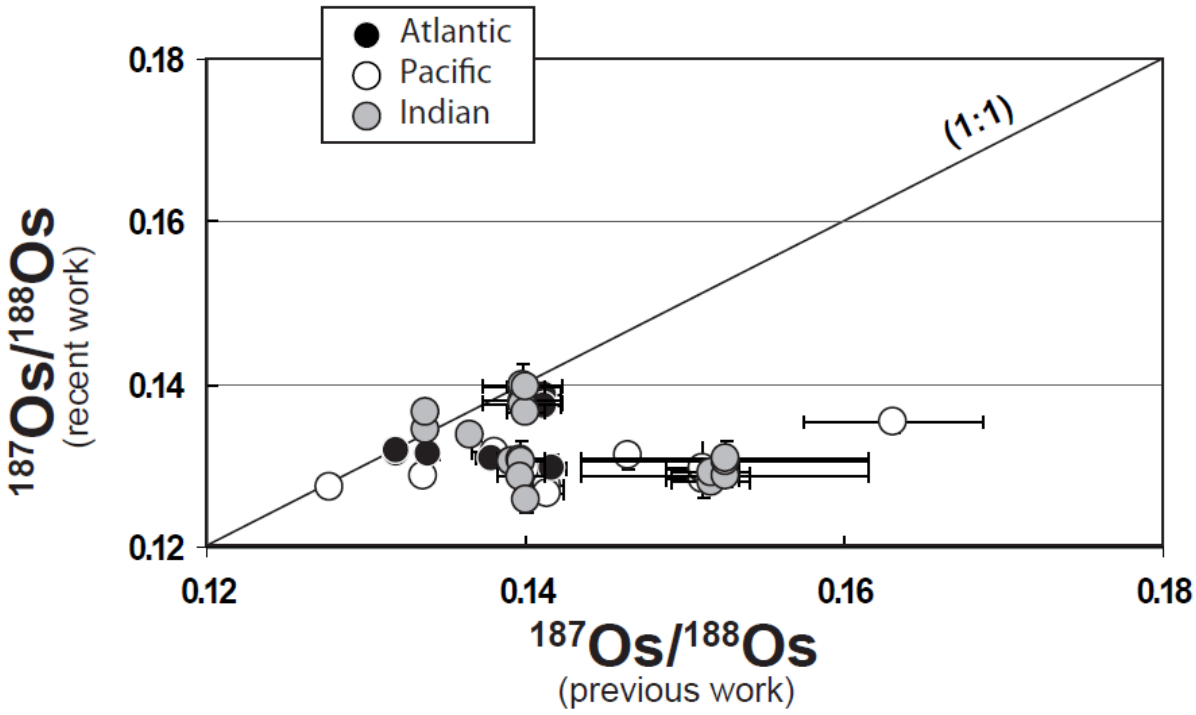
Atlantic
Pacific
Indian
(1:1)
0.18
0.16
0.14
0.12
0.12
0.14
0.16
0.18
$^{187}Os/^{188}Os$
(recent work)
$^{187}Os/^{188}Os$
(previous work)

Figure 17

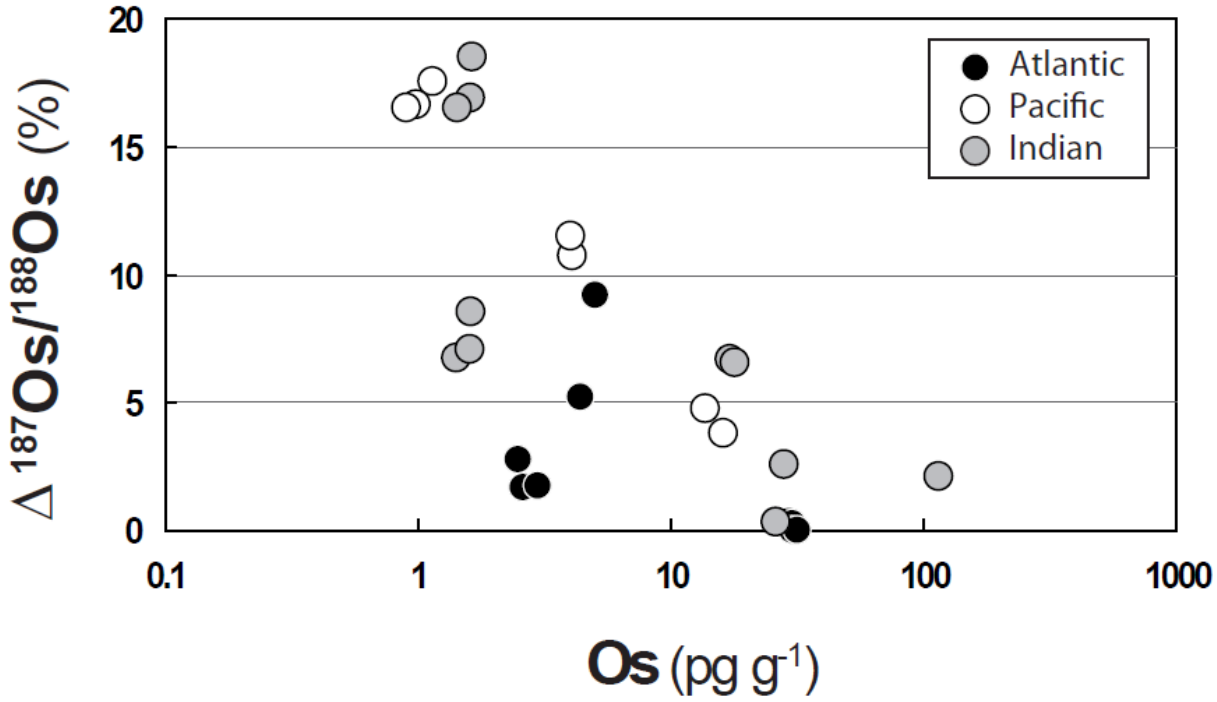
20
15
10
5
0
0.1
1
10
100
1000
Atlantic
Pacific
Indian
Δ 187Os/188Os (%)
Os (pg g-1)

Figure 18

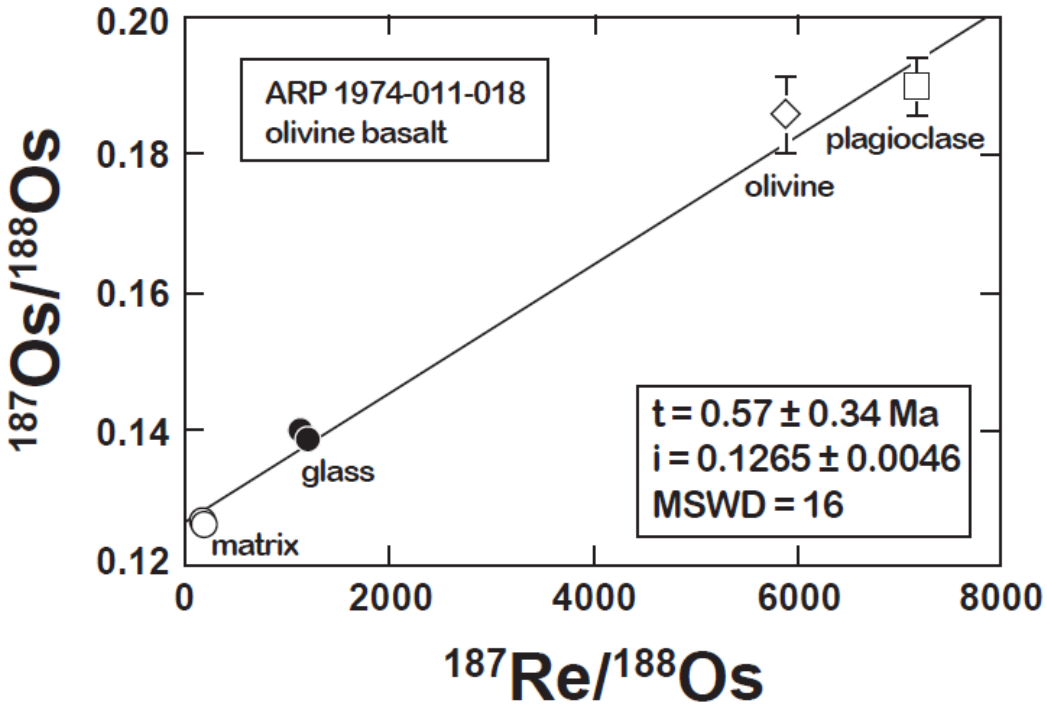
ARP 1974-011-018
olivine basalt
t = 0.57 ± 0.34 Ma
i = 0.1265 ± 0.0046
MSWD = 16
plagioclase
olivine
glass
matrix
0.20
0.18
0.16
0.14
0.12
0
2000
4000
6000
8000
187Os/188Os
187Re/188Os

Figure 19

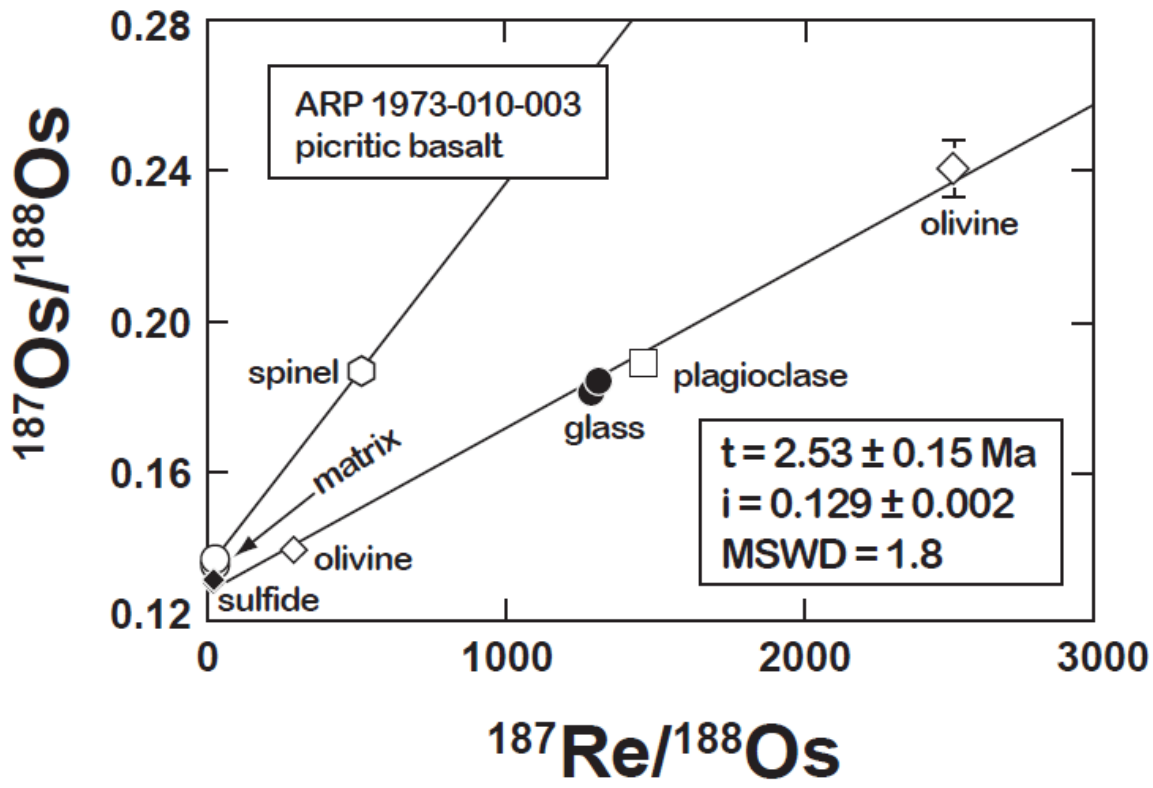
ARP 1973-010-003
picritic basalt
olivine
spinel
plagioclase
glass
matrix
olivine
sulfide
t = 2.53 ± 0.15 Ma
i = 0.129 ± 0.002
MSWD = 1.8
0.28
0.24
0.20
0.16
0.12
0
1000
2000
3000
187Os/188Os
187Re/188Os

Figure 20

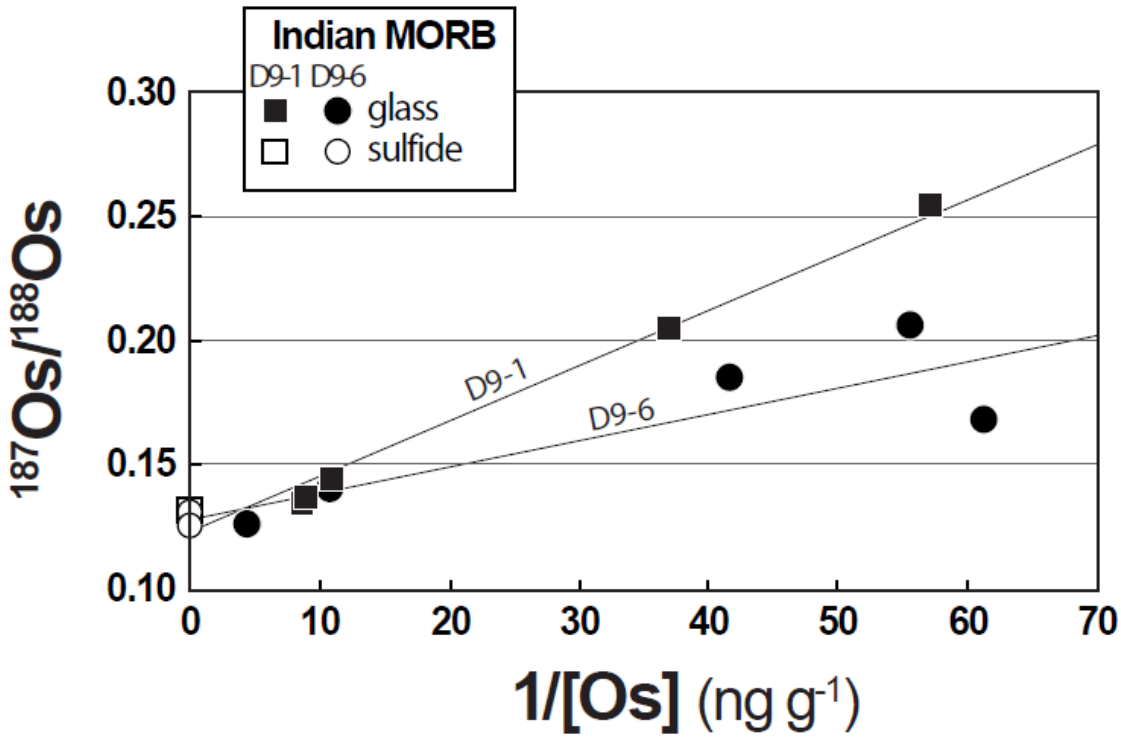
Indian MORB
D9-1 D9-6
glass
sulfide
0.30
0.25
0.20
0.15
0.10
0
10
20
30
40
50
60
70
D9-1
D9-6
187Os/188Os
1/[Os] (ng g-1)

3667 Figure 21
3668

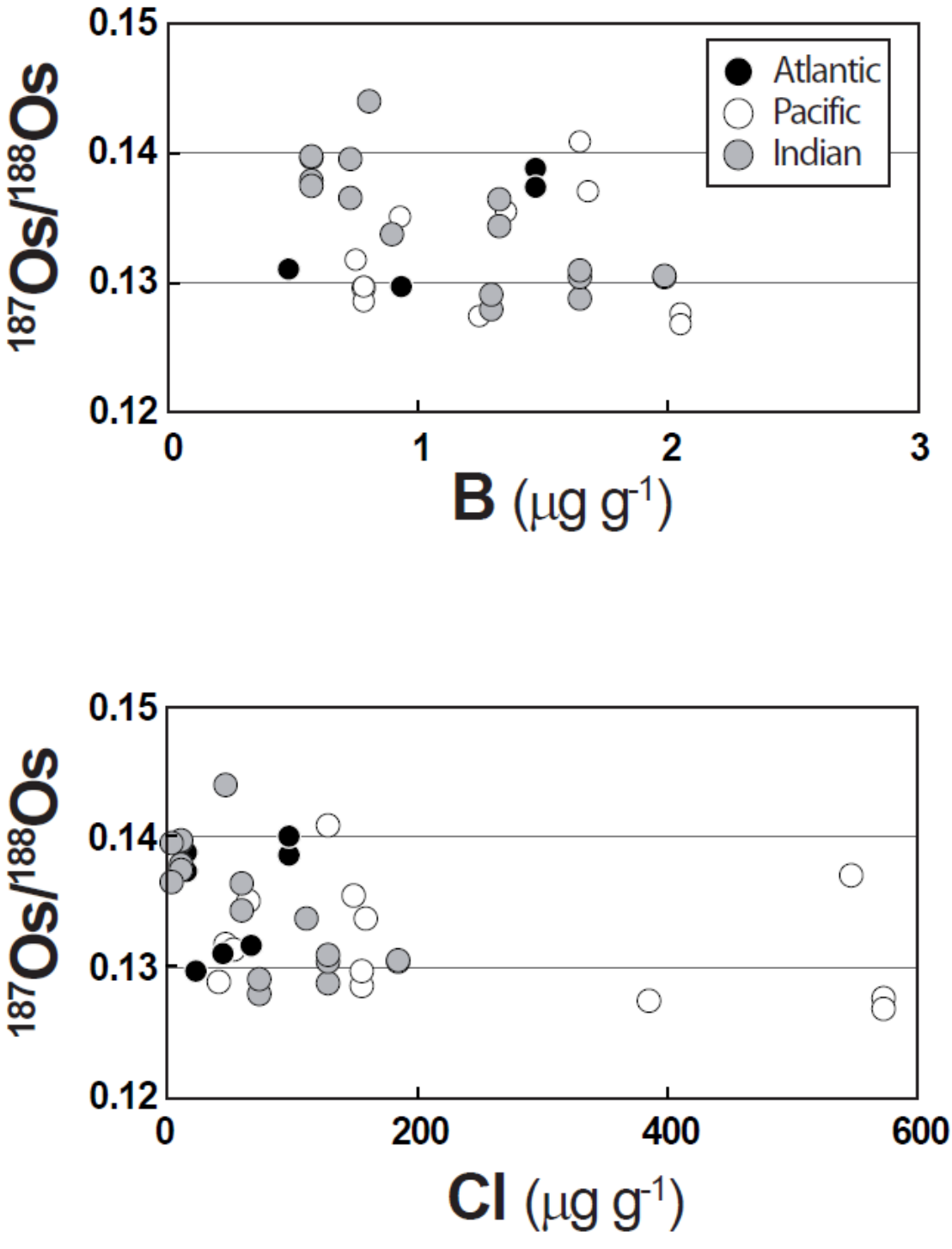

3669
3670
3671
3672
3673

Figure 22

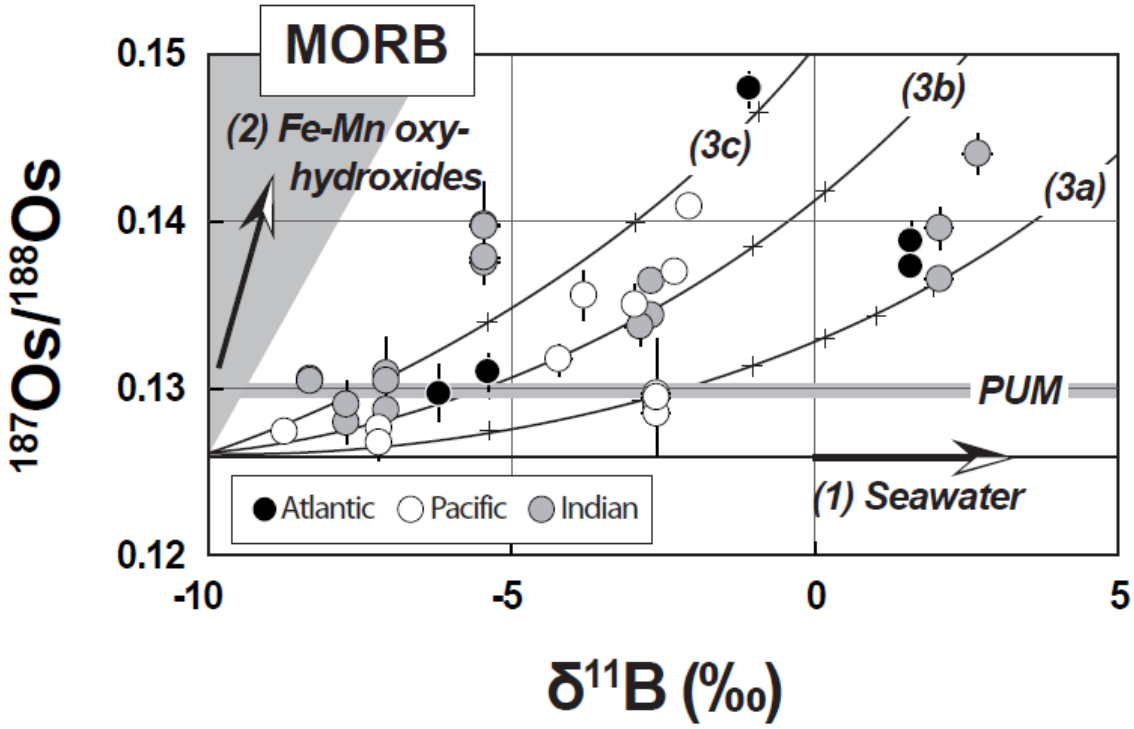
MORB
(2) Fe-Mn oxy-hydroxides
(3c)
(3b)
(3a)
PUM
(1) Seawater
Atlantic
Pacific
Indian
0.15
0.14
0.13
0.12
-10
-5
0
5
$^{187}Os/^{188}Os$
$\delta^{11}B$ (‰)

3700 Figure 23a
3701

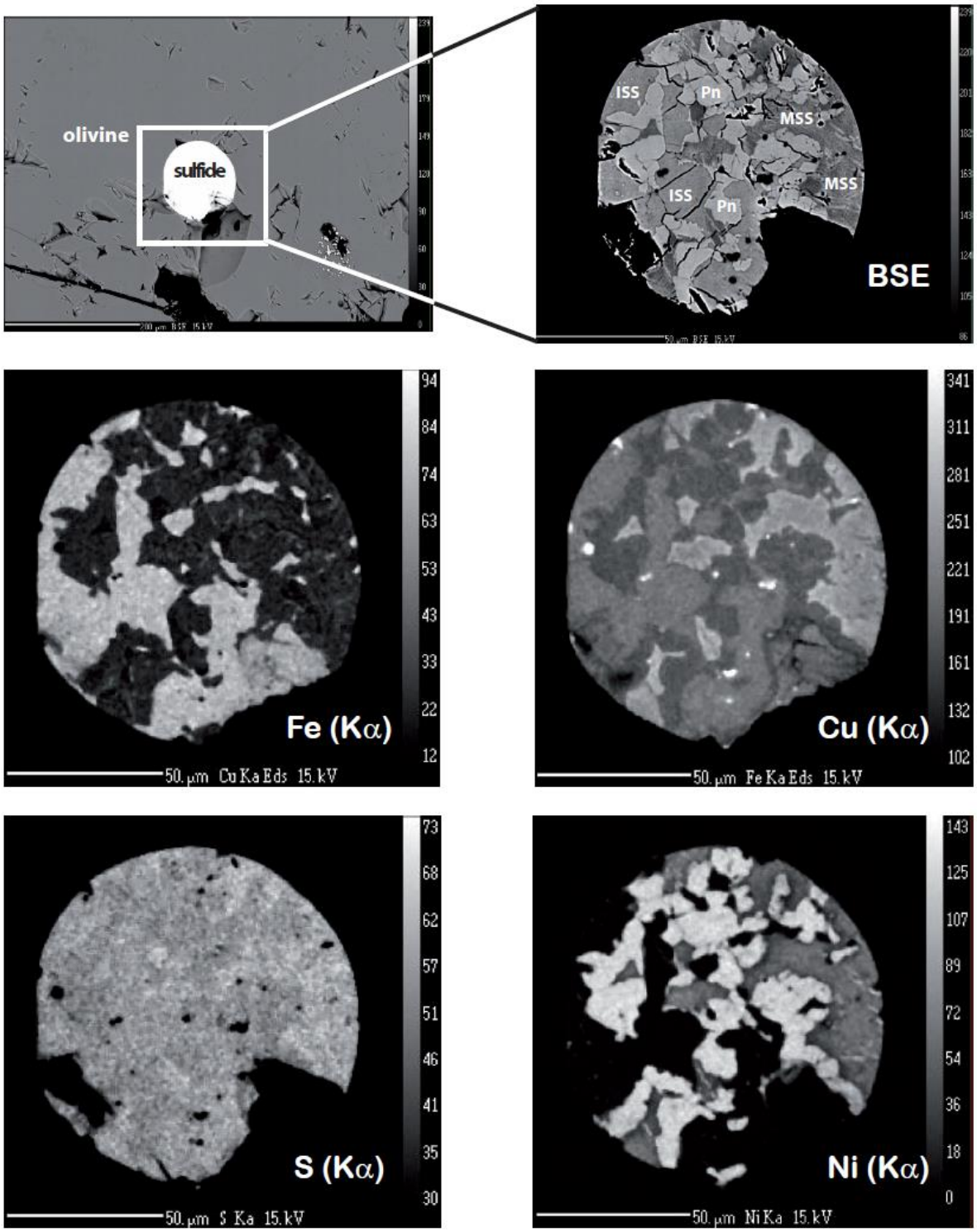

3702
3703
3704
3705
3706

Figure 23b

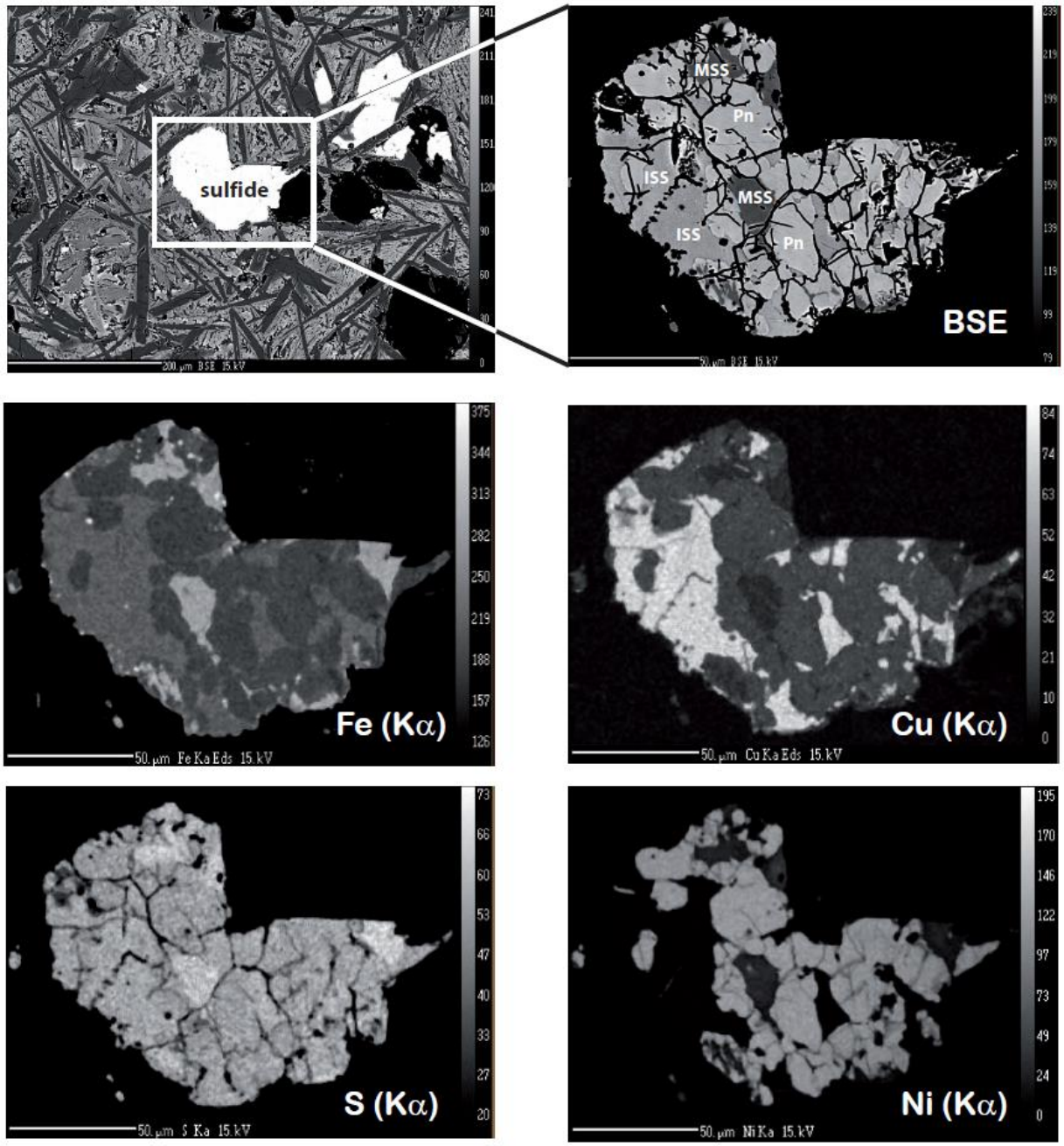

Figure 24

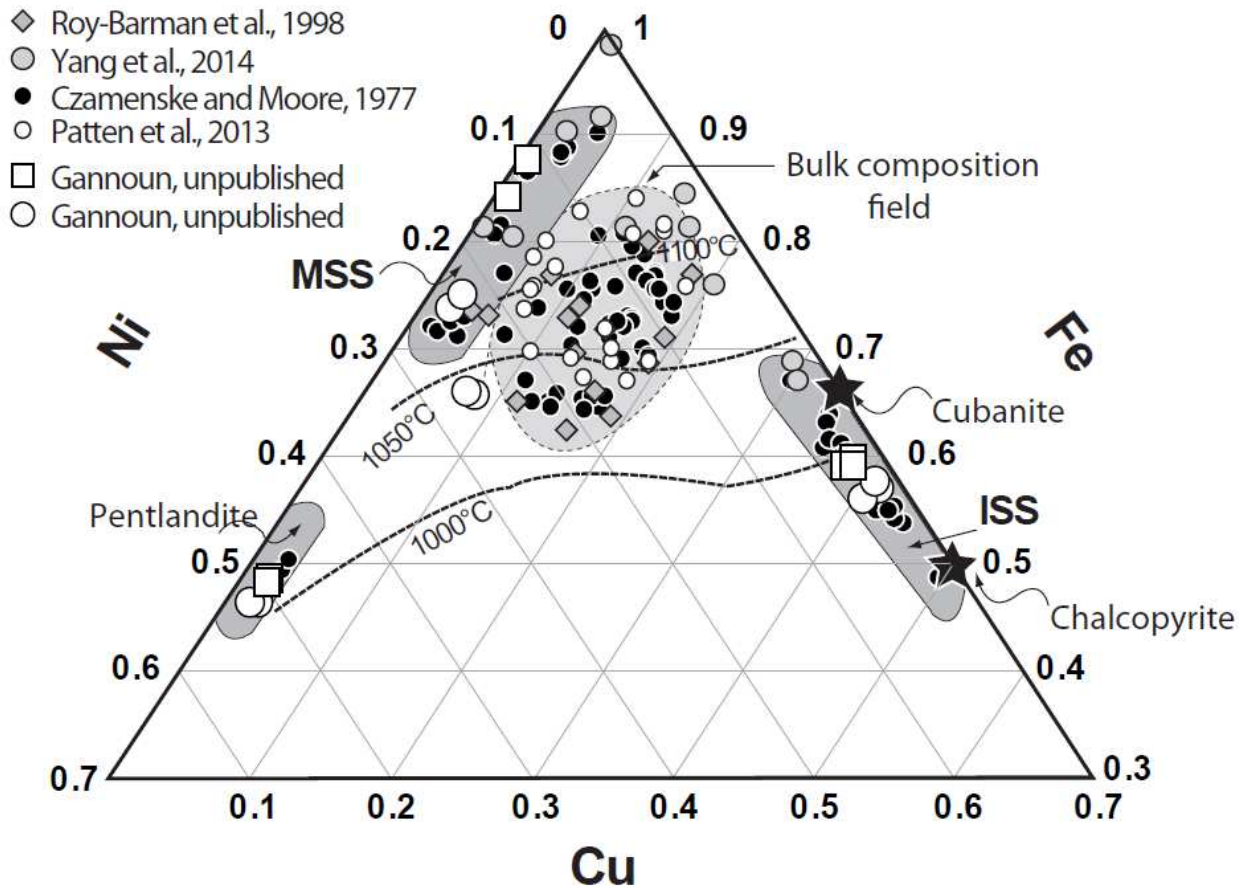
Roy-Barman et al., 1998
Yang et al., 2014
Czamenske and Moore, 1977
Patten et al., 2013
Gannoun, unpublished
Gannoun, unpublished
Bulk composition field
MSS
ISS
Cubanite
Chalcopyrite
Pentlandite
1100°C
1050°C
1000°C
Ni
Fe
Cu
0
1
0.1
0.9
0.2
0.8
0.3
0.7
0.4
0.6
0.5
0.5
0.6
0.4
0.7
0.3
0.1
0.2
0.3
0.4
0.5
0.6
0.7

Figure 25

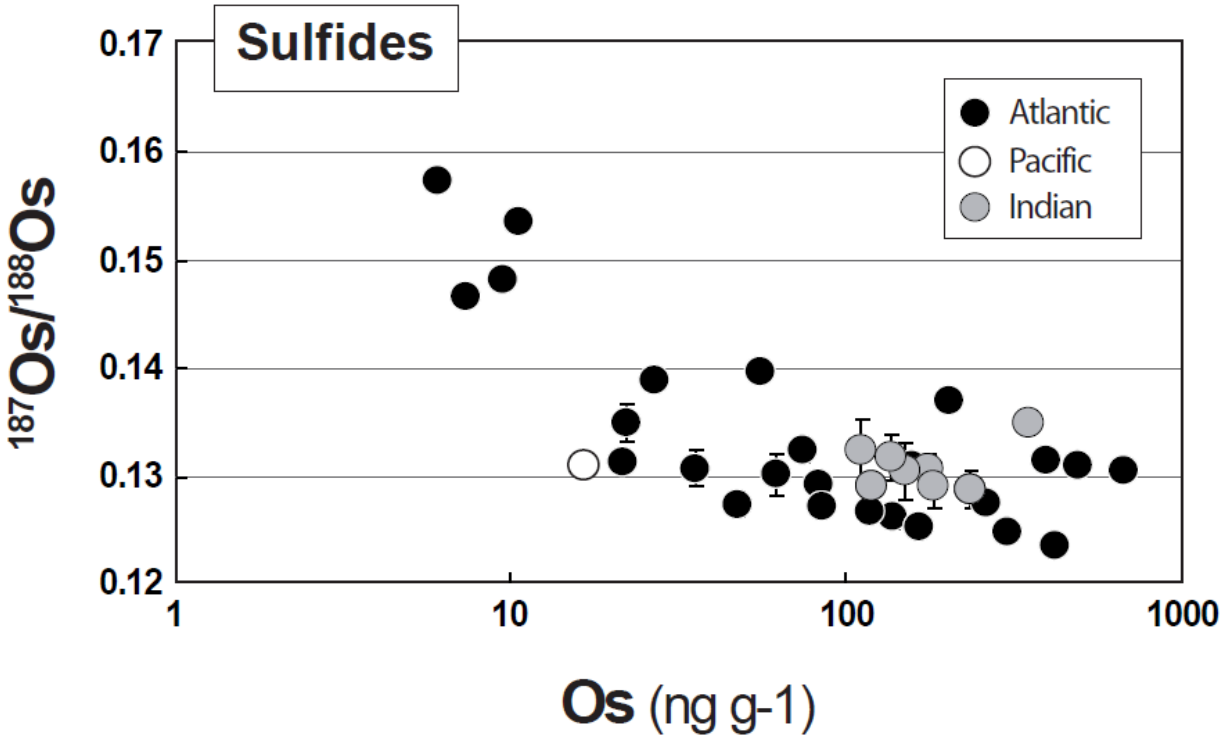
Sulfides
Atlantic
Pacific
Indian
0.17
0.16
0.15
0.14
0.13
0.12
1
10
100
1000
187Os/188Os
Os (ng g-1)

3774 Figure 26
3775

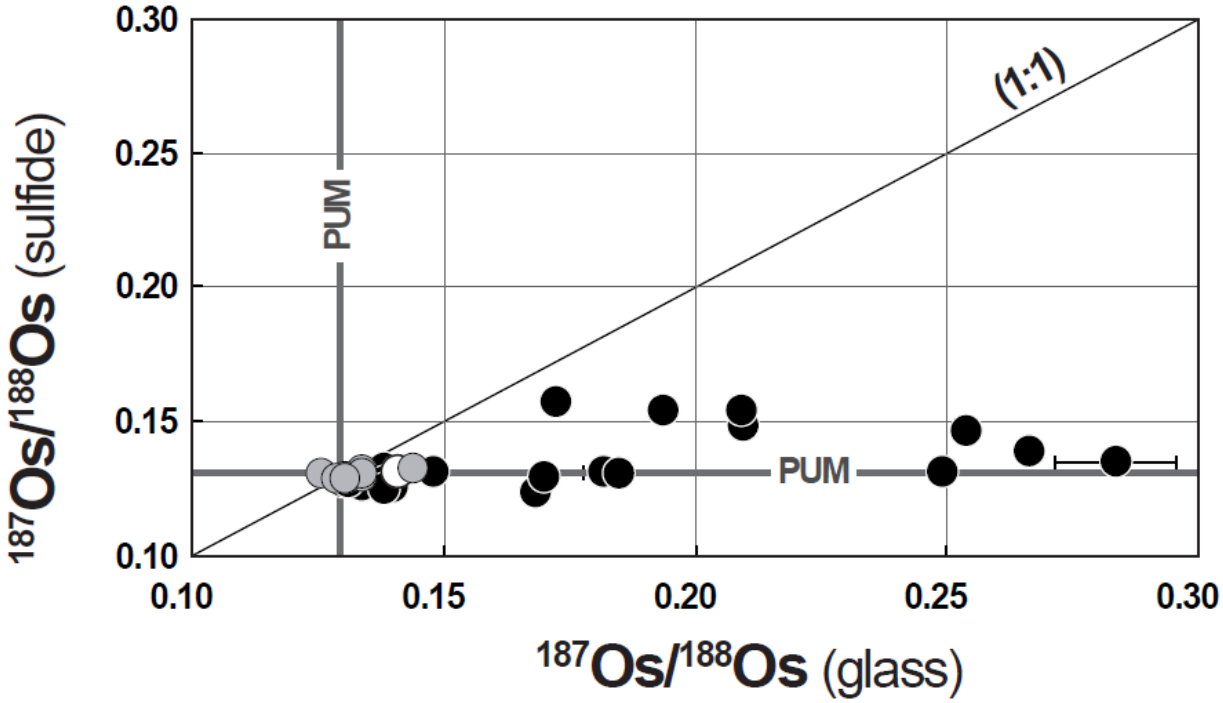

3776
3777
3778
3779
3780
3781
3782
3783
3784
3785
3786
3787
3788
3789
3790
3791
3792
3793
3794
3795
3796
3797
3798
3799
3800
3801
3802

3803 Figure 27
3804

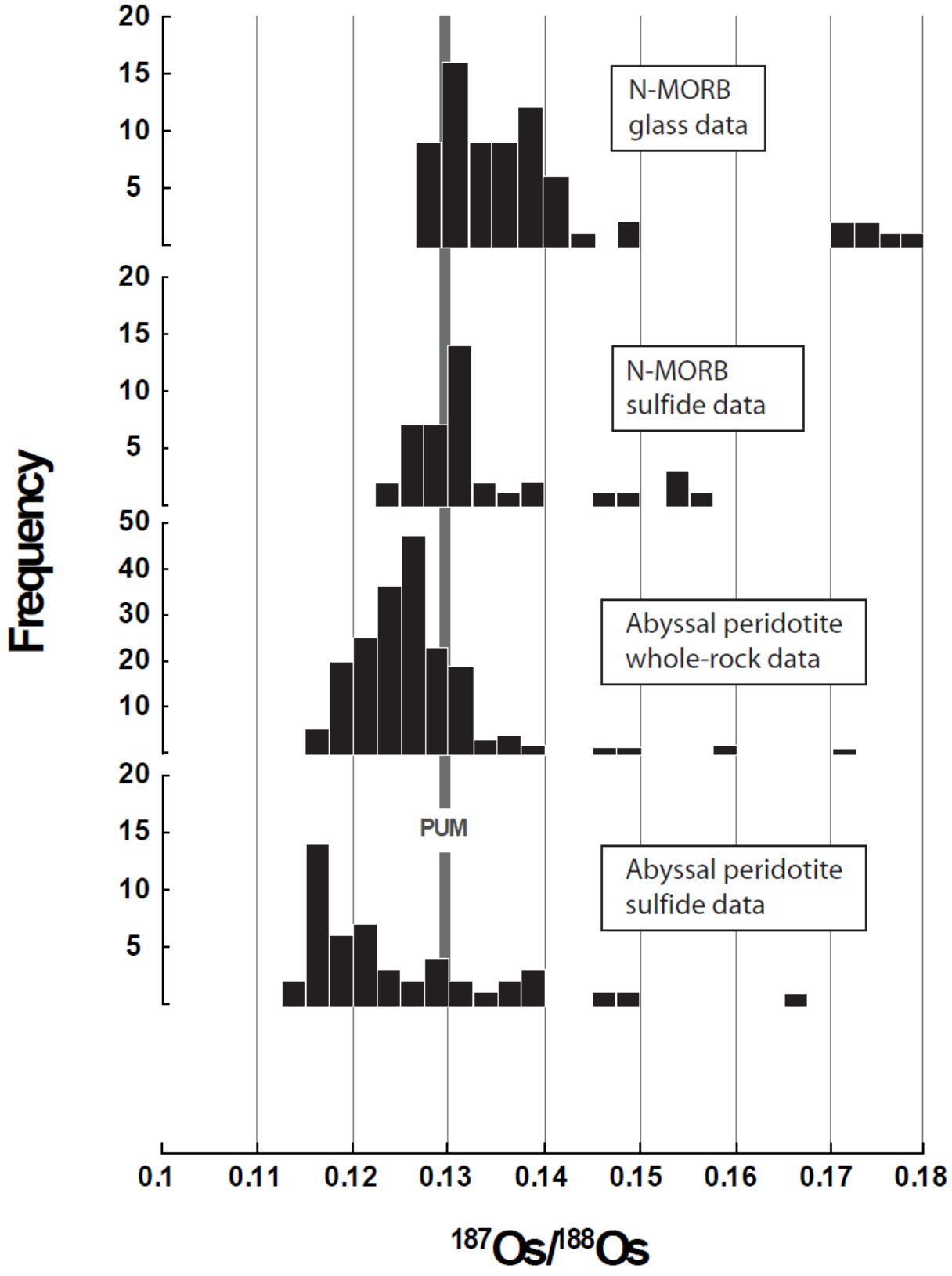

3805
3806

Figure 28

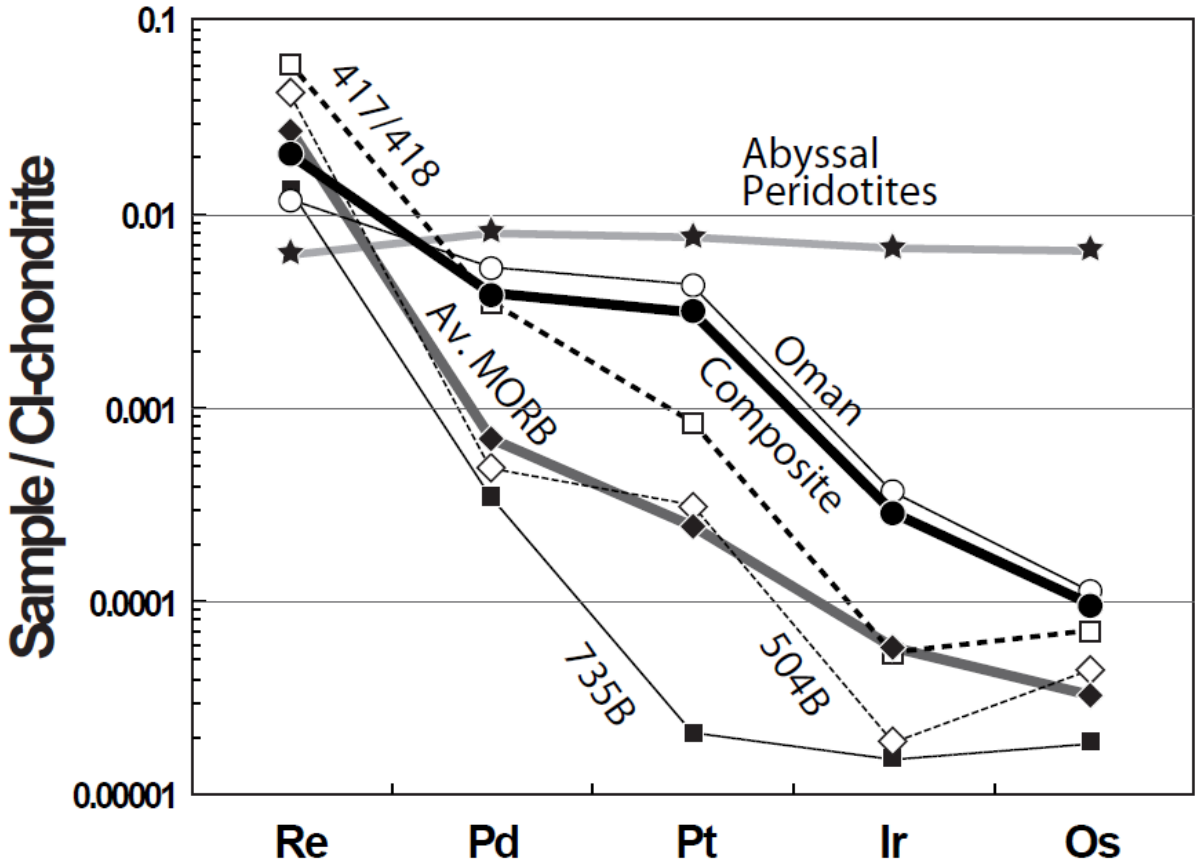
0.1
0.01
0.001
0.0001
0.00001
Sample / CI-chondrite
Re
Pd
Pt
Ir
Os
417/418
Abyssal
Peridotites
Av. MORB
Oman
Composite
735B
504B

Figure 29

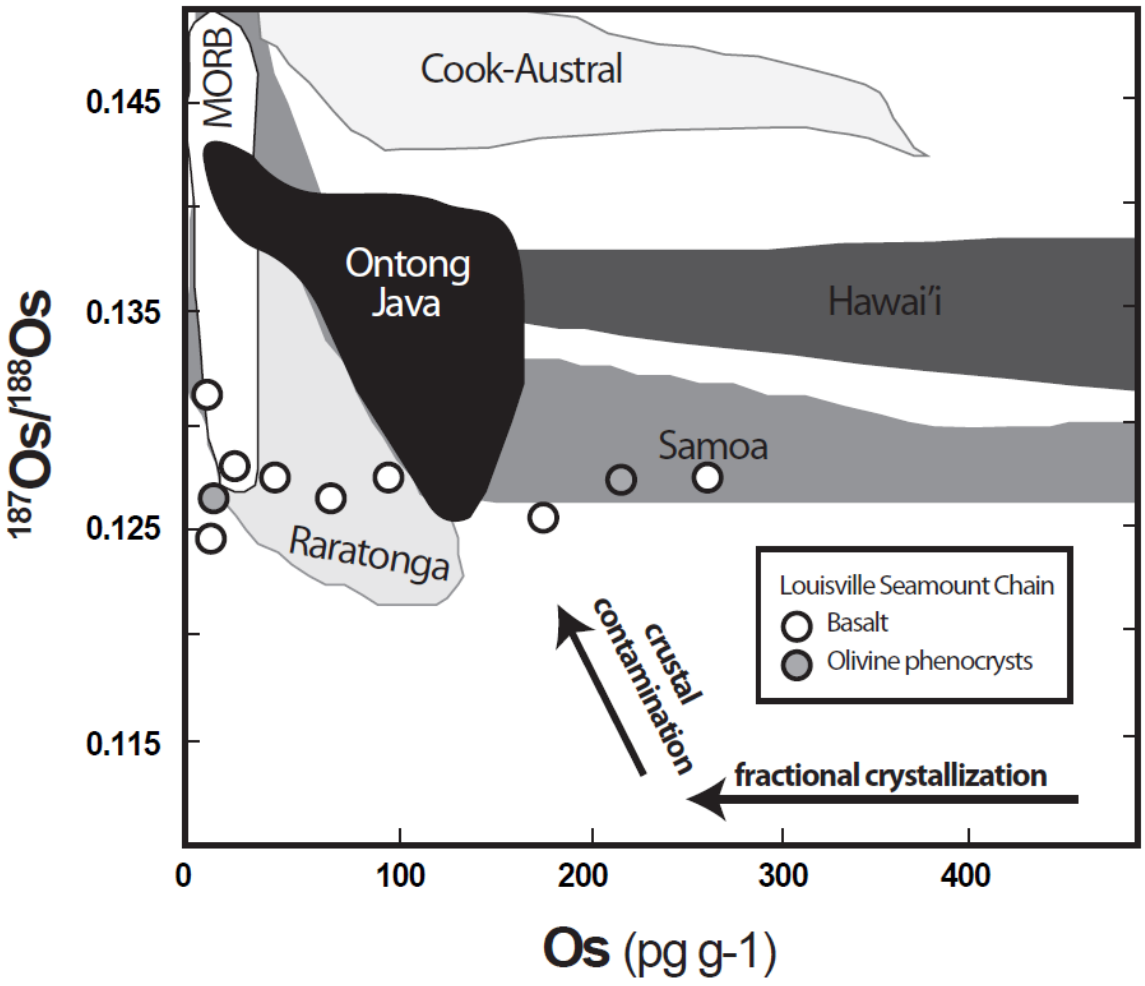
MORB
Cook-Austral
Ontong Java
Hawai'i
Samoa
Raratonga
Louisville Seamount Chain
Basalt
Olivine phenocrysts
crustal contamination
fractional crystallization
0.145
0.135
0.125
0.115
0
100
200
300
400
$^{187}Os/^{188}Os$
Os (pg g-1)

Figure 30

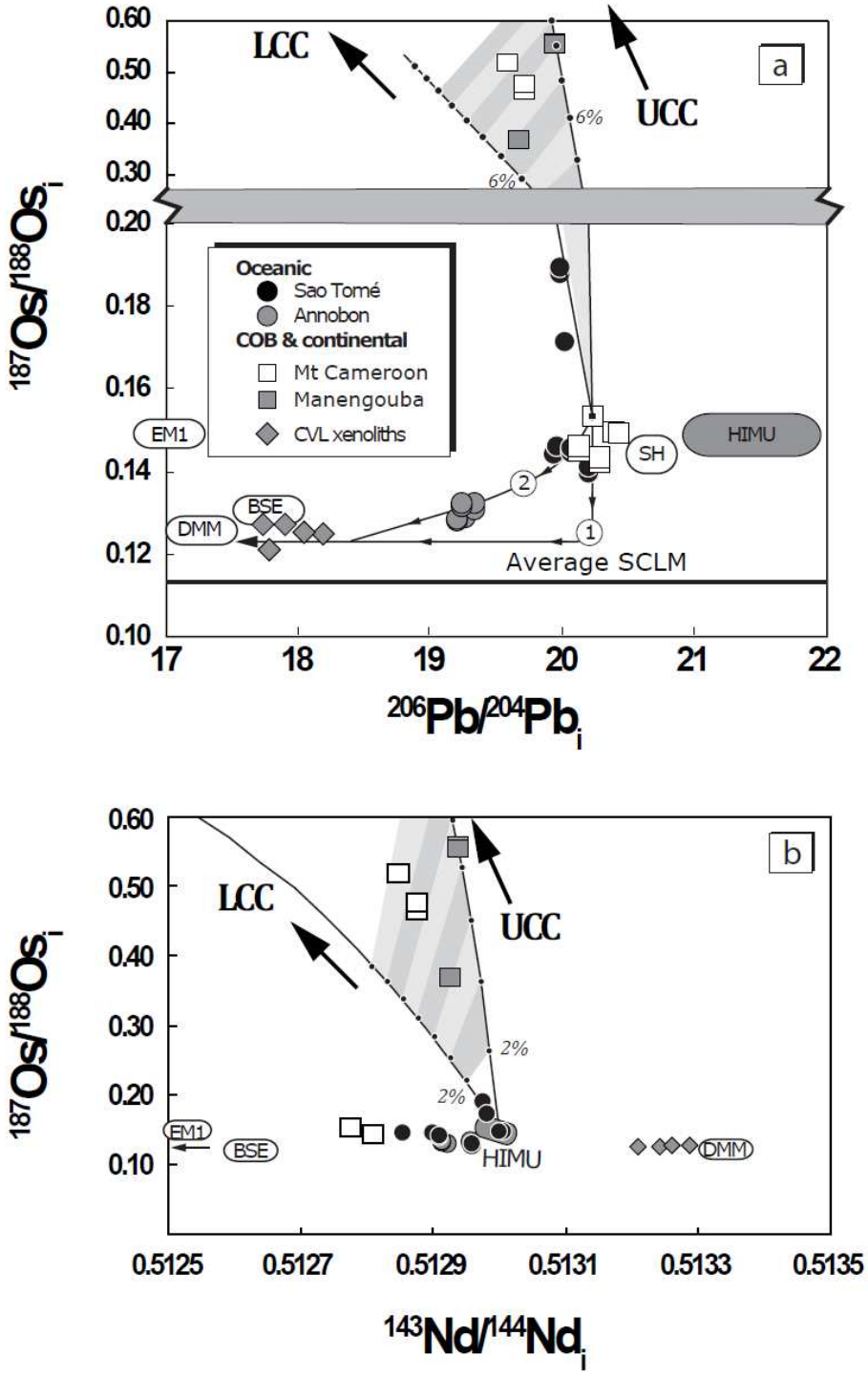
a
LCC
UCC
6%
6%
Oceanic
Sao Tomé
Annobon
COB & continental
Mt Cameroon
Manengouba
CVL xenoliths
EM1
HIMU
SH
BSE
DMM
2
1
Average SCLM
0.60
0.50
0.40
0.30
0.20
0.18
0.16
0.14
0.12
0.10
17
18
19
20
21
22
$^{187}Os/^{188}Os_i$
$^{206}Pb/^{204}Pb_i$
b
LCC
UCC
2%
2%
EM1
BSE
HIMU
DMM
0.5125
0.5127
0.5129
0.5131
0.5133
0.5135
$^{187}Os/^{188}Os_i$
$^{143}Nd/^{144}Nd_i$

Figure 31

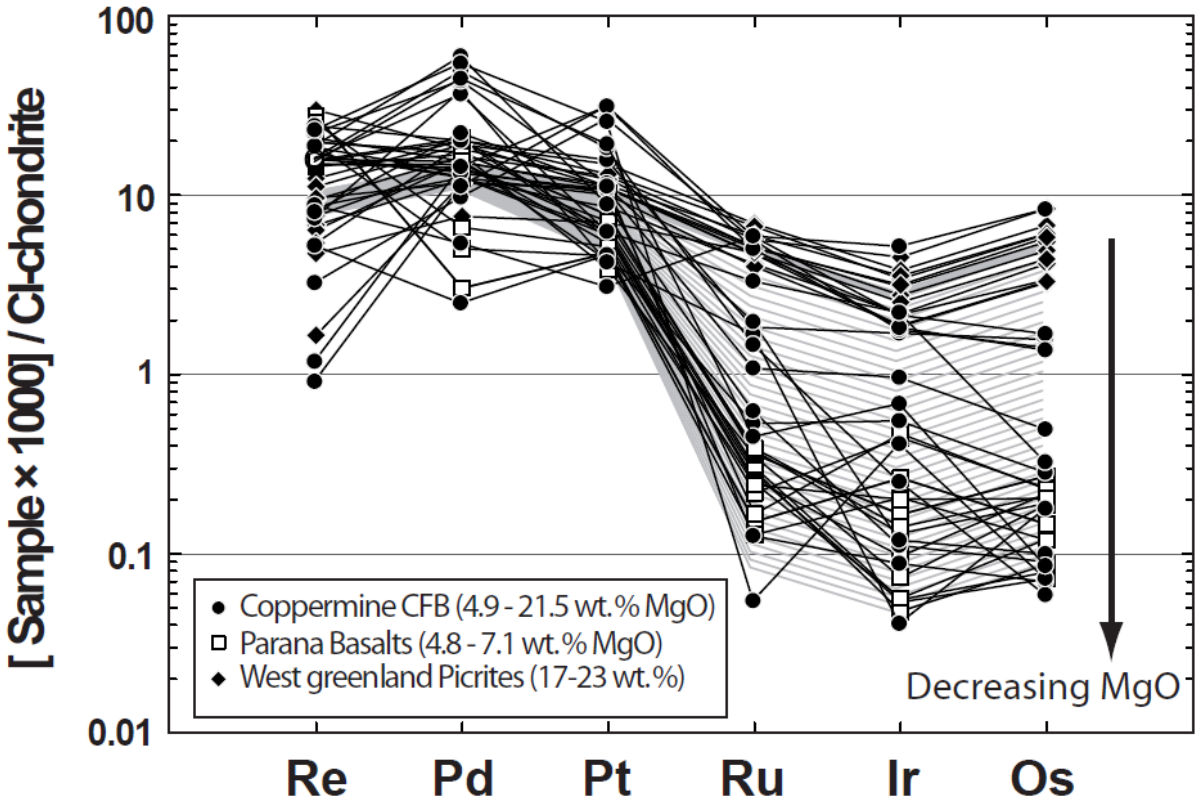
100
10
1
0.1
0.01
[Sample × 1000] / Cl-chondrite
Coppermine CFB (4.9 - 21.5 wt.% MgO)
Parana Basalts (4.8 - 7.1 wt.% MgO)
West greenland Picrites (17-23 wt.%)
Decreasing MgO
Re
Pd
Pt
Ru
Ir
Os

Figure 32

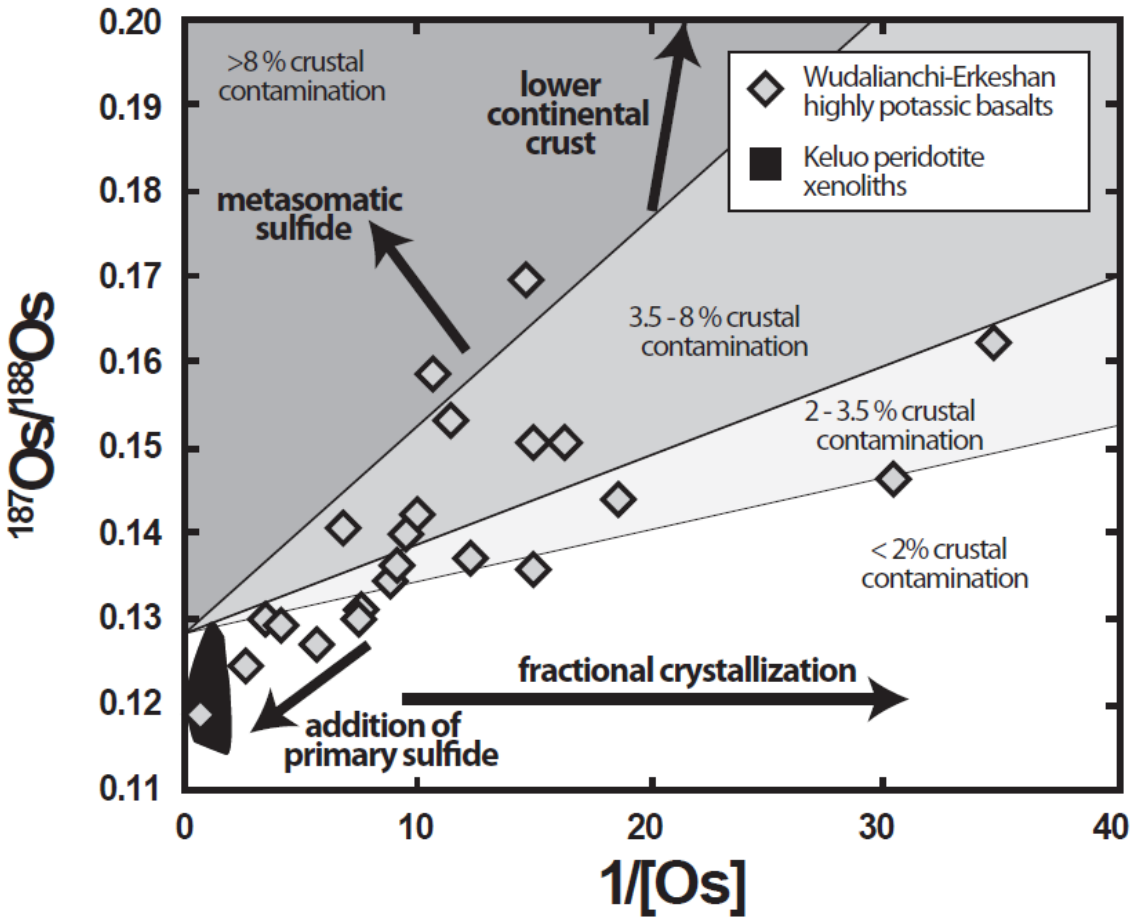
0.20
0.19
0.18
0.17
0.16
0.15
0.14
0.13
0.12
0.11
0
10
20
30
40
$^{187}Os/^{188}Os$
1/[Os]
>8 % crustal contamination
lower continental crust
metasomatic sulfide
Wudalianchi-Erkeshan highly potassic basalts
Keluo peridotite xenoliths
3.5 - 8 % crustal contamination
2 - 3.5 % crustal contamination
< 2% crustal contamination
fractional crystallization
addition of primary sulfide

Figure 33

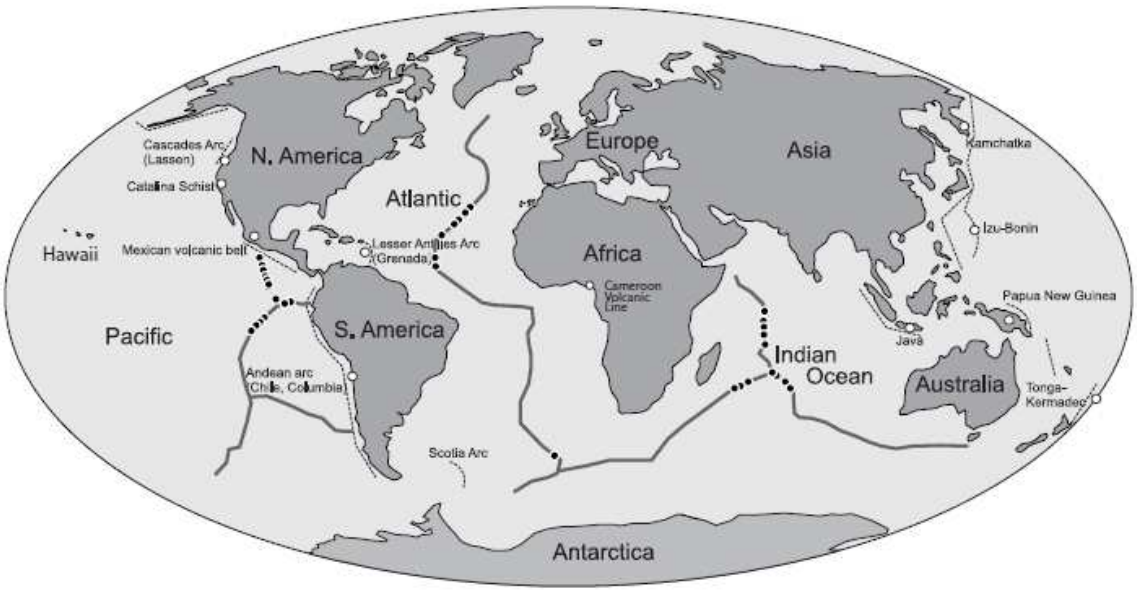
Cascades Arc
(Lassen)
N. America
Catalina Schist
Atlantic
Europe
Asia
Kamchatka
Izu-Bonin
Hawaii
Mexican volcanic belt
Lesser Antilles Arc
Grenada
Africa
Cameroon
Volcanic
Line
Papua New Guinea
Pacific
S. America
Java
Indian
Ocean
Australia
Tonga-
Kermadec
Andean arc
(Chile, Columbia)
Scotia Arc
Antarctica

3942 Figure 34
3943

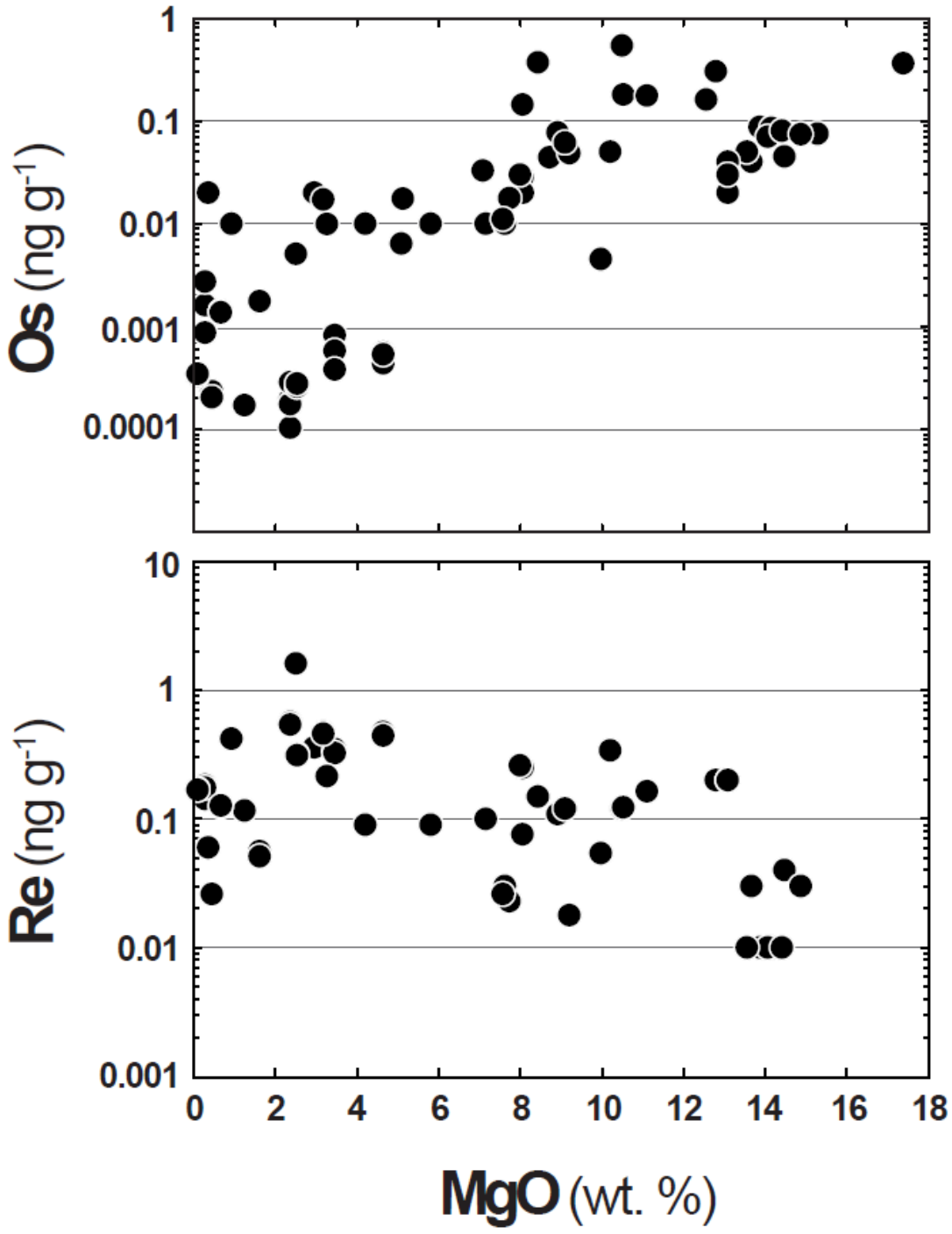

3944
3945
3946
3947
3948
3949
3950

3951 Figure 35
3952

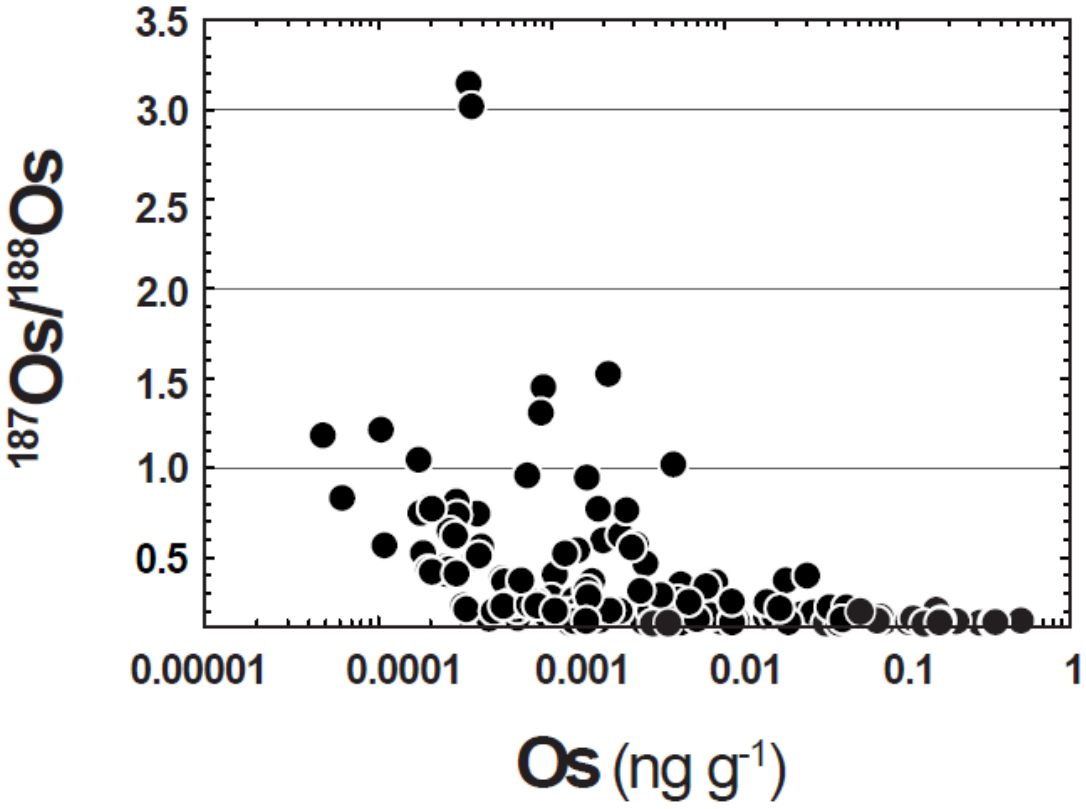
3.5
3.0
2.5
2.0
1.5
1.0
0.5
187Os/188Os
0.00001
0.0001
0.001
0.01
0.1
1
Os (ng g-1)

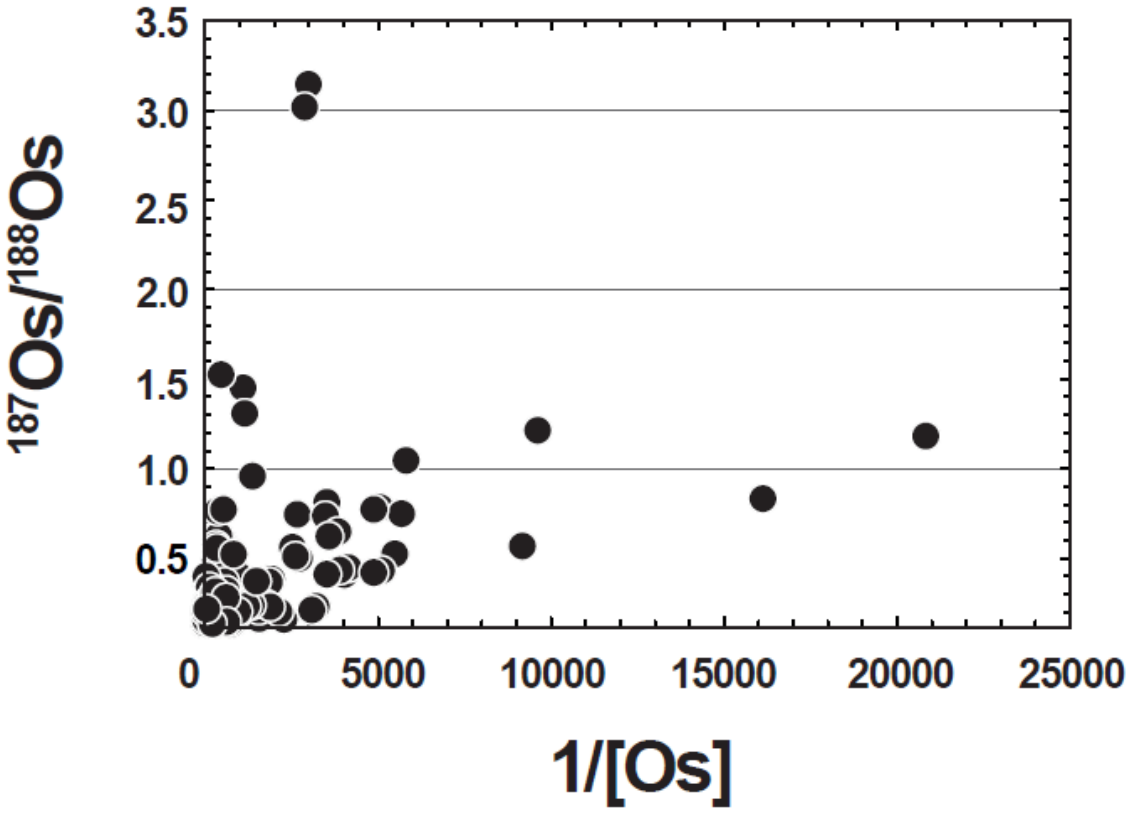
3.5
3.0
2.5
2.0
1.5
1.0
0.5
187Os/188Os
0
5000
10000
15000
20000
25000
1/[Os]

3953

Figure 36

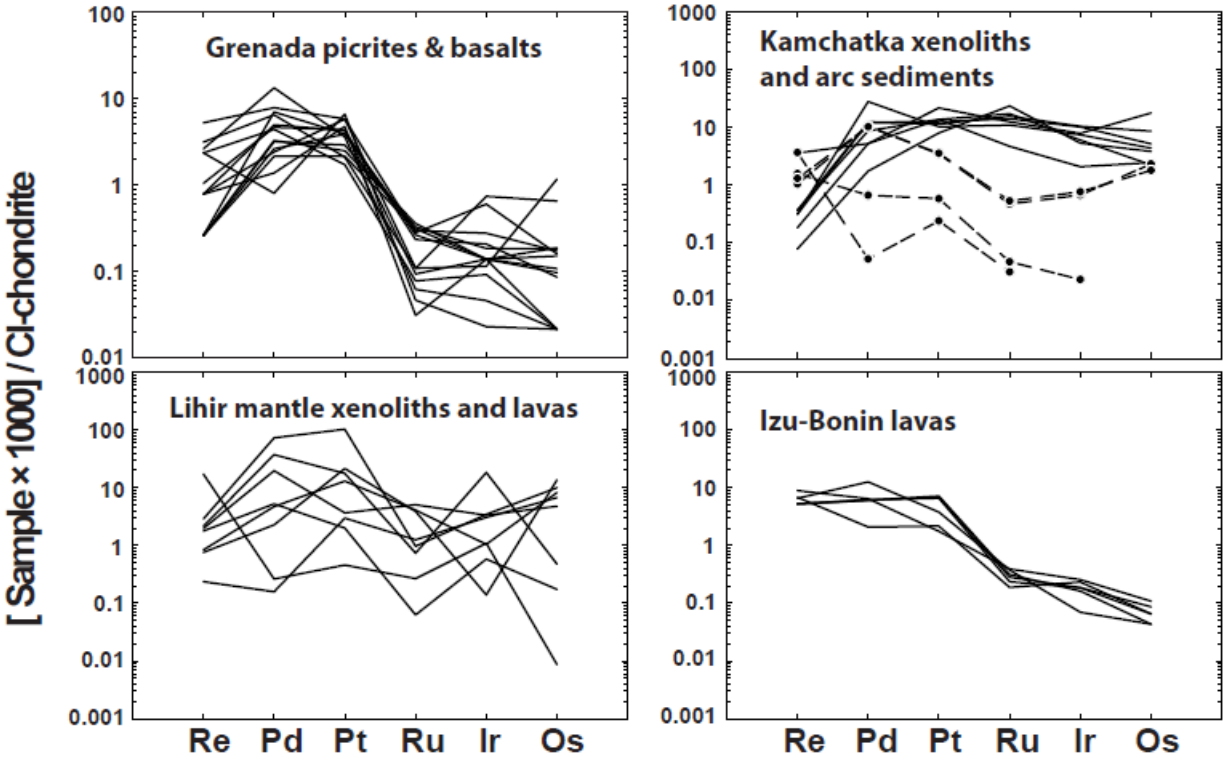
[Sample × 1000] / CI-chondrite
Grenada picrites & basalts
Kamchatka xenoliths
and arc sediments
Lihir mantle xenoliths and lavas
Izu-Bonin lavas
Re Pd Pt Ru Ir Os

Figure 37

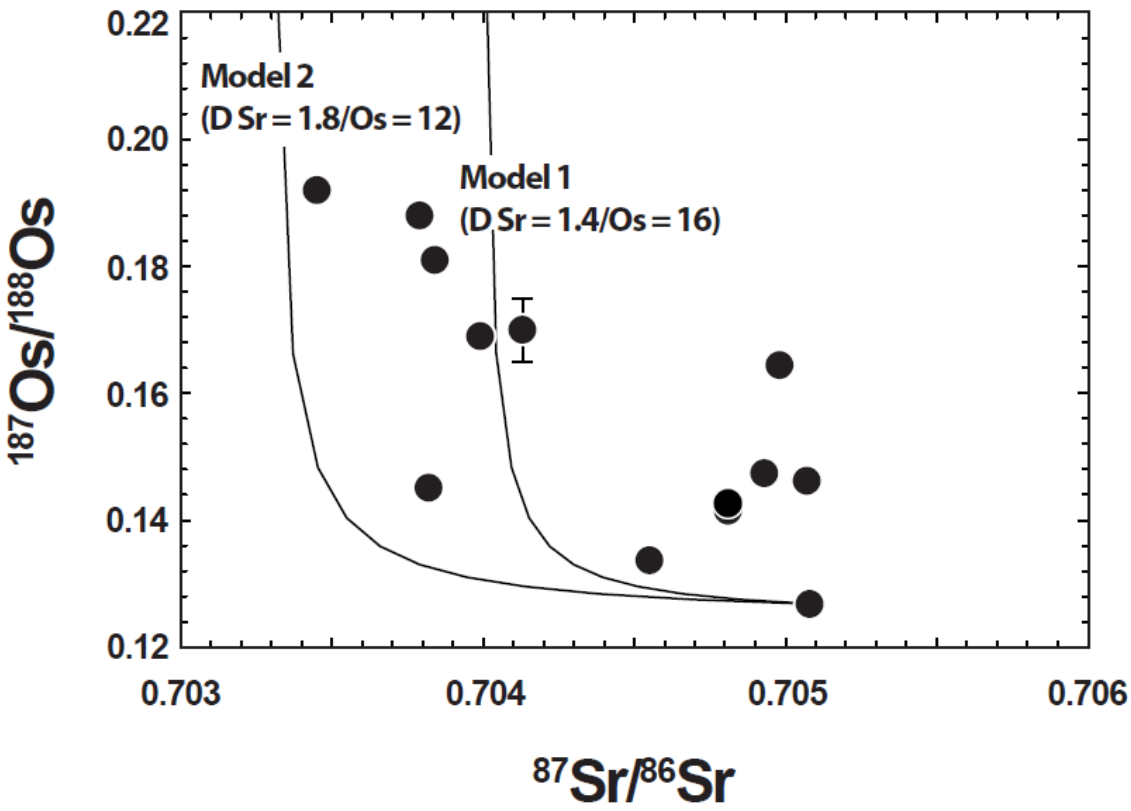
Model 2
(D Sr = 1.8/Os = 12)
Model 1
(D Sr = 1.4/Os = 16)
0.22
0.20
0.18
0.16
0.14
0.12
0.703
0.704
0.705
0.706
187Os/188Os
87Sr/86Sr

Figure 38

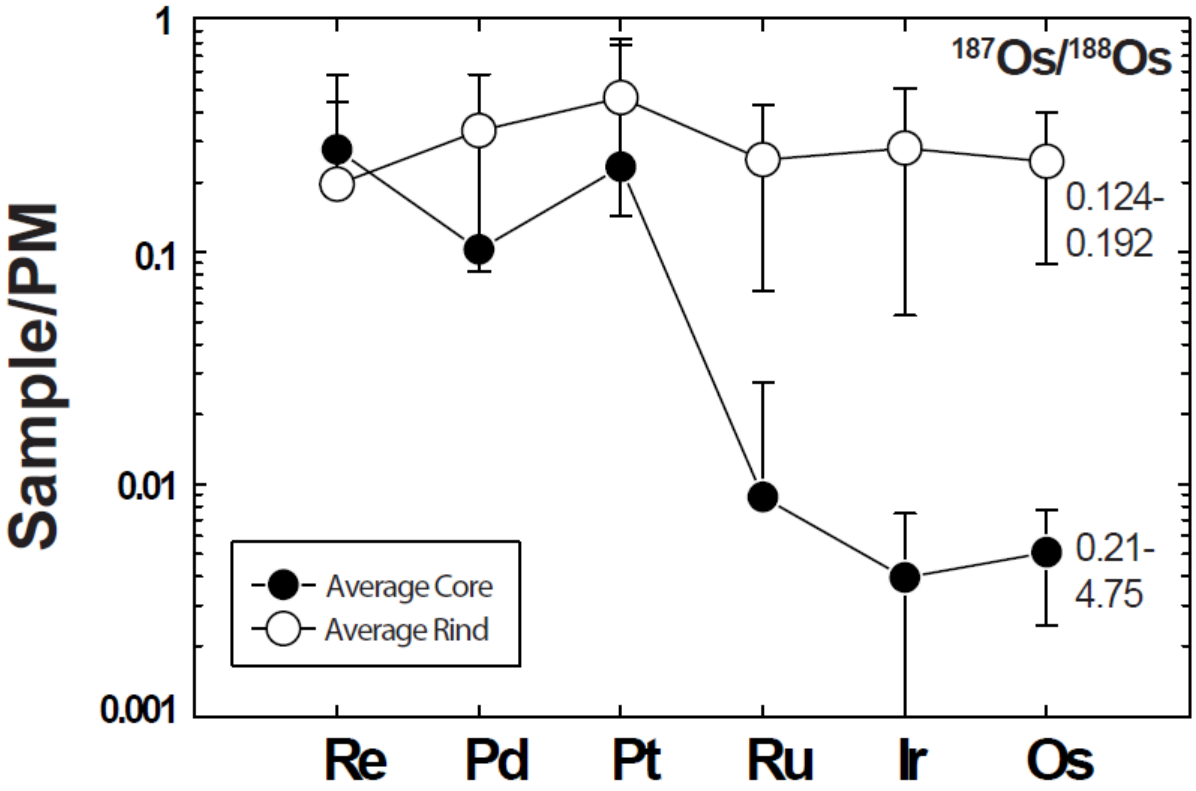
1
0.1
0.01
0.001
Sample/PM
$^{187}Os/^{188}Os$
0.124-
0.192
0.21-
4.75
Average Core
Average Rind
Re
Pd
Pt
Ru
Ir
Os